A THEORETICAL AND EXPERIMENTAL STUDY OF NEUTRON WAVE PROPAGATION IN MODERATING MEDIA

By

RAY STURGIS BOOTH

A DISSERTATION PRESENTED TO THE GRADUATE COUNCIL OF
THE UNIVERSITY OF FLORIDA
IN PARTIAL FULFILLMENT OF THE REQUIREMENTS FOR THE
DEGREE OF DOCTOR OF PHILOSOPHY

UNIVERSITY OF FLORIDA

April, 1965

UNIVERSITY OF FLORIDA
3 1262 08552 5599

Copyright by
Ray Sturgis Booth
and
Department of Nuclear Engineering
University of Florida
1965

ACKNOWLEDGMENTS

The author wishes to express his sincere appreciation to the members of his supervisory committee for their assistance in the preparation of this dissertation. Special recognition is due Dr. Rafael B. Perez for his continual guidance and encouragement. His advice and profound insight have been invaluable throughout all phases of this work.

The author is grateful to Dr. M. J. Ohanian for his major contribution to the theoretical aspects of the dissertation through stimulating discussions and the contribution of useful computer codes. Important in the experimental work has been the generous aid of Robert H. Hartley and his careful and exacting experimental technique during the acquisition of mutually valuable data.

Other persons whose contributions to this work are gratefully recognized include Robert B. Razminas for the sharing of his DIAGONAL-CORRECTOR code, the staff of the University of Florida Computing Center for valuable assistance in connection with many codes, George Fogle for the contribution of his technical know-how to the experiment, and Barbara Gyles, who took more than a typist's interest in turning out the final manuscript.

The author is deeply indebted to his wife, Judy, for her devoted encouragement, understanding, and patience. Her valuable help in the preparation of the manuscript is also appreciated.

TABLE OF CONTENTS

		Page
ACKNOWLEDGMENTS		iii
LIST OF TABLES		vi
LIST OF FIGURES		vii
LIST OF SYMBOLS		x
ABSTRACT		xiii
Chapter		
I.	INTRODUCTION	1
II.	REVIEW OF THE LITERATURE	5
III.	THE BOLTZMANN EQUATION IN THE DIFFUSION APPROXIMATION WITHIN THE FRAMEWORK OF NEUTRON THERMALIZATION THEORY	11
IV.	THE EXPERIMENT IN GRAPHITE	58
V.	COMPARISON OF THE THEORY WITH THE EXPERIMENT	99
VI.	RELATIONSHIPS BETWEEN THE NEUTRON WAVE EXPERIMENT AND DIE-AWAY EXPERIMENT IN THE DETERMINATION OF DIFFUSION AND THERMALIZATION PARAMETERS	124
VII.	CONCLUSIONS AND RECOMMENDATIONS	136
LIST OF REFERENCES		144
APPENDIX		149
BIOGRAPHICAL SKETCH		178

LIST OF TABLES

Table		Page
1.	The Energy Points Used in the Discrete Energy Representation and the Calculated Values of the Diffusion Coefficient at These Points	39
2.	Parameters Used in the Numerical Calculations	41
3.	Eigenvalues of the Space and Energy Dependent Boltzmann Operator Using the SUMMIT Kernel and the MASSMK Kernel	45
4.	The Experimental and Theoretical Values for the $P^{(n)}$ Coefficients	122
5.	The Experimental and Theoretical Values for the $Q^{(n)}$ Coefficients	132
6.	The Static and Dynamic Parameters	133
7.	Parameters as Determined from Various Die-Away Experiments Compared with the Results of This Work	134

LIST OF FIGURES

Figure		Page
1.	Flow Diagram of Several of the Computer Codes Used in the Theory	38
2.	Several Eigenfunctions of the Space and Energy Dependent Boltzmann Operator Using the SUMMIT Kernel.	43
3.	Several Eigenfunctions of the Space and Energy Dependent Boltzmann Operator Using the MASSMK Kernel.	44
4.	Real Component of the Complex Inverse Relaxation Length for the Fundamental and First Four Energy Harmonics as Calculated Using the MASSMK Kernel.	50
5.	Imaginary Component of the Complex Inverse Relaxation Length for the Fundamental and First Four Energy Harmonics as Calculated Using the MASSMK Kernel.	51
6.	Real Component of the Complex Inverse Relaxation Length for the Fundamental and First Three Energy Harmonics as Calculated Using the SUMMIT Kernel.	53
7.	Imaginary Component of the Complex Inverse Relaxation Length for the Fundamental and First Three Energy Harmonics as Calculated Using the SUMMIT Kernel.	54
8.	Real Component of the Complex Inverse Relaxation Length for the Fundamental and First Two Space Harmonics as Calculated Using the MASSMK Kernel.	55
9.	Imaginary Component of the Complex Inverse Relaxation Length for the Fundamental and First Two Space Harmonics as Calculated Using the MASSMK Kernel.	56

LIST OF FIGURES (Continued)

Figure		Page
10.	Arrangement of the Experiment and Details of the Thermalizing Tank (from Reference 14).	60
11.	A Block Diagram of the Electronic Equipment Used in the Wave Experiment.	66
12.	Time Sequence of Electrical Signals Associated with the Electronic Equipment Used in the Wave Experiment	68
13.	A Block Diagram of Electronic Equipment Used in the Pulse Propagation Experiment (from Reference 14)	71
14.	Thermal Wave of the 200 cps Wave Experiment for Several z Positions	72
15.	Thermal Pulse for the Pulse Propagation Experiment for Several z Positions (from Reference 14)	74
16.	Amplitude of the 400 cps Wave as Obtained from the First Harmonic of the 200 cps Wave Data and the Fundamental of the 400 cps Wave Data	82
17.	Phase of the 400 cps Wave as Obtained from the First Harmonic of the 200 cps Wave Data and Fundamental of the 400 cps Wave Data.	83
18.	Combined Amplitude Curves for Several Frequencies	93
19.	Combined Phase Curves for Several of the Frequencies	94
20.	Comparison of the Theoretically Derived α to the Experimental Results	100
21.	Comparison of the Theoretically Derived ξ to the Experimental Results	101
22.	Comparison of the Theoretically Derived $2\alpha\xi$ to the Experimental Results	106

LIST OF FIGURES (Continued)

Figure		Page
23.	Comparison of the Theoretically Derived $\alpha^2 - \xi^2$ to the Experimental Results for Frequencies up to 1,400 cps.	107
24.	Comparison of the Theoretically Derived $\alpha^2 - \xi^2$ to the Experimental Results for Frequencies up to 400 cps.	108
25.	The $P^{(n)}$ as a Function of the Maximum Frequency Included in the Least-Squares Fit . .	112
26.	The Experimentally Determined Real Part of $\bar{t}$ versus Distance from the Source.	115
27.	The Experimentally Determined Imaginary Part of $\bar{t}$ versus Distance from the Source. .	116
28.	The Experimentally Determined α' and ξ' as a Function of Frequency.	117
29.	The First Frequency Derivatives of $2\alpha\xi$ and $\alpha^2 - \xi^2$ versus ω	118
30.	A Pictorial Representation of the Die-Away and Neutron Wave Experiments	126

LIST OF SYMBOLS

B_1^2	Transverse buckling of the fundamental space mode (cm^{-2})
B^2	Square of the fundamental complex inverse relaxation length for $B_1^2=0$. Also used as a general eigenvalue in one part of the theory (cm^{-2})
B_n^2	Square of the complex inverse relaxation length for $B_1^2=0$ associated with the higher energy modes (cm^{-2})
$B^{(K)}$	The Kth coefficient of the Maclaurin's series expansion of B^2 ($cm^{-2}secK$)
C_o	Diffusion cooling coefficient (cm^4sec^{-1})
$D(E)$	Energy dependent diffusion coefficient
D_o	Energy averaged diffusion coefficient (cm^2sec^{-1})
E	Neutron energy (ev)
F_o	Coefficient of the B^6 term in the power series expansion of λ in power of B^2 (cm^6sec^{-1})
L_{mn}	Matrix elements of the energy expansion in eigenfunctions of the $\underline{P}$ operator ($cm^{-2}sec$)
$M(E)$	Maxwellian distribution (number density)
$\underline{P}$	Energy and space dependent Boltzmann operator
$P^{(n)}$	The coefficients of the power series fit of the experimental data ($cm^{-2}sec^n$)
$Q^{(n)}$	Coefficients of the power series expansion of ρ^2 $(cm^2)^{n-1}$

LIST OF SYMOBLS (continued)

S_n	The nth ratio associated with the fundamental eigenvalue
$S_n^{(K)}$	The Kth coefficient in the Maclaurin's series of S_n (sec^K)
t	Time (sec)
u(I-J)	Heaviside unit step function
v_o	Reference neutron speed for thermal neutrons (2.198×10^5 cm sec^{-1})
$W_n(q,\nu)$	The nth Fourier width of the measured pulse in the pulse propagation experiment
x,y,z	Space variables of the rectangular coordinate system (cm)
α_o	$v_o \Sigma_{ao}$ (sec^{-1})
δ_{mn}	Kronecker delta
η	Variable used in the discrete energy representation ($\eta = (E/KT)^{1/2}/(1+(E/KT)^{1/2})$
λ	Decay constant measured in the die-away experiment or calculated from the $Q^{(n)}$ with $\alpha_o=0$ (sec^{-1})
λ^w	Decay constant calculated from the $Q^{(n)}$ with $\alpha_o \neq 0$ (sec^{-1})
ν,f	Frequency (cps)
ρ^2	Squared fundamental complex inverse relaxation length. Also used in one section of the theory as the general eigenvalue (cm^{-2})
ρ_{no}^2	The nth eigenvalue of the $\underline{P}$ operator (cm^{-2})
Σ_{ao}	Energy averaged macroscopic absorption cross section (cm^{-1})

LIST OF SYMBOLS (continued)

$\Sigma_s(E)$	Energy dependent macroscopic scattering cross section (cm^{-1})
$\Sigma_a(E)$	Energy dependent macroscopic absorption cross section (cm^{-1})
$\Sigma_{s1}(E)$	Energy dependent second Legendre moment of the angular dependent scattering cross section
$\Sigma_s(E',E)$	Energy dependent differential scattering cross section (cm^{-1}/ev)
$\Sigma_t(E)$	Energy dependent macroscopic total collision cross section (cm^{-1})
$\phi(\vec{r},E,t)$	Neutron flux (n $cm^{-2}sec^{-1}ev^{-1}$)
$\phi_{\ell,m}(x,y)$	Spatial eigenfunction used in the space expansion
$\chi(E)$	Summetrized neutron flux
$\psi_n(E)$	The nth eigenfunction of the $\underline{P}$ operator
$\psi(q,t)$	The measured pulse of the pulse propagation experiment
$\psi_n(q,\nu)$	The nth Fourier moment of $\psi(q,t)$
ω	Frequency (rad/sec)
∇^2	Laplacian operator
$\nabla^2_{x,y}$	Laplacian operator for the x and y variables

Abstract of Dissertation Presented to the Graduate Council
in Partial Fulfillment of the Requirements for
the Degree of Doctor of Philosophy

A THEORETICAL AND EXPERIMENTAL STUDY OF NEUTRON WAVE PROPAGATION IN MODERATING MEDIA

By

Ray Sturgis Booth

April, 1965

Chairman: Dr. Rafael B. Perez
Major Department: Nuclear Engineering

The space, energy, and time or frequency dependent Boltzmann equation in the diffusion approximation has been used within the framework of neutron thermalization theory to predict thermal neutron wave propagation in a moderating medium. This theory was then compared with the experiment conducted on a graphite pile.

In the theoretical section the energy dependence was expanded in the space-energy eigenfunctions of the Boltzmann operator, and the transverse-space dependence was expanded in the orthogonal solutions to the Helmholtz equation with homogeneous boundary conditions. It was then shown that each of these space and energy modes thus formed propagate with characteristic complex inverse

relaxation lengths. The perturbation method developed by Perez was used to expand these complex eigenvalues in a Maclaurin's series of the frequency variable. In cases where this series did not rapidly converge a direct solution of the complex secular determinant was obtained. Two scattering kernels were selected for implementation into the theory, the MASSMK kernel and the SUMMIT kernel based primarily upon derivations by Parks. The numerical calculations of the theory were performed on an IBM-709 digital computer and founded upon the previous work of Ohanian.

In the experimental section an accurate technique for conducting neutron wave experiments in multiplying or diffusing media was presented along with the results of the graphite experiment. The excitation of neutron waves, both by modulated and pulsed sources, and the electronic systems associated with their detection were discussed. Special attention was given to the analysis of data for which several computer codes were developed.

In the comparison of theory and experiment it was shown that the neutron wave technique allows for the separation of diffusion and thermalization effects, thereby yielding a more exacting comparison of theoretical and experimental results. Polynomial fits of functions formed

from the experimental results yielded coefficients to be compared with the theoretically derived terms of the perturbation expansion. The results of the thermal pulse propagation experiment were also analyzed by a method suggested by Moore, and confirmation of his predictions was established.

The diffusion and thermalization parameters determined from the data analysis were then compared with results of several die-away experiments and with the theory. The complementary relationships between the neutron wave and die-away experiments were also presented.

The diffusion and thermalization parameters determined in this work for graphite of density 1.60 gm/cm^3 were $v\Sigma_a = (91.\pm 1.)sec^{-1}$, $vD = (2.16\pm .01)x10^5\ cm^2sec^{-1}$, $C = (39.\pm 2.)x10^5\ cm^4sec^{-1}$, $F = (12.\pm 2.)x10^7\ cm^6sec^{-1}$.

CHAPTER I

INTRODUCTION

Placement of a modulated or pulsed source of thermal neutrons at one boundary of a nuclear assembly creates a disturbance which can be analyzed in terms of wave components propagating from this source with frequency dependent phase shift and attenuation factors. The importance of the neutron wave experiment is based upon the fact that these two independently measurable quantities are strongly dependent upon the diffusion and thermalization properties of the assembly. Thus accurate determinations of physical constants and severe tests of theoretical models are possible through an experimental determination of the frequency dependent dispersive properties (dispersion law) of the system.

Several experimental methods for investigation of moderating and multiplicative assemblies are now in extensive use. They include, among others, exponential experiments, "poisoning" experiments, and the die-away technique. It is interesting to note that the neutron wave technique, which is the subject of this dissertation, is related to each of the three methods mentioned above. Basically, the neutron

wave experiment is an extension of the exponential experiment in that the constant source of the latter is replaced by a modulated or pulsed source. One then measures the complex inverse relaxation length, ρ, of the neutron waves as they travel through the assembly. An extrapolation to zero frequency of the real part of ρ yields the same value, B_m^2, as obtained by the exponential experiment. Using a modulated source, the material buckling is obtained through an extrapolation of a curve, which is nearly constant near the zero frequency intercept, rather than by measuring a single point on the curve. Also the imaginary part of ρ is still available for determining another parameter or comparing with the theory. Still another possibility with the neutron wave experiment is the appearance of resonance phenomena arising from the splitting of each spatial mode into various energy modes which propagate with different complex inverse relaxation lengths.

Increasing the frequency of modulation in a neutron wave experiment can be considered equivalent to "poisoning" the medium with a 1/v poison. Therefore, determining the bucklings and relaxation lengths at several poison concentrations in the "poisoning" experiment and finding the complex relaxation length as a function of frequency in the wave experiment are complementary measurements. Moreover, the frequency-dependent, energy spectrum of the neutron wave experiment bears a close resemblance to the energy spectrum

associated with the "poisoning" experiment as a function of the poison concentration. In the wave experiment, however, solids as well as liquids can be homogeneously "poisoned."

The neutron wave technique and the die-away experiment also bear a close resemblance. The modulus of the complex inverse relaxation length can be thought of as a negative buckling. Its relationship to ω/v, the "poisoning" term, is quite similar to the relationship between the geometric buckling and the decay constant as measured by the die-away technique. In the die-away experiment one determines λ, the lowest time-energy eigenvalue of the Boltzmann operator, as a function of the geometric buckling. This method, though quite effective for the determination of diffusion parameters, has severe limitations when applied to the determination of thermalization parameters unless the time-dependent, energy spectrum is measured. At high bucklings, thermalization effects cause the curve of λ versus buckling to deviate slightly from the linear relationship predicted by diffusion theory. This second-order effect occurs precisely at the range of buckling where the least confidence can be given to the experimental results; for it is in this range of buckling that the extrapolation distance is most important, transport corrections become significant, and the energy dependence takes the longest time to stabilize. Also an asymptotic decay is never attained in some crystalline moderators because of the so-called "trapped neutrons" which decay

in time much slower than those associated with the fundamental eigenvalue. Thermalization effects are of first-order significance in the neutron wave experiment. Diffusion theory predicts that the real part of ρ^2 should be independent of frequency, whereas it is in fact nearly linearly related to the square of the frequency. The measurement of thermalization parameters via the neutron wave technique can be accomplished in large systems where angular dependence and extrapolation distances are of comparatively minor importance.

The purpose of this dissertation is to present both theoretical and experimental investigations of the propagation of neutron waves in a moderating medium. The Boltzmann equation in the diffusion approximation is used as the theoretical model, and its energy dependence is expanded in the space-energy eigenfunctions of the Boltzmann operator. A perturbation method is used to expand the square of the complex inverse relaxation length in a Maclaurin's series of the $j\omega$ variable and in the x variable which is related to the frequency of excitation by the expression $\omega = xe^x$. In the experimental section an accurate technique for conducting neutron wave experiments in multiplying or diffusing media is presented along with the experiment in graphite. Special attention is then given to the analysis of the data thereby obtained and to its comparison with the theory.

CHAPTER II

REVIEW OF THE LITERATURE

The propagation of neutron waves caused by oscillating a thermal-neutron absorber in a chain-reacting pile was investigated by Weinberg and Schweinler (1).* Weinberg and Wigner (2) derived equations for the attenuation distance, wave length, and propagation velocity as a function of frequency for waves excited by a localized source in an infinite diffusing or multiplying medium. It was shown that the diffusion coefficient and the prompt material buckling could be determined by measuring the propagation characteristics of these neutron waves. Experimental measurements of diffusion parameters in graphite and heavy water were performed by Raievski and Horowitz (3) by using a mechanical source and a frequency range which varied from 50 cps to 500 cps. Their results were in good agreement with theoretical predictions, but no attempt was made to extend the theory to include thermalization effects.

---

* Underlined numbers in parentheses refer to the List of References.

Preliminary experiments in graphite and in water-moderated subcritical assemblies were done by Uhrig (4,5). He used one-group diffusion theory to derive equations relating the prompt material buckling and diffusion coefficient to the neutron wave's phase shift and attenuation and compared his results to experiments conducted on the graphite, subcritical reactor at Iowa State University (6). A mechanical source was used in these experiments; and the basic unit in the detection system was a dual, coincidence-anticoincidence switching circuit which directed the detector pulses to four slave scalers so that each scaler counted during a different phase interval of the modulated source (7). It was determined that the waves do follow the tendency predicted by theory; however, the wave velocity was in all cases higher than expected, with the deviation becoming greater as the oscillation frequency increased.

The theoretical work of Uhrig was extended by Booth (8) to a two-group diffusion theory model. It was shown that when two energy groups are considered two thermal waves propagate in the fundamental spatial mode, that the relative magnitude of the Fermi age compared with the square of the diffusion length is of predominant importance in determining the propagating characteristics of the two waves, that K_∞ is a second-order effect with respect to these same characteristics, and that the material buckling can be measured

from experiments conducted in the central region of the assembly. Several methods for the detection of neutron waves were also presented by Booth.

Perez and Uhrig (9) investigated the propagation of neutron waves in a moderating media with a one-group diffusion model and a thermalization model. In the thermalization model the energy dependence was expanded in the Associated Laguerre Polynomials of order one. The complex inverse relaxation length was expressed in a power series of the ratio ω/vD, and it was shown that the coefficients of this expansion are functions of the thermalization and diffusion properties of the moderator. The authors demonstrated that the neutron wave technique affords a complementary method to the "poisoning" technique and that the difficulties encountered in the die-away experiment because of the trap effect should not be present in a neutron wave experiment.

The diffusion and cooling coefficients of graphite were determined experimentally by Perez, Booth, and Hartley (10) by the neutron wave technique. The value of D_0 agreed with previous measurements, but the value of C_0 was a factor of two larger than that obtained by Starr and Price (11) using the die-away technique. The propagation of neutron waves in a subcritical assembly using multigroup diffusion theory was investigated by Perez, Booth, Denning, and

Hartley (12). It was shown that for "n" groups each spatial mode splits into "n" damped waves of the same frequency but with different phase shift and attenuation factors, and that the interaction of these waves presents the possibility for measurable resonance effects which are quite sensitive to the lattice parameters of the system. An attempt was made to demonstrate thermalization effects in moderators by the reflection of neutron waves by Denning, Booth, and Perez (13). In the experiment a sinusoidally modulated source of neutrons was placed at one face of a 26.7 cm. long graphite block with transverse buckling of 4.0×10^{-3} cm^{-2} which preceded a 62 cm. long heavy-water region of the same transverse area. Theoretical investigations indicated that if any reflection occurred at the graphite, heavy-water interface it would have to be caused by energy modes which propagate only when the energy dependence of the neutrons differs from a Maxwellian distribution. This was qualitatively confirmed by the experiment.

The propagation of thermal pulses was demonstrated by Hartley (14) and Miley and Doshi (15). Hartley produced thermal pulses of about one millisecond width by use of a neutron generator and thermalizing tank, recorded the pulses at various distances from the source, and compared the results in the time domain to a one-group diffusion theory model. An extension of the theory to that of Perez and

Uhrig met with severe difficulties when the inversion to the time domain of the complicated Laplace-transformed flux was encountered. The disagreement between the experiment and the one-group diffusion theory showed the sensitivity of the experiment to thermalization effects. Miley and Doshi used the TRIGA Reactor as a source and thermal pulses were produced of width ranging between 32 and 66 milliseconds. The measured asymptotic velocity of the pulse yielded a value of D_o; but because of the large pulse width (i.e., lack of high frequency content), the more interesting thermalization effects observed by Hartley were not detected. Diffusion theory was compared with the experiment, and corrections were made for the source distribution.

A method of comparing theory and experiment in the neutron wave experiment with pulsed, thermal sources was suggested by Moore (16) so that the inversion of the theory to the time domain (which proved so difficult for Hartley) would not be necessary. In essence, Moore suggested that comparisons be made in the frequency domain by numerically determining Fourier moments and widths of the data measured in the time domain. Fourier widths were defined and shown to be proportional to the derivatives with respect to frequency of the dispersion law of the medium. This theory was shown to be especially applicable when the fundamental solution of the dispersion law was expressed in the perturbation expansion introduced by Perez and Uhrig (9, 17).

Kunaish (18) used time, energy, and space dependent neutron thermalization theory in the consistent P_1 approximation to develop a theory for comparison with neutron wave and die-away experiments. The non-Maxwellian component of the energy dependence was expanded in a Taylor series, a heavy-gas scattering kernel was used, and the results provided an accurate description of the neutron wave experiment for source frequencies up to 500 cps.

CHAPTER III

THE BOLTZMANN EQUATION IN THE DIFFUSION APPROXIMATION WITHIN THE FRAMEWORK OF NEUTRON THERMALIZATION THEORY

Presentation of the Theoretical Model and the Method Used for Its Solution

Introduction

Placement of a sinusoidally modulated or pulsed source of thermal neutrons at one boundary of a moderating medium generates thermal neutron waves which propagate from the source with frequency and space dependent amplitude and phase. The positional variation of this frequency dependent thermal neutron flux is what one measures experimentally, and it will receive the principal emphasis in the theory which follows. Attention will be given to the space, energy, and time or frequency dependent thermal neutron flux in a moderating medium within the framework of neutron thermalization theory. The main objective will be to calculate the complex inverse relaxation length as a function of frequency for the fundamental space and energy mode.

The energy distribution of thermal neutrons in a finite moderating medium deviates from a Maxwellian distribution for several reasons. The preferential leakage of

higher energy neutrons from the assembly produces a "cooling" effect upon the spectrum, and the preferential absorption of slower neutrons causes a "hardening" effect. The prediction of this spectrum is further complicated by the thermal velocity of the scattering nuclei and the chemical binding and crystalline effects in the moderator.

The probability of a scattering interaction between neutrons and the moderator nuclei is expressed by the differential scattering cross section $\Sigma_s(E',E)$ for energy transfer from E' to E. It is the essential physical parameter in the thermal region, and the prediction of transient and asymptotic phenomena can be only as accurate as this scattering kernel. For this reason, care has been taken to select as accurate a scattering kernel as possible. The more accurate scattering kernels are much too complicated to be considered analytically; and when using them, one must employ numerical methods.

The Boltzmann Equation in the Diffusion Approximation

To investigate the effect of the energy spectrum upon thermal neutron wave propagation, one can use the Boltzmann equation in the diffusion approximation. For a finite, isotropic, homogeneous, and non-multiplying medium it is expressed as

$$\frac{1}{v}\frac{\partial\phi(\vec{r},E,t)}{\partial t} = D(E)\nabla^2\phi(\vec{r},E,t) - [\Sigma_s(E) + \Sigma_a(E)]\phi(\vec{r},E,t) +$$

$$+ \int_0^\infty \Sigma_s(E',E)\phi(r,E',t)dE' \qquad (1)$$

where

t = the time variable

$\vec{r}$ = the position vector

E = the energy variable

v = the speed variable

∇^2 = the Laplacian operator

$\phi(\vec{r},E,t)d\vec{r}dE$ = the total flux of neutrons at time t in the volume element $d\vec{r}$ about point $\vec{r}$ which have energies between E and E + dE (neutrons/cm^2/sec/ev.)

$\Sigma_a(E)\phi(\vec{r},E,t)dE$ = the total number of absorptions per unit volume about r and per unit time at time t due to neutrons with energy between E and E + dE

$\Sigma_s(E)\phi(\vec{r},E,t)dE$ = the total number of scattering collisions per unit volume about $\vec{r}$ and per unit time at time t due to neutrons with energy between E and E + dE

$\Sigma_s(E',E)\phi(\vec{r},E',t)dE'dE$ = the total number of scattering collisions per unit volume about $\vec{r}$ and per unit time at time t due to neutrons of initial energy between E' and E' + dE' and of final energy between E and E + dE

$D(E)$ = the energy dependent diffusion coefficient (cm.)

Within the diffusion approximation, D(E) is given by the expression

$$D(E) = \frac{1}{3[\Sigma_t(E) - \Sigma_{s1}(E)]} \qquad (2)$$

where

$$\Sigma_t(E) = \Sigma_s(E) + \Sigma_a(E) \tag{3}$$

and

$\Sigma_{s1}(E)$ = the second Legendre moment of the angular dependent scattering cross section

$$\Sigma_{s1}(E) = \int_{-1}^{1} \Omega\cdot\Omega'\Sigma_s(E,\Omega\cdot\Omega')d(\Omega\cdot\Omega')$$

From the definitions of $\Sigma_s(E)$ and $\Sigma_s(E',E)$ it is evident that

$$\Sigma_s(E) = \int_{0}^{\infty} \Sigma_s(E,E')dE' \tag{4}$$

In the experiment the source is placed near the exposed, z=0 face of a long rectangular stack of cadmium-covered moderator. Thus homogeneous boundary conditions can be applied at extrapolated boundaries of the x and y variables, the source condition is applied at z=0, and the flux can be specified to vanish at an infinite value for the z variable (i.e., end effects are considered negligible since measurements will not be made at the far end of the pile). Specifically, the boundary conditions that should be applied to equation (1) for the solution of this problem are

$$\phi(\mp a,y,z,E,t) = 0 \tag{5}$$

$$\phi(x, \mp b,z,E,t) = 0 \tag{6}$$

$$\phi(x,y,\infty,E,t) = 0 \tag{7}$$

and

$$-D(E) \frac{\partial^2}{\partial z^2} \phi(x,y,z,E,t)\Big|_{z=0} = 1/2\ S(x,y,E,t) \tag{8}$$

where $S(x,y,E,t)$ is the space, energy, and time dependent source of thermal neutrons.

Under these conditions, it will be advantageous to expand the flux in an orthogonal set of functions in the x and y variables. In view of the linear character of the problem and since our main interest is focused upon the frequency dependence of the flux, it can also be separated into a steady part(due to the constant component of the source) and an oscillatory part. Considering only the oscillatory component of the solution to equation (1), we can expand it in the form

$$\phi(\vec{r},E,t) = \mathrm{Re}\left[\sum_{\ell,m} \phi_{\ell,m}(x,y)\phi_{\ell,m}(z,E)\ \exp(j\omega t)\right] \tag{9}$$

where $\phi_{\ell,m}(x,y)$ satisfies the Helmholtz equation with homogeneous boundary conditions, which is expressed as

$$(\nabla^2_{x,y} + B^2_{\perp\ell,m})\ \phi_{\ell,m}(x,y) = 0 \tag{10}$$

with

$B^2_{\perp \ell,m}$ = the transverse buckling of the ℓ,m spatial mode and

$\nabla^2_{x,y}$ = the Laplacian operator for the x and y variables.

The substitution of equation (9) into equation (1) with the use of equation (10), multiplication of the result by $\phi_{p,k}(x,y)$, and integration over the x and y variables results in

$$\left[-D(E)B^2_{\perp p,k} - \Sigma_a(E) - \Sigma_s(E) + D(E)\frac{\partial^2}{\partial z^2} - \frac{j\omega}{v}\right]\phi_{p,k}(z,E) + \int_0^\infty \Sigma_s(E',E)\phi_{p,k}(z,E')dE' = 0 \qquad (11)$$

In the experiment, one would like to measure only the fundamental spatial mode so it is of major concern in the theory. Since the equations for the various spatial modes differ only by the magnitude of the transverse buckling, one can, without serious loss in generality, remove the subscripts. The symbols $B^2_\perp$ and $\phi(z,E)$ are now understood to represent the transverse buckling and the flux associated with the fundamental spatial mode, respectively. It is also convenient at this point to express equation (11) in a more compact, operator formalism by use of the substitution*

---

* The author wishes to express his thanks to Dr. Frank J. Munno for helpful discussions in connection with this substitution.

$$\phi(z,E) = \frac{\chi(E,z)\sqrt{vM(E)}}{\sqrt{D(E)}} \tag{12}$$

where M(E), the Maxwellian distribution, is expressed as

$$M(E) = C(E/kT)^{1/2} \exp(-E/kT) \tag{13}$$

By substituting equation (12) into equation (11) and dividing the result by $\sqrt{vM(E)D(E)}$, one obtains

$$\left[-B_{\perp}^2 - \frac{\Sigma_a(E)}{D(E)} - \frac{\Sigma_s(E)}{D(E)} + \frac{\partial^2}{\partial z^2} - \frac{j\omega}{vD(E)}\right]\chi(z,E) + \int_0^{\infty} \frac{\Sigma_s(E',E)\chi(z,E')\sqrt{v'M(E')}}{\sqrt{vM(E)}\sqrt{D(E')}\sqrt{D(E)}}\,dE' = 0 \tag{14}$$

or

$$\left[-B_{\perp}^2 + \frac{\partial^2}{\partial z^2} - \frac{j\omega}{vD(E)}\right]\chi(z,E) + \underline{P}\chi(z,E) = 0 \tag{15}$$

where

$$\underline{P}\chi(z,E) = \int_0^{\infty} dE' \left\{ \frac{\Sigma_s(E',E)\sqrt{v'M(E')}}{\sqrt{vM(E)}\sqrt{D(E')}\sqrt{D(E)}} - \delta(E'-E)\left[\frac{\Sigma_a(E)}{D(E)} + \frac{\Sigma_s(E)}{D(E)}\right]\right\} \chi(z,E') \tag{16}$$

Solution of the Eigenvalue Problem Associated with the Space and Energy Dependent Boltzmann Operator

It is instructive to consider equation (15) for the case when the transverse leakage and frequency of excitation are both zero (i.e., a semi-infinite plane with a constant source). The incentive for this deviation comes from the work of Ohanian (19) and Ohanian and Daitch (20) in their theoretical investigation of the die-away experiment. We shall assume that the solution to the equation thus formed may be written as

$$\chi(z,E) = \sum_{n=1}^{\infty} a_n \psi_n(E) \exp[-\rho_{no} z] \tag{17}$$

with the understanding that the above expansion is convergent only if the $\psi_n(E)$ form a complete set. Substitution of the above expansion into equation (15) with both $B_\perp^2$ and ω equal to zero results in

$$-\sum_{n=1}^{\infty} a_n \rho_{no}^2 \psi_n(E) \exp(-\rho_{no} z) = \sum_{n=1}^{\infty} \underline{P} a_n \psi_n(E) \exp(-\rho_{no} z) \tag{18}$$

If the initial assumption of completeness is correct, the $\psi_n(E)$ will be linearly independent. Therefore, equation (18) must hold separately for each value of "n" and reduces to

$$-\rho_{no}^2 \psi_n(E) = \underline{P} \psi_n(E) \tag{19}$$

Thus ρ_{no}^2 and $\psi_n(E)$ are the eigenvalues and corresponding eigenfunctions of the $\underline{P}$ operator. An inspection of this

operator with reference to the principle of detailed balance,

$$v'\Sigma_s(E',E)M(E')dE'dE = v\Sigma_s(E,E')M(E)dEdE' \tag{20}$$

reveals that it is both real and symmetric. Thus its eigenfunctions must be real, satisfy the orthogonality condition,

$$\int_0^\infty \psi_n(E)\psi_m(E)dE = 0 \qquad \text{for } n \neq m, \tag{21}$$

and be linearly independent (21). This latter characteristic assures that the expansion expressed by equation (17) and the subsequent manipulations were valid.

The facility of the substitution expressed by equation (12) and of the investigation of the semi-infinite, zero-frequency problem now becomes evident. If one expands the energy dependence of equation (15) in terms of the eigenfunctions obtained above, equation (19) can be used to exchange for the complicated $\underline{P}\psi_n(E)$ expression its simple equivalent $-\rho_{no}^2\psi_n(E)$. Thus the solution of equation (15) by this method is not directly complicated by the consideration of realistic and therefore involved energy exchange kernels since more difficult kernels simply result in different eigenfunctions for use in the expansion. Or, expressed differently, the complicated characteristics of the energy exchange kernel are carried to the solution of equation (15) by the eigenfunctions and eigenvalues obtained from the $\underline{P}$

operator.* Moreover, the homogeneous equations and secular determinant resulting from the above mentioned expansion will be much simpler than that obtained by using other orthogonal functions which do not bear as close a relationship to the actual solution.

The eigenfunctions and their corresponding eigenvalues also have physical significance. They are the thermalization theory solution to the exponential experiment in a semi-infinite plane. The $\psi_1(E)$ function is the fundamental energy mode which is exponentially attenuated with distance from the source, and its corresponding eigenvalue is the square of the asymptotic inverse relaxation length. The one-group diffusion theory equivalent to this eigenvalue is $1/L^2$. Thus $\psi_n(E)$ and ρ_{no}^2 represent, respectively, the eigenfunctions and eigenvalues of the space and energy dependent Boltzmann operator and are what one encounters when performing the exponential experiment in a very large moderating medium. More important physical significance can be assigned to these eigenvalues in the context of this work when one recalls that the exponential experiment can be considered a neutron wave experiment

---

* This argument is based upon the assumption that the difficulty involved in the solution to the eigenvalue problem is not dependent upon the complexity of the scattering kernel. This is, in general, the case since, as explained in the second part of this chapter, a discrete energy representation of the eigenvalue problem is solved on a computer. Thus more involved scattering kernels simply result in different numbers being read as input to the code.

performed at zero frequency. From this viewpoint it becomes apparent that the ρ_{no}^2 are the zero intercepts of the squared complex inverse relaxation lengths plotted as a function of frequency. A knowledge of these zero intercepts is useful because their closeness to the fundamental eigenvalue is quite indicative of the amount of higher-energy-mode contamination predicted by the particular scattering kernel under investigation.

Further insight into the nature of these eigenfunctions and eigenvalues can be obtained by a more detailed investigation of the eigenvalue problem represented by equation (19). With the $\underline{P}$ operator explicitly expressed and some terms rearranged, equation (19) becomes

$$\left[\frac{\Sigma_a(E) + \Sigma_s(E)}{D(E)} - \rho_{no}^2\right]\psi_n(E) = \int_0^\infty \frac{\Sigma_s(E',E)\sqrt{v'M(E')}}{\sqrt{vM(E)}\sqrt{D(E)}\sqrt{D(E')}}\psi_n(E')dE' \tag{22}$$

For the special case in which $\Sigma_a(E) = 0$, the lowest eigenvalue is zero and its corresponding eigenfunction is $\sqrt{vM(E)D(E)}$; which is easily verified by direct substitution and by use of the principle of detailed balance. This is consistent with the fact that in an infinite medium with no absorption the flux will attain an equilibrium Maxwellian distribution in energy and a constant value in space. From the arrangement of equation (22) it is evident that it will be satisfied by two types of solutions:

1. $\rho_{no}^2 \neq \Sigma_t(E)/D(E)$ for any value of E. This results in discrete eigenvalues and the more common continuous eigenfunctions as solutions.

2. $\rho_{no}^2 = \Sigma_t(E)/D(E)$. In this case the expression enclosed in brackets is zero. The right-hand side of equation (22) is not necessarily zero, however, so that if the eigenfunctions are to satisfy the equation in this circumstance they must exhibit in part a singular behavior. Moreover, condition (2) can be satisfied for any value of the continuous variable E under the condition $\rho_{no}^2 \geq [\Sigma_t(E)/D(E)]_{MIN}$. Thus above this limit point a continuous eigenvalue spectrum is obtained.

Expansion of the Frequency Dependent Equation in Eigenfunctions of the Space and Energy Dependent Boltzmann Operator

The energy dependence of the flux can now be developed in terms of the eigenfunctions mentioned above. An exponential dependence upon the z variable will be assumed so that the solution to equation (15) can be expressed in the form

$$\chi(z,E) = \sum_{n=1}^{\infty} A_n \psi_n(E) \exp(-\rho z) \quad * \qquad (23)$$

---

* A more rigorous expression for this expansion would be

$$\chi(z,E) = \sum_{n=1}^{N} \{A_n^{(d)} \psi_n^{(d)}(E) + \int_{[\Sigma_t(E)/D(E)]_{MIN}}^{\infty} A^{(c)}(\rho_o^2) \psi^{(c)}(E,\rho_o^2) d\rho_o^2\} \exp[-\rho z]$$

where the $\psi_n(E)$ satisfy the eigenvalue equation, and they have been normalized so that

$$\int_0^\infty \psi_n(E)\psi_m(E)dE = \delta_{mn} \tag{24}$$

Substitution of equation (23) into equation (15) results in

$$\sum_{n=1}^{\infty} \left[-B_\perp^2 + \rho^2 - \frac{j\omega}{vD(E)}\right] A_n(\exp[-\rho z])\psi_n(E) +$$

$$+ \sum_{n=1}^{\infty} A_n(\exp[-\rho z])\underline{P}\psi_n(E) = 0 \tag{25}$$

which, when multiplied by $\psi_m(E)$ and integrated over all energy, yields

$$\sum_{n=1}^{\infty} [(\rho^2 - B_\perp^2 - \rho_{no}^2)\delta_{mn} - L_{mn}j\omega]A_n = 0$$

$$m = 1,2,3,\cdots \tag{26}$$

---

where the superscripts "d" and "c" represent, respectively, the discrete and continuum sets. However, in the actual solution a discrete energy formalism is used and calculations are performed only at a finite number of discrete energy values. Eigenvalues in the continuum, which actually are a function of energy, and their corresponding eigenfunctions are obtained only at particular energy points. Thus equation (23) correctly expresses the actual expansion used, which is the discrete approximation to the more rigorous and less convenient representation.

where use has been made of equations (19) and (24) and

$$L_{mn} = \int_0^\infty \psi_m(E) \, [1/vD(E)] \, \psi_n(E) dE \tag{27}$$

Equation (26) expresses in a compact form a set of linear, homogeneous, algebraic equations for the modal amplitudes A_n and the eigenvalues ρ^2. One is able to solve the set only for the relative magnitudes of the A_n, and the number of eigenvalues which allow a solution will be equal to the number of equations considered. Also there will be a different set of ratios for each eigenvalue. The compatibility condition for the above set of homogeneous equations yields the secular determinant or dispersion law

$$\left| (B^2 - \rho_{no}^2)\delta_{mn} - j\omega L_{mn} \right| = 0 \tag{28}$$

with

$$B^2 = \rho^2 - B_\perp^2 \tag{29}$$

which can be used to determine the complex eigenvalues that will allow solutions for equation (26). These eigenvalues are the squared complex inverse relaxation lengths which are to be compared with the experiment. It is satisfying to note that for $\omega=0$ the secular determinant, equation (28), reduces to a diagonal determinant yielding the ρ_{no}^2 for the B^2 eigenvalues.

Determination of the Fundamental Complex Inverse Relaxation Length from the Complex Homogeneous Equations

The perturbation method developed by Perez and Uhrig (9) and systematized by Kunaish (18) will be used to develop each of the eigenvalues and modal amplitudes in a power series expansion of the frequency variable. This power series representation is used because it allows one to compare very easily various theoretical models with one another and with the experimental results. Once the coefficients are calculated, the eigenvalue can be determined for any frequency within the radius of convergence of the series. To initiate this expansion, the first equation and the first term of each of the other equations in the homogeneous set represented by equation (26) are explicitly expressed. Considering the first "N" equations of this set, one obtains

$$(B^2 - \rho_{10}^2) - L_{11}j\omega - \sum_{n=2}^{N} L_{1n}j\omega S_n = 0 \qquad \text{for } m = 1 \tag{30}$$

$$-L_{m1}j\omega - \sum_{n=2}^{N} \{(B^2 - \rho_{no}^2)\delta_{mn} - L_{mn}j\omega\} S_n = 0 \qquad \text{for } m = 2,3,4,\cdots \tag{31}$$

where each equation has been divided by A_1 so that the set could be solved for the ratios

$$S_n = A_n/A_1 \qquad n = 2,3,4,\cdots \tag{32}$$

and for the eigenvalue B^2. In this method, B^2 and each of its corresponding ratios, S_n, are expanded in a Maclaurin's series. Thus we let

$$B^2 = \sum_{K=0}^{I} \frac{B^{(K)}(j\omega)^K}{K!} \tag{33}$$

and

$$S_n = \sum_{K=0}^{I} \frac{S_n^{(K)}(j\omega)^K}{K!} \tag{34}$$

where

$$B^{(K)} = \frac{\partial^K}{\partial^K j\omega} B^2\Big|_{j\omega=0} \tag{35}$$

and

$$S_n^{(K)} = \frac{\partial^K}{\partial^K j\omega} S_n\Big|_{j\omega=0} \tag{36}$$

The Kth coefficient of B^2 and those of each of the S_n are obtained from equations (30) and (31), respectively, after differentiating them "K" times with respect to $j\omega$ and setting $j\omega$ equal to zero.

It should be emphasized at this point that we are presently expanding only the fundamental eigenvalue along with its corresponding ratios. However, it will be shown that the other N-1 eigenvalues and their ratios are obtained in exactly the same way after rearranging the initial equations and redefining some terms.

By letting $j\omega=0$ in equation (30) and equation (31), it can easily be determined that

$$B^{(0)} = \rho_{10}^2 \tag{37}$$

and

$$S_n^{(0)} = 0 \qquad n = 2,3,4,\cdots \tag{38}$$

Using the identity

$$\frac{\partial^I}{\partial x^I}[A(x)B(x)] = \sum_{K=0}^{I} \binom{I}{K} A^K(x)B^{(I-K)}(x) \tag{39}$$

where

$$\binom{I}{K} = \frac{I!}{K!(I-K)!} \tag{40}$$

one can differentiate equation (30) and equation (31) "I" times to obtain at $j\omega=0$

$$B^{(I)} - \rho_{10}^2\delta_{I0} - L_{11}\delta_{I1} - u(I-2)\sum_{K=0}^{I}\sum_{n=2}^{I}\binom{I}{K} L_{1n}\delta_{K1}S_n^{(I-K)}=0 \tag{41}$$

$$- L_{m1}\delta_{I1} + \sum_{n=2}^{N} \sum_{K=0}^{I} \binom{I}{K} \{(B^{(K)} - \rho_{no}^2 \delta_{K0})\delta_{mn} - L_{mn}\delta_{K1}\} S_n^{(I-K)} = 0$$

$$m = 2,3,4,\cdots \qquad (42)$$

where u(I-2) is the unit-step function. By evaluating the summation over "K" in equation (41) and rearranging terms, one obtains

$$B^{(I)} = \rho_{10}^2 \delta_{I0} + L_{11}\delta_{I1} + u(I-2) \sum_{n=2}^{N} \binom{I}{1} L_{1n} S_n^{(I-1)} \qquad (43)$$

which can be used to determine each $B^{(I)}$ if the $S_n^{(I-1)}$ are known. Equation (42) can be simplified by separating out from the rest of the series in the "K" summation the terms for which K=0 and K=1. By performing this manipulation, extracting the $S_m^{(I)}$ coefficient from the term for which K=0, and rearranging terms, an expression for the $S_m^{(I)}$ ratios is obtained

$$S_m^{(I)} = \frac{L_{m1}\delta_{I1} - u(I-2) \sum_{n=2}^{N} \binom{I}{1} (B^{(1)}\delta_{mn} - L_{mn}) S_n^{(I-1)}}{(\rho_{mo}^2 - \rho_{10}^2)} -$$

$$- \frac{u(I-3) \sum_{n=2}^{N} \sum_{K=2}^{I-1} \binom{I}{K} B^{(K)} S_n^{(I-K)}}{(\rho_{mo}^2 - \rho_{10}^2)} \quad ; \qquad m = 2,3,4,\cdots \tag{44}$$

The summation over "K" in the above expression is extended only to "I-1" since $S_m^{(0)}$ is zero, and the step functions are introduced because some terms were extracted from the summations.

The procedure used for evaluating the $B^{(I)}$ and $S_m^{(I)}$ is initiated by first determining $B^{(1)}$ and $S_m^{(1)}$ from equations (43) and (44), respectively. Knowing these terms, $B^{(2)}$ can be calculated from equation (43) and placed in equation (44) in order to find the $S_m^{(2)}$. This process of alternately using the two expressions to first calculate $B^{(I)}$ then $S_m^{(I)}$ when all the $B^{(J)}$ and $S_m^{(J)}$ are known for $J<I$ can be repeated to determine as many terms as one needs. Then using the $B^{(I)}$ in equation (33), the frequency dependent complex inverse relaxation length for the fundamental mode can be evaluated.

It may happen, however, that the series does not converge very rapidly. In fact, this is the case for one of the scattering kernels selected. For this situation, a more convenient series can be obtained by a change of variable of the form

$$j\omega = j\chi e^{\chi} \tag{45}$$

One can then derive a power series expansion for B^2 in terms of χ. Recognizing that

$$\frac{d^n}{d\chi^n} (j\chi e^{\chi})\Big|_{\chi=0} = jn \tag{46}$$

andusing the procedure as explained with the ω expansion, one can obtain expressions for the $B^{(I)}$ and the $S_m^{(I)}$ for the power series expansions in the χ variable. As in the ω expansion

$$B^{(0)} = \rho_{10}^2 \tag{47}$$

and all of the $S_m^{(0)}$ are zero. For I = 1, one finds

$$B^{(1)} = jL_{11} \tag{48}$$

$$S_m^{(1)} = jL_{m1}/(\rho_{mo}^2 - \rho_{10}^2) \qquad m = 2,3,4,\cdots \tag{49}$$

and, in general, for $I \geq 2$

$$B^{(I)} = jIL_{11} - \sum_{n=2}^{N} \sum_{K=1}^{I-1} \binom{I}{K} jKL_{1n} S_n^{(I-K)} \tag{50}$$

and

$$S_m^{(I)} = \frac{jIL_{m1} - \sum_{K=1}^{I-1} \binom{I}{K} B^{(K)} S_m^{(I-K)} + \sum_{n=2}^{N} \sum_{K=1}^{I-1} \binom{I}{K} jKL_{mn} S_n^{(I-K)}}{(\rho_{mo}^2 - \rho_{10}^2)}$$

$$m = 2,3,4,\cdots \qquad (51)$$

In the determination of ρ^2 as a function of frequency, both of these power series expansions will be used.

An alternative to the series representation is to solve the complex secular determinant directly for several values of ω. For reasons previously discussed, this method is not as appealing as the ones derived above; and it will be used only as a last resort, that is, for cases in which both of the series converge slowly or not at all.

Determination of the Higher Order Complex Inverse Relaxation Lengths

It was stated that the equations obtained for the $B^{(I)}$ and the $S_m^{(I)}$ were derived to evaluate only the fundamental ρ^2. To calculate the other eigenvalues, one can rearrange the equations expressed by equation (26) so that the same expressions can be used to calculate coefficients associated with all of the eigenvalues. To explain this procedure, consider the case where m=3 in equation (26). Allowing n to range from one to three, one obtains

$$[(\rho^2 - B_\perp^2 - \rho_{10}^2) - L_{11}j\omega]A_1 - L_{12}j\omega A_2 - L_{13}j\omega A_3 = 0 \tag{52}$$

$$- L_{21}j\omega A_1 + [(\rho^2 - B_\perp^2 - \rho_{20}^2) - L_{22}j\omega]A_2 - L_{23}j\omega A_3 = 0 \tag{53}$$

$$- L_{31}j\omega A_1 - L_{32}j\omega A_2 - [(\rho^2 - B_\perp^2 - \rho_{30}^2) - L_{33}j\omega]A_3 = 0 \tag{54}$$

Let us specify that the eigenvalue associated with the second equation is desired (i.e., the eigenvalue whose zero intercept is $\rho_{20}^2 + B_\perp^2$). If we exchange equations (53) and (52) and rearrange terms in each of the equations, the result is

$$[(\rho^2 - B_\perp^2 - \rho_{20}^2) - L_{22}j\omega]A_2 - L_{21}j\omega A_1 - L_{23}j\omega A_3 = 0 \tag{55}$$

$$- L_{12}j\omega A_2 + [\rho^2 - B_\perp^2 - \rho_{10}^2) - L_{11}j\omega]A_1 - L_{13}j\omega A_3 = 0 \tag{56}$$

$$- L_{32}j\ A_2 - L_{31}j\omega A_1 - [(\rho^2 - B_\perp^2 - \rho_{30}^2) - L_{33}j\omega]A_3 = 0 \tag{57}$$

An inspection of these last three equations and the ones from which they were derived indicates that both sets are of exactly the same form since they differ only in subscripts. Thus the same expressions used for the solution of the fundamental eigenvalue are also valid for the second

if care is taken to correctly rearrange the L_{mn} and ρ_{no}^2 matrix elements and to assign subscripts to them corresponding to their new positions before applying the equations. By analogy, the arrangement of terms for calculating the nth eigenvalue and its ratios is obtained by exchanging the first and the nth equations and then exchanging the first and n^{th} terms in all of the equations.

Numerical Calculations Associated with the Theory

Introduction

The derivations thus far presented are founded upon the theoretical formalizations of Perez and Uhrig (9) and Ohanian and Daitch (20). The work of the former authors indicated the method by which, beginning with the Boltzmann equation in the diffusion approximation, one could formulate a power series expansion for the complex inverse relaxation length. They used Associated Laguerre Polynomials in expanding the energy dependence, whereas here the eigenfunctions of the space and energy dependent Boltzmann operator form the orthogonal functions for this expansion. This more elegant method has practical value since the secular determinant used to determine the eigenvalues, B_n^2, has a much simpler form and one need not calculate the complicated matrix elements of the scattering operator. As a by-product of this method, one obtains all of the zero intercepts of the B_n^2 (i.e., ρ_{no}^2).

For the determination of the B_n^2 and their corresponding eigenfunctions, use was made of the numerical techniques developed by Ohanian for his calculation of the eigenfunctions of the time and energy dependent Boltzmann operator. In fact, after minor modification, several of the computer codes developed by Ohanian were used in this work.

Evaluation of the Eigenvalues and Eigenfunctions of the Space and Energy Dependent Boltzmann Operator in the Diffusion Approximation

The Discrete Energy Formulation of the Eigenvalue Problem -- In the discrete energy representation, equation (15) becomes a set of "J" equations of the form

$$-\rho_{no}^2\psi_n(E_i) = \sum_{j=1}^{J}{}' K(E_j,E_i)\psi_n(E_j)\Delta E_j - \left[\frac{\Sigma_a(E_i)}{D(E_i)} + \frac{\Sigma_s(E_i)}{D(E_i)}\right]\psi_n(E_i)$$

$$i = 1,2,3,\cdots,J \qquad (58)$$

where

$$K(E_j,E_i) = \frac{\Sigma_s(E_j,E_i)\sqrt{v_j M(E_j)}}{\sqrt{v_i M(E_i)}\sqrt{D(E_j)}\sqrt{D(E_i)}} \qquad (59)$$

$$\Sigma_s(E_i) = \sum_{\ell=1}^{J}{}' \Sigma_s(E_i,E_\ell)\Delta E_\ell \qquad (60)$$

ΔE_j depends upon the numerical integration scheme selected, "J" is equal to the number of energy points, and the prime on the summation indicates that the term involving $\Sigma_s(E_i,E_i)$ has been eliminated from the summation in the interest of greater numerical accuracy (19). An inspection of the above equations with all terms included reveals that for i=j the term $\Sigma_s(E_i,E_i)$ in the j summation in equation (58) should be canceled by an identical term in the expression $\frac{\Sigma_s(E_i)}{D(E_i)}$. It was determined by Ohanian that greater accuracy could be achieved by elimination of these terms altogether before introducing equation (58) into the computer. This is a very fortunate development since, as explained later in this section, it was necessary to adjust the diagonal elements of the scattering kernel calculated by the SUMMIT code. Since the diagonal elements are not needed in this numerical solution to the eigenvalue equation, this modification should not have any direct influence upon that solution.

The set of equations represented by equation (58) can be more simply expressed as

$$-\rho_{no}^2(\psi_n) = (\underline{P})(\Delta E)(\psi_n) \qquad (61)$$

where

(ψ_n) is a column vector composed of the values of the ψ_n eigenfunctions at each of the j energy points,

(ΔE) is a diagonal matrix containing the weights for the numerical integration,

and

($\underline{P}$) is a square matrix representing the $\underline{P}$ operator.

The elements of the ($\underline{P}$) matrix are given by the expression

$$P_{ij} = K(E_j,E_i)(1 - \delta_{ij}) - \frac{\delta_{ij}}{\Delta E_j}\left[\frac{\sum_{\ell=1}^{J'} \Sigma_s(E_i,E_\ell)\Delta E_\ell}{D(E_i)} + \frac{\Sigma_a(E_i)}{D(E_i)}\right] \tag{62}$$

We have now arrived at the equation which is to be solved by the EIGENVALUE code. Note that the symmetry of the $\underline{P}$ operator is preserved in the discrete representation and that since (ΔE) is simply a diagonal matrix to provide weighting for the integration the numerical eigenvalue problem also contains a symmetric operator.

Evaluation of the Scattering Kernel and Formulation of the Symmetrized P Operator -- All of the theoretical calculations were performed on an IBM 709 digital computer. In essence, the implementation of the theory derived in the preceding section was accomplished through the use of an echelon of computer codes, beginning with one which calculated the scattering kernel and ending with the EIGENVALUE code. Each code made use of the results of one or more of its predecessors and, in turn, contributed to the codes farther on in the chain. The format for the discussion in

this section can therefore be logically based upon the flow diagram shown in Figure 1.* In the discussion which follows, pertinent information pertaining to the computational methods will be presented. For a complete discussion of the workings and input-output information for the computer codes used the reader is referred to the reports submitted by the author to his committee supervisor.

One of the more important considerations in the implementation of this numerical method was the determination of what variable to use in order to most advantageously express the energy dependence. This problem was solved by Ohanian (19) by the use of a variable defined as

$$\eta = (E/KT)^{1/2} / (1 + (E/KT)^{1/2}) \qquad (63)$$

The 33 energy points, corresponding to 32 equally spaced increments of the η variable, that he used were adopted for this work and are listed in Table 1. Also shown in the table are the $D(E_i)$ as obtained by the use of SUMMIT, PINNACLE, and DIAGONAL CORRECTOR codes. For the numerical integrations encountered, except those in SUMMIT and

---

* This computation was done under the direct supervision of Dr. M. J. Ohanian, with initial inspiration from Dr. R. B. Perez. The author is grateful to Robert B. Razminas for the use of his DIAGONAL CORRECTOR CODE and for his contribution to the matching of several of the codes.

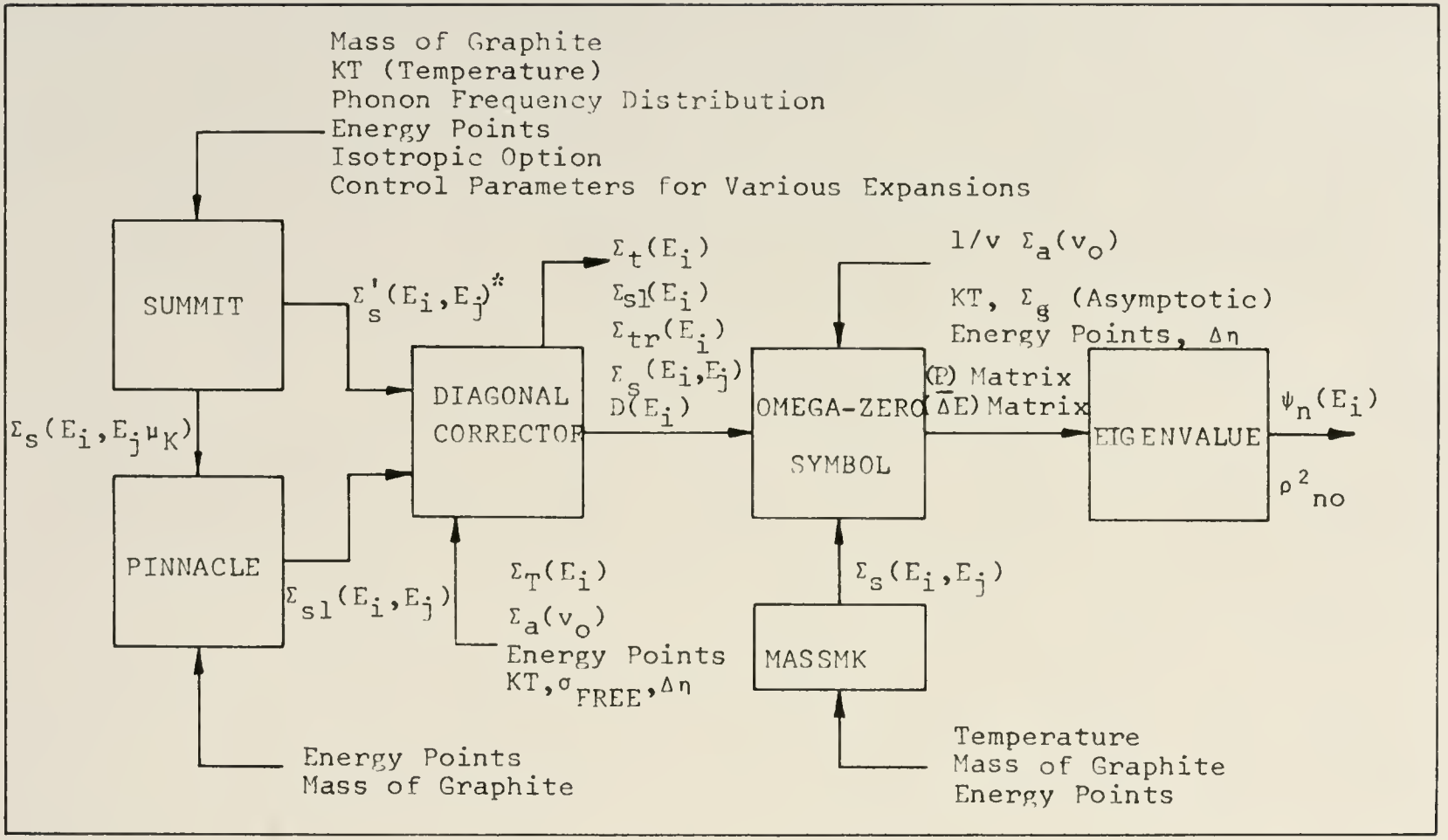

* Diagonal elements from SUMMIT were not complete.

Fig. 1. Flow Diagram of Several of the Computer Codes Used in the Theory.

TABLE I

THE ENERGY POINTS USED IN THE DISCRETE ENERGY REPRESENTATION AND THE CALCULATED VALUES OF THE DIFFUSION COEFFICIENT AT THESE POINTS

ENERGY POINTS (EV.)	DIFFUSION COEF. (CM.)
0.19489899E-04	0.90540472E 00
0.82478099E-04	0.16644209E 01
0.19665200E-03	0.28357907E 01
0.37111399E-03	0.38656164E 01
0.61667299E-03	0.50007596E 01
0.94622400E-03	0.61531631E 01
0.13752100E-02	0.77092278E 01
0.19221999E-02	0.51939103E 00
0.26096600E-02	0.70397882E 00
0.34648699E-02	0.94295391E 00
0.45211899E-02	0.12733748E 01
0.58196499E-02	0.96080945E 00
0.74110299E-02	0.95736114E 00
0.93586800E-02	0.91105106E 00
0.11742199E-01	0.11272739E 01
0.14662799E-01	0.10718941E 01
0.18249500E-01	0.81394893E 00
0.22669999E-01	0.79333499E 00
0.28143399E-01	0.84320298E 00
0.34960400E-01	0.82992154E 00
0.43512300E-01	0.82778580E 00
0.54334600E-01	0.80977708E 00
0.68173099E-01	0.77186675E 00
0.86089300E-01	0.78670610E 00
0.10963000E-00	0.79197136E 00
0.14111499E-00	0.77184059E 00
0.18413600E-00	0.78138231E 00
0.24448000E-00	0.76182067E 00
0.33191600E-00	0.78947944E 00
0.46393500E-00	0.91681817E 00
0.67426600E 00	0.96415816E 00
0.10345899E 01	0.14859277E 02
0.17191599E 01	0.15770610E 01

PINNACLE, Simpson's rule was used since most of the functions to be integrated were generally smooth. Comparatively few quantities were needed as input parameters, and the more important ones are listed in Table 2.

Figure 1 shows the sequence of the numerical calculations and the input and output of each code in the chain. For the first task, that of calculating the scattering kernel, two different models were used. The first, and more realistic, kernel was formulated by Parks (22,23) and incorporated by Bell (24) into a computer code called SUMMIT. The P_1 kernel was calculated from the output of SUMMIT by the PINNACLE code. The code multiplied the angular dependent scattering kernel from SUMMIT by the cosine of the scattering angle, performed a Gaussian integration over the angle, and multiplied the result by an appropriate energy dependent factor. The second scattering kernel considered was a free-gas energy-exchange kernel obtained by the use of the MASSMK code (25). Note that the calculations involving the MASSMK kernel differed from those of the SUMMIT code only by the scattering kernel $\Sigma_s(E_i,E_j)$. All other inputs to the OMEGA-ZERO SYMBOL via DIAGONAL CORRECTOR (26) were the same as those obtained from the SUMMIT kernel.

The scattering kernel calculated by SUMMIT does not include the elastic contribution. For this reason, it was necessary to correct the diagonal elements of this kernel so that the scattering cross sections obtained from it were consistent with values taken from the "barn book" (BNL-325).

TABLE 2

PARAMETERS USED IN THE NUMERICAL CALCULATIONS

Parameter	Value	Units
Mass of Graphite	12.011	amu.
α_o	90.04	sec^{-1}
v_o	2.198×10^5	cm/sec
N (number density)	0.0803	n/cm^3.
kT	0.02526	ev.
$\Delta\eta$	0.027027	----
σ_s FREE	4.6949	barns

This was accomplished in the DIAGONAL CORRECTOR code. As shown in Figure 1, several other quantities were also obtained from this code. The (P) matrix was calculated using the OMEGA-ZERO SYMBOL code. This code was obtained by modifying the SYMBOL code written by Ohanian to account for the differences between the (P) matrix of equation (62) and the one obtained by him for his eigenvalue problem.

The eigenvalues and eigenfunctions of the space and energy dependent Boltzmann operator were computed by the EIGENVALUE code using the Jacobi method of matrix diagonalization (Appendix A of reference (19)). This was not the same code as used by Ohanian but it was similar to it.* The code used in this work was modified to accept the diagonalization when the smallest diagonal element became more than 10^{16} greater than the largest off-diagonal element.

Presentation of the Eigenfunctions and Eigenvalues -- Several of the eigenfunctions and all of the eigenvalues computed by the method outlined above are presented, respectively, in Figure 2 and Table 3 for the SUMMIT kernel and Figure 3 and Table 3 for the MASSMK kernel. Some problems were encountered in drawing the eigenfunctions

---

* The code was obtained by Dr. Ohanian and converted for use on the University of Florida IBM 709 computer by the author.

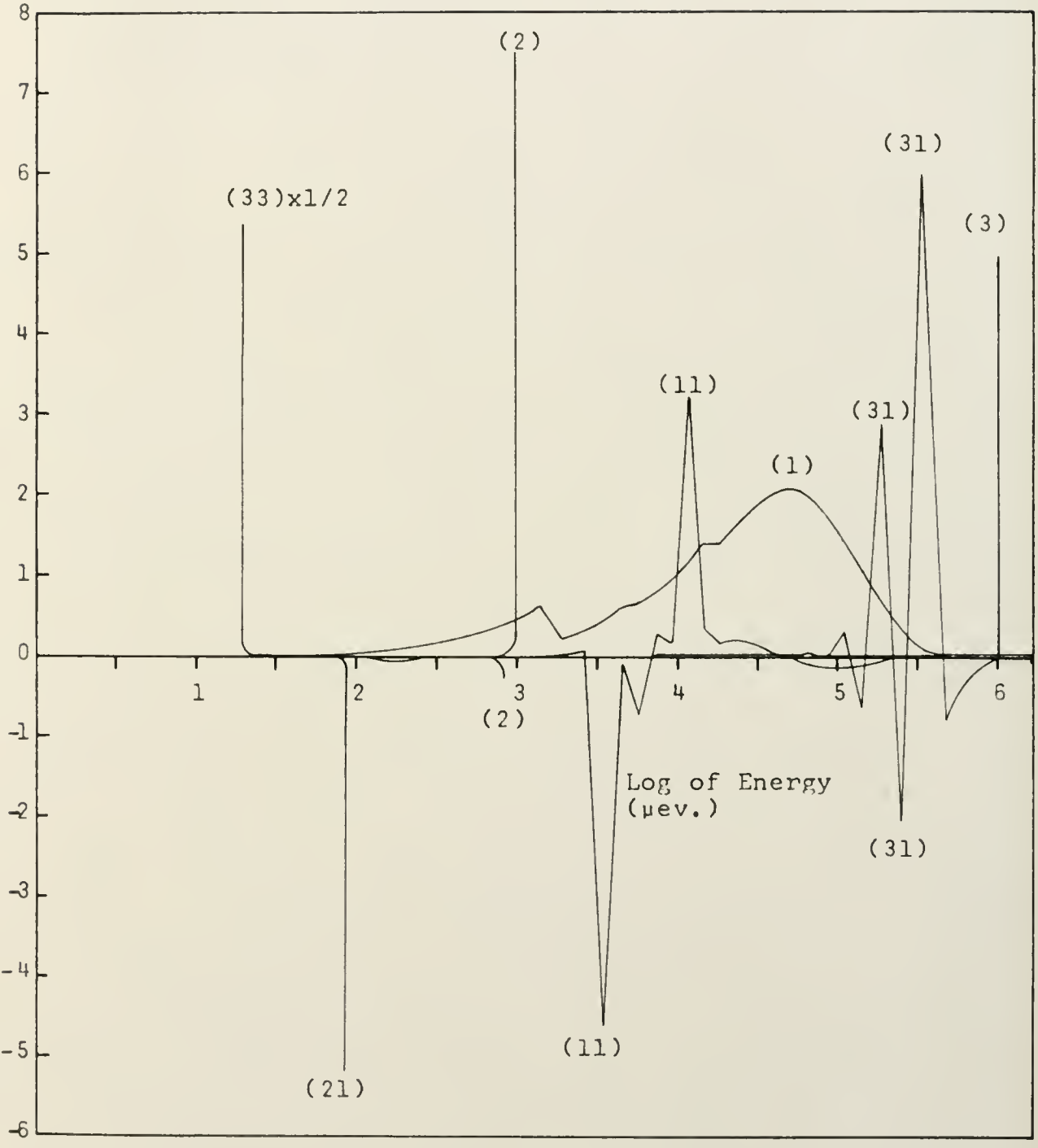

ig. 2. Several Eigenfunctions of the Space and Energy Dependent Boltzmann Operator Using the SUMMIT Kernel.

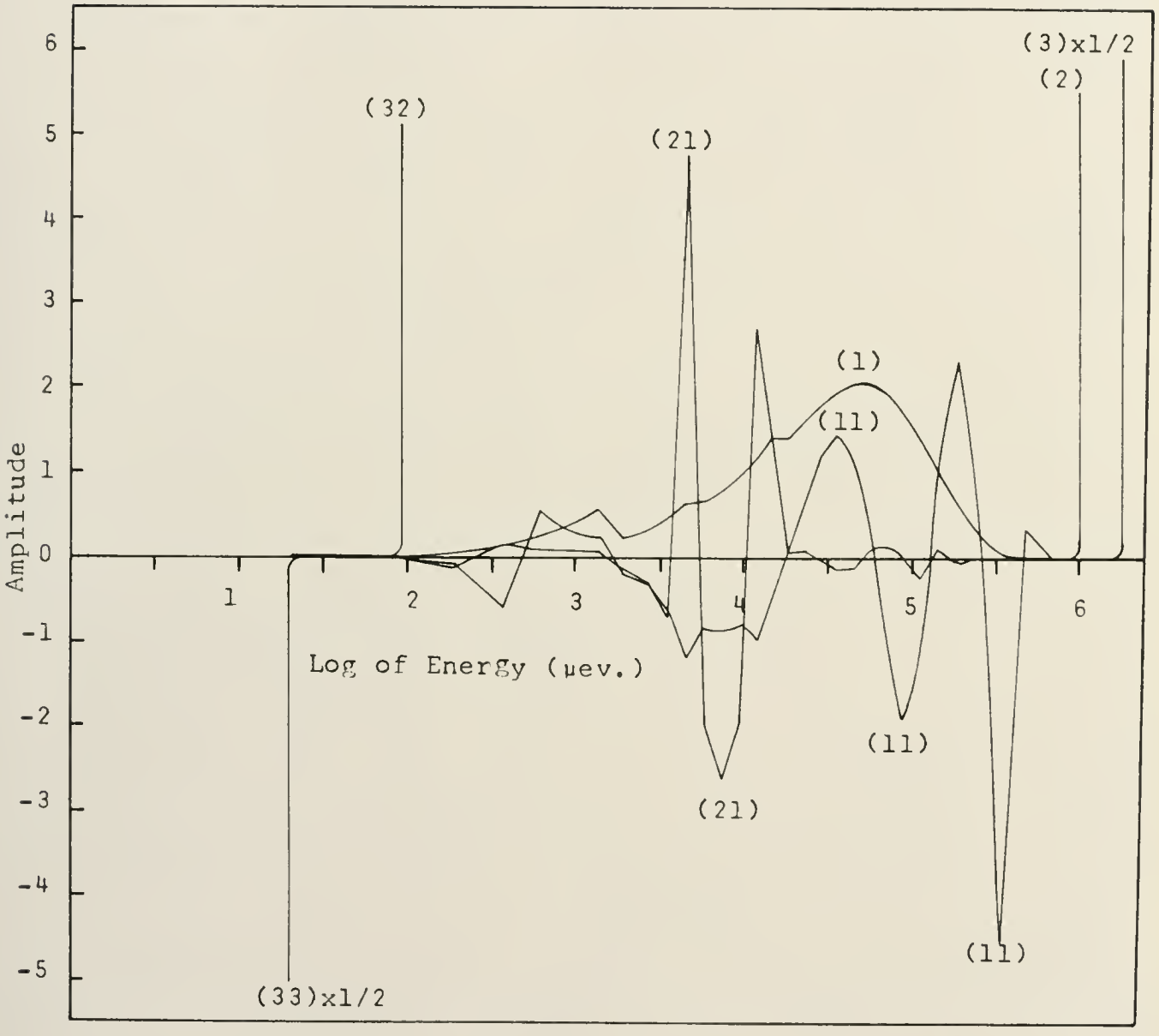

Fig. 3. Several Eigenfunctions of the Space and Energy Dependent Boltzmann Operator Using the MASSMK Kernel.

TABLE 3

EIGENVALUES OF THE SPACE AND ENERGY DEPENDENT BOLTZMANN OPERATOR USING THE SUMMIT KERNEL AND THE MASSMK KERNEL

SUMMIT	MASSMK
0.42844241E-03	0.42994279E-03
0.30875468E-02	0.30594949E-02
0.37078650E-02	0.14320712E-01
0.44850244E-02	0.63025152E-01
0.65955998E-02	0.80414867E-01
0.10662339E-01	0.10734916E-00
0.14949699E-01	0.98474810E-01
0.17229941E-01	0.12307265E-00
0.20076749E-01	0.14447561E-00
0.19529168E-01	0.17164934E-00
0.20320657E-01	0.22728613E-00
0.21378068E-01	0.24452724E-00
0.22301081E-01	0.26831973E-00
0.24511521E-01	0.16281100E-00
0.27752671E-01	0.30214746E-00
0.29222453E-01	0.34459867E-00
0.35146919E-01	0.32484750E-00
0.40474408E-01	0.35953601E-00
0.36619057E-01	0.39137711E-00
0.43478405E-01	0.40926518E-00
0.50642820E-01	0.38388654E-00
0.49833021E-01	0.43537266E-00
0.55298758E-01	0.44520015E-00
0.65017583E-01	0.43975324E-00
0.77065729E-01	0.44780591E-00
0.81092229E-01	0.44983647E-00
0.91628064E-01	0.47610663E-00
0.11717452E-00	0.48240651E-00
0.12339253E-00	0.50220024E 00
0.10396006E-00	0.71235961E 00
0.13176729E-00	0.10231198E 01
0.14078926E-00	0.12931190E 01
0.19005135E-00	0.48972284E 01

because they can have more than one singularity and in the discrete representation it is difficult to distinguish between multiple discontinuities and oscillations. The possibility for multiple discontinuities is attributed to the many fluctuations in $\Sigma_t(E)/D(E)$. This function can be identical to a particular eigenvalue for several energy values thereby causing the corresponding eigenfunction to have several discontinuities. From the characteristics of the eigenfunctions, it appears that only the fundamental eigenvalue is discrete; and the remaining ones represent particular eigenvalues in the continuum. As shown in Table 3, beyond ρ_{20}^2 the larger eigenvalues associated with the SUMMIT kernel are closer to the fundamental eigenvalues than are the ones from the MASSMK kernel.

The Energy Expansion of the Frequency Dependent Boltzmann Equation in the Diffusion Approximation

The expansion of the energy dependence of equation (15) in terms of the eigenfunctions of the $\underline{P}$ operator requires the evaluation of only one matrix element, L_{mn}, expressed by equation (27). In the discrete energy representation this integration becomes

$$L_{mn} = \sum_{i=1}^{J} \psi_m(E_i) \left[\frac{1}{v(E_i)D(E_i)}\right] \psi_n(E_i)\Delta E_i \qquad (64)$$

where ΔE_i is the weighting factor for the numerical integration A L-MATRIX ELEMENTS code was written which evaluated these matrix elements using both Simpson's rule and Weddle's rule (27) and which also checked the orthonormality condition. The numerical integrations were evaluated using the η variable since the eigenfunctions obtained from the EIGENVALUE code were expressed in this variable and the discrete energy representation was based upon the selection of equal η increments for the evaluation of the energy points. It was felt that since each of the continuum eigenfunctions exhibited at least one discontinuity, and since $D(E_i)$ is not a smooth function, it would be necessary to apply very elaborate integration schemes in order to obtain accurate results. If any integration other than Simpson's rule was used, it was found that for some of the eigenfunctions the orthonormality check was not satisfied (i.e., the integration over energy of all $\psi_m(E_i)$ times $\psi_n(E_i)$ was not necessarily much less than the integration of all $[\psi_m(E_i)]^2$). This fact is not surprising since the eigenfunctions obtained from the EIGENVALUE code were obtained with a Simpson's rule weighting function. For this reason, it was felt that continuity of the numerical methods, that is, the use of Simpson's rule throughout, would result in the more consistent set of L_{mn} elements. Some justification for this reasoning is found in the work of Ohanian (19) since a similar integration was required in his

calculation of the cooling coefficient for water and accurate results were obtained.*

A pragmatic consideration of this calculation provides some satisfaction since its use resulted in theoretical curves which were in good agreement with the experiment. Also the diagonal elements of the L_{mn} matrix were, in general, much larger than the off-diagonal elements since in the evaluation of the former, the large discontinuity of both eigenfunctions occurred at the same energy point. Thus after a careful investigation of the integrands arising in the evaluation of the L_{mn} matrix elements, some justification can be obtained for their accuracy. But, in the general case, the numerical integration of such "wild" functions by Simpson's rule cannot be defended.

Evaluation and Presentation of the Complex Inverse Relaxation Lengths

With the L_{mn} matrix elements determined, one can apply equations (43) and (44) to evaluate the coefficients of the expansion of ρ^2 in powers of $(j\omega)$ and equations (50) and (51) to evaluate the same expansion in powers of χ. In cases where neither series converges rapidly, the

---

* Also in calculations performed by Razminas and the author under the direction of Ohanian, the cooling coefficient for graphite was calculated by Ohanian's method. It agreed quite well with the one obtained by Honeck using the same kernel.

eigenvalues were evaluated directly from the secular determinant at particular values of frequency. Computer codes were written to calculate the coefficients for both the $j\omega$ expansion and the χ expansion of any of the 33 ρ^2 along with their corresponding ratios, S_n. If more than a few terms were used in the $j\omega$ expansion, however, it was necessary to divide the equations by L_{11} and derive expressions for the expansion in powers of $L_{11}j\omega$. This was because at high frequencies, ω^n became larger than 10^{38}, the largest number acceptable to the computer. This problem did not arise in the χ expansion since for a frequency of about 1000 cps χ need be only about 7. Problems were also encountered in the coefficients. For the $j\omega$ and $L_{11}j\omega$ expansions, the series could not be carried past the fifteenth term since,in the former case, underflow occurred in the computer and in the latter case, overflow occurred. In the χ expansion the coefficients did not change as rapidly and no underflow or overflow problem occurred; but since factorial 33 is nearly 10^{38}, the series was cut off at the 33rd term. This, however, was not the limiting factor in the χ expansion for it appeared that after the 20th term round off errors built up rapidly.

Shown in Figure 4 and Figure 5 are the frequency dependent real and imaginary components of the complex inverse relaxation length for the fundamental energy mode

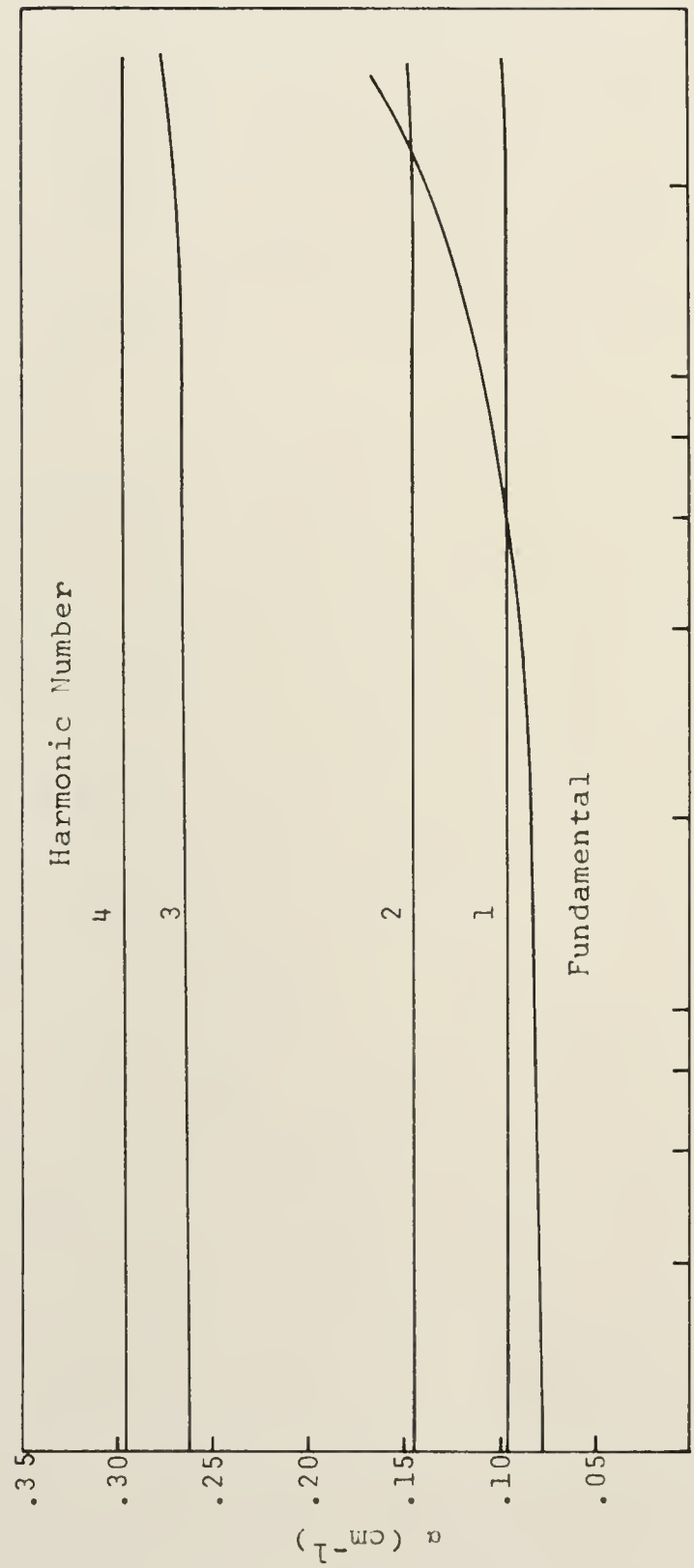

Fig. 4. Real Component of the Complex Inverse Relaxation Length for the Fundamental and First Four Energy Harmonics as Calculated Using the MASSMK Kernel.

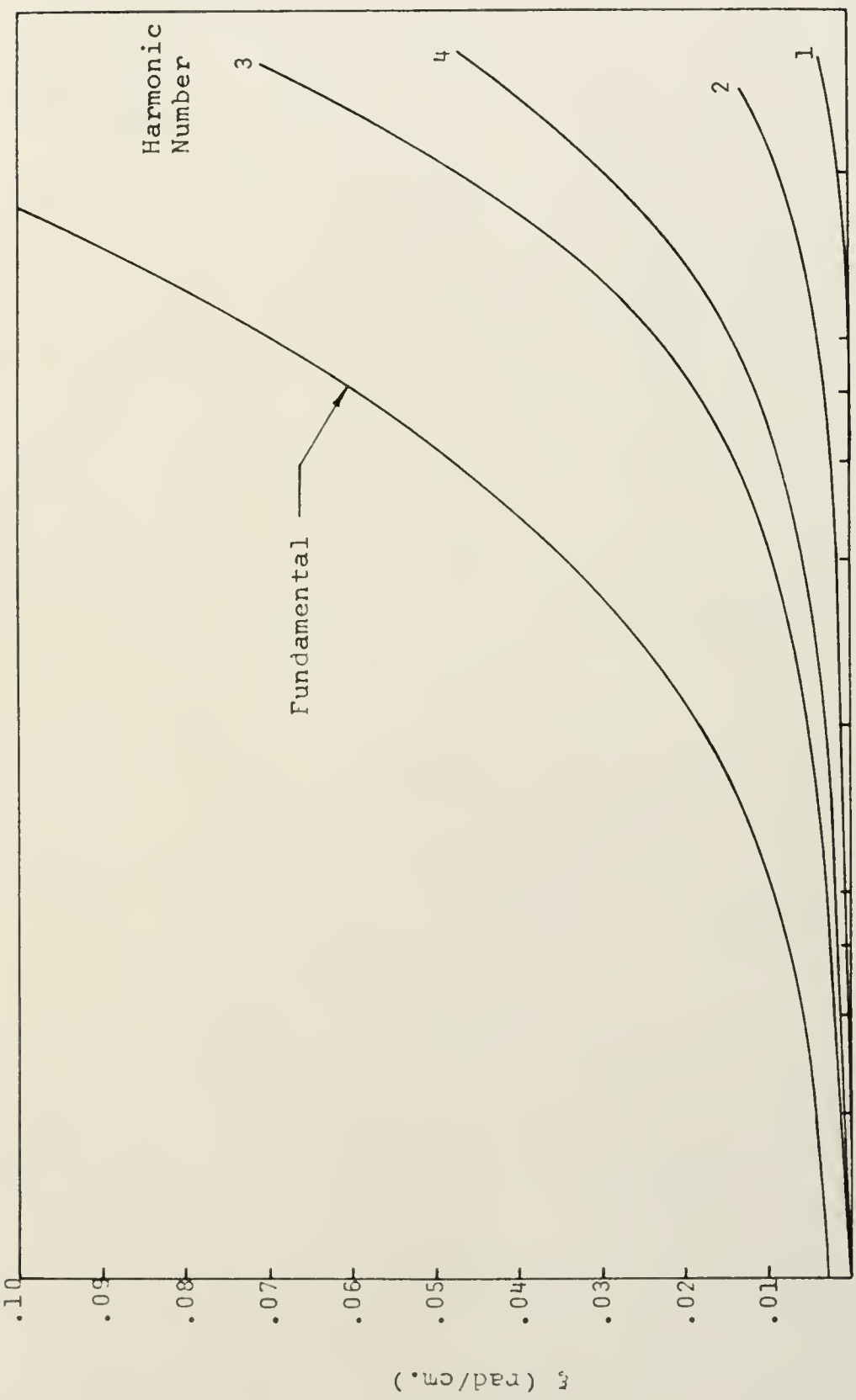

Fig. 5. Imaginary Component of the Complex Inverse Relaxation Length for the Fundamental and First Four Energy Harmonics as Calculated Using the MASSMK Kernel.

and the first four energy harmonics as generated by using the MASSMK kernel. Presented in Figure 6 and Figure 7 are these same eigenvalues up to the third harmonic obtained by use of the SUMMIT code. Figure 8 and Figure 9 show the fundamental and first two space harmonics for the MASSMK calculation. The transverse bucklings used in this last set of curves are indicated on the figures, and for all other curves a value of 5.96×10^{-4} cm^{-2} was used since this was the calculated value for the graphite pile investigated. The omega expansion was used in the generation of all the MASSMK curves, and the method presented previously for the generation of higher energy harmonics was successfully applied with this scattering kernel. Six terms were sufficient for convergence in this case. For the SUMMIT kernel, however, the omega expansion did not converge when as many as 15 terms were used; and for this scattering kernel the χ expansion and the direct numerical solution of the complex secular determinant yielded the eigenvalues.* As shown in Figures 6 and 7, the 18-term χ expansion appears to have converged since agreement exists between it and the direct solution for the fundamental

---

* The code used for this calculation was obtained by Victor Cain from the SHARE Program Library. The code, called EIGENVALUES OF COMPLEX MATRICES, has as its identification number NU EIG4.

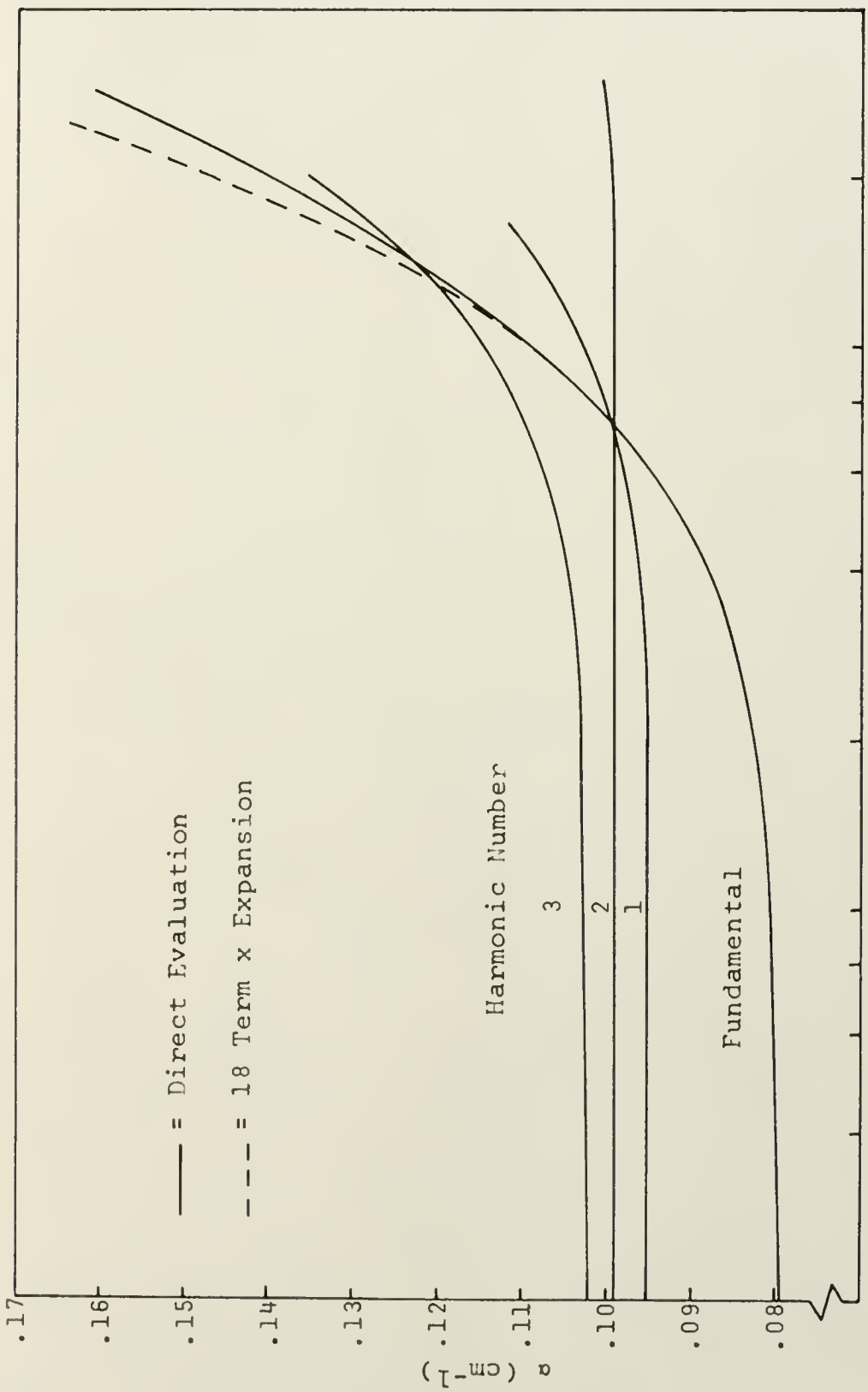

Fig. 6. Real Component of the Complex Inverse Relaxation Length for the Fundamental and First Three Energy Harmonics as Calculated Using the SUMMIT Kernel.

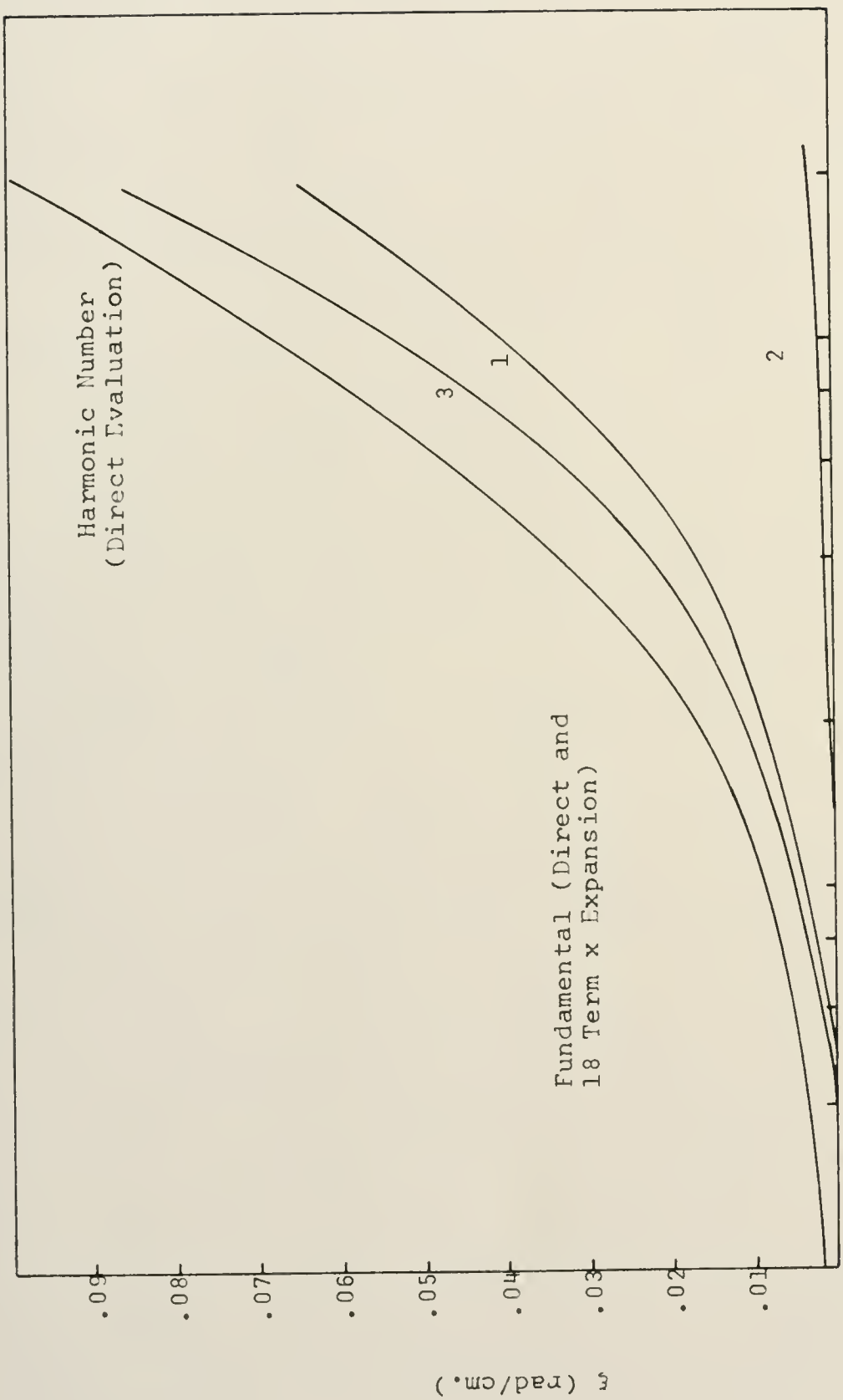

Fig. 7. Imaginary Component of the Complex Inverse Relaxation Length for the Fundamental and First Three Energy Harmonics as Calculated Using the SUMMIT Kernel.

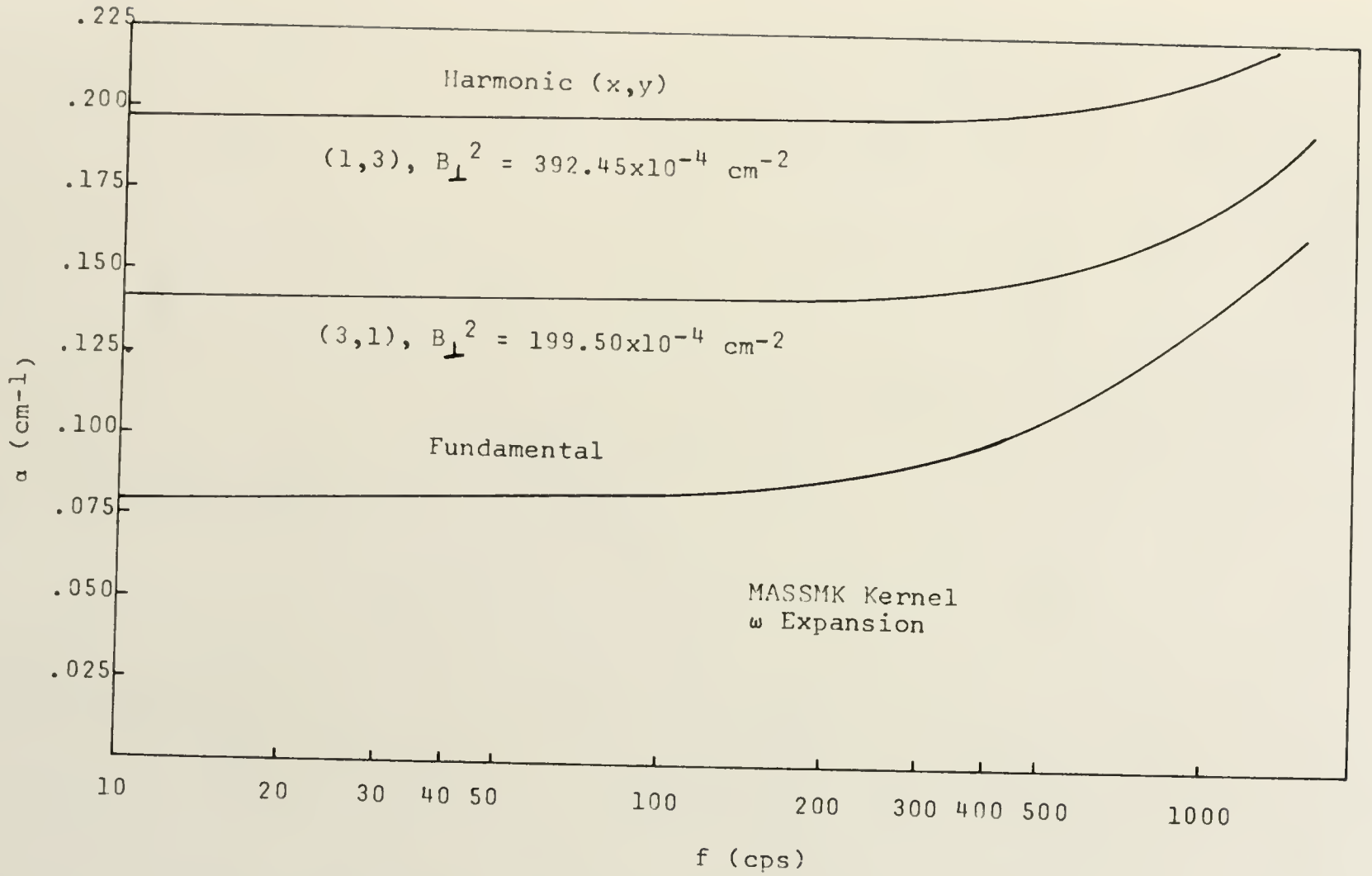

Fig. 8. Real Component of the Complex Inverse Relaxation Length for the Fundamental and First Two Space Harmonics as Calculated Using the MASSMK Kernel.

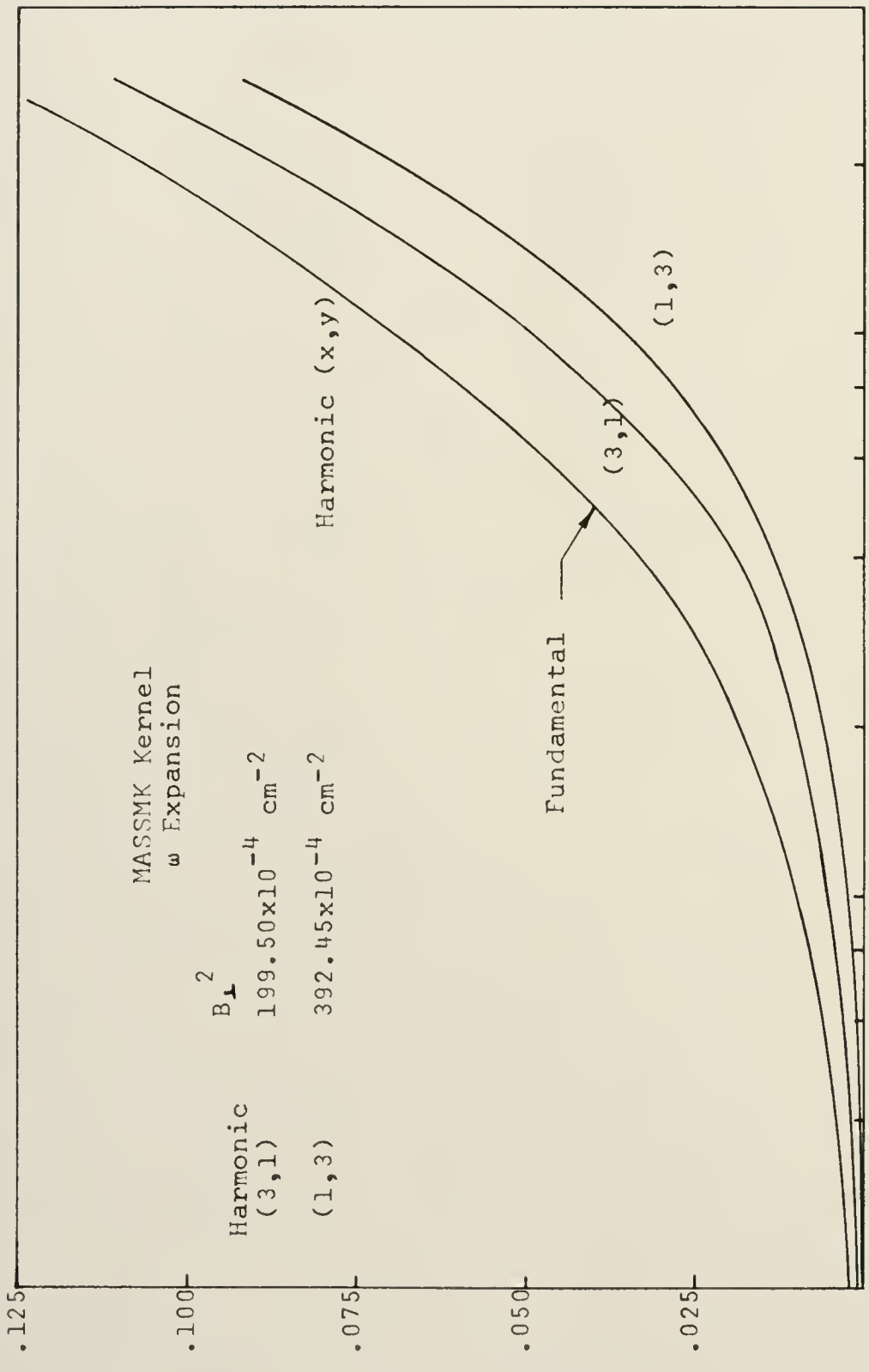

Fig. 9. Imaginary Component of the Complex Inverse Relaxation Length for the Fundamental and First Two Space Harmonics as Calculated Using the MASSMK Kernel.

eigenvalue. The higher energy mode eigenvalues for the SUMMIT kernel were calculated by the direct method.

Some concern can be caused by a careful inspection of the higher energy modes. For higher frequencies, these modes appear to be less attenuated than the fundamental mode; and, therefore, modal contamination is predicted. The less accurate MASSMK kernel does not predict as serious energy mode contamination. One must recall, however, that in order for these higher energy modes to propagate, they must be excited by the source or the medium; and even in the finite, absorbing medium to be investigated they will account for only a small percentage of the energy spectrum compared with the fundamental Maxwellian distribution. Also Kunaish has shown that for the heavy mass scattering kernel the total energy spectrum, calculated from as many as nine of his energy harmonics, will propagate with a complex inverse relaxation length which is within 1 per cent of that of the fundamental.

From the curves showing the higher spatial mode eigenvalues, it can be concluded that for this experiment they will be of secondary importance in comparison with the higher energy modes. Calculations by Perez (9) and Kunaish (18) predict that higher spatial contamination should be reduced to a negligible amount at points farther than 20 cm. from the source. The calculations presented here confirm these predictions.

CHAPTER IV

THE EXPERIMENT IN GRAPHITE

Introduction

The experimental techniques currently used at the University of Florida for the production and detection of neutron pulses and waves were developed over a period of nearly four years through the efforts of many persons. As a half-time graduate assistant on the neutron wave project, the author has been intimately involved in all phases of this developmental work. The methods for analyzing the data have also evolved over a period of years. The principal contribution of the author has been in this area; for he has, under the guidance of his chairman and with suggestions from co-workers, written every computer code required for the data analysis and analyzed or co-analyzed all the data taken thus far in the neutron wave project. Also this work represents by no means the first, nor the last, experimental results to be derived from the neutron wave project, as is evident from an inspection of the Review of the Literature.

The medium investigated in this experiment was a rectangular pile of AGOT graphite 44.7 cm. by 71 cm. by 125 cm. covered, except on the source face, with 30 mil. thick cadmium. The discussion of the experiment which follows is divided into three general areas. Consideration is given to the methods used to excite the thermal neutron waves. Attention is then focused upon the systems employed in their detection. The third section deals with the analysis of data and will be given special emphasis.

The Source

The source of thermal neutron waves used in this experiment was a Cockcroft-Walton type neutron generator placed in a thermalizing tank as shown in Figure 10. The neutron generator, manufactured by Texas Nuclear Corporation of Austin, Texas, produced either a sinusoidally modulated or a pulsed intensity of 14 Mev neutrons which were then slowed down to thermal energy and directed to the graphite pile by the thermalizing tank. The sinusoidally modulated intensity of neutrons was obtained by varying the extraction voltage of the ion source bottle, thereby controlling the intensity of the deuterium beam which impinged upon the tritium target. The pre-acceleration pulsing unit consists of deflection plates, Einzel lens, and focus lens. This unit deflects the deuterium beam to the base of the Einzel lens during the wait time between pulses and allows it to

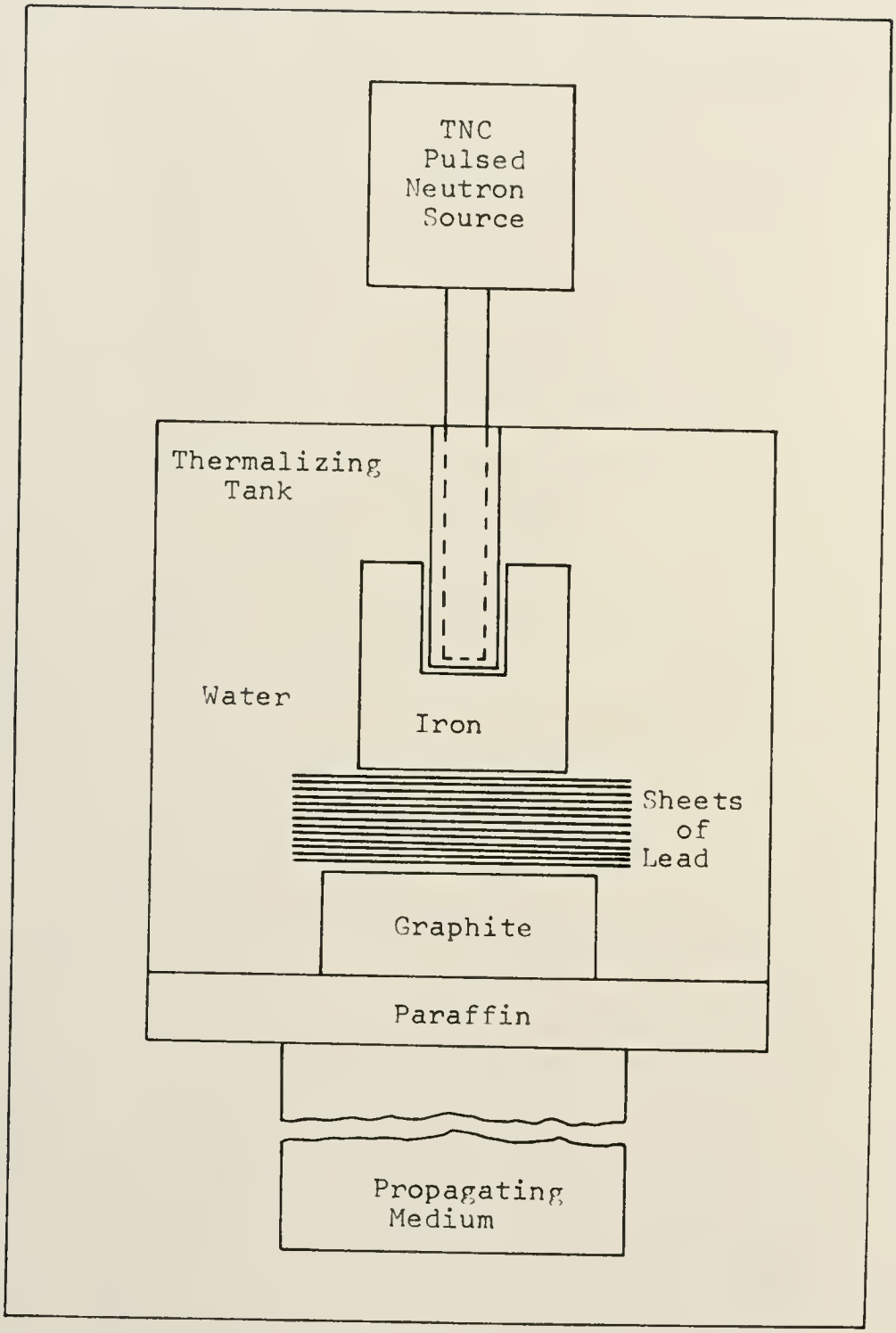

Fig. 10. Arrangement of the Experiment and Details of the Thermalizing Tank (from Reference 14).

pass on to the target for the duration of the pulse. For the data obtained with the modulated source, the frequency varied between 50 and 1226 cps, the ratio of maximum to minimum neutron count rate was roughly 9 to 1, and harmonic and 60 cycle contamination were quite small. For data taken in the pulsing mode, the maximum to minimum thermal neutron yield was about 1000 to 1; and the total pulse width was about 1 millisecond at the z position in the graphite which was closest to the source.* More detailed discussions of the sinusoidal and pulsed mode are given, respectively, in References (8) and (14).

As previously mentioned, the thermalizing tank was used to thermalize the 14 Mev neutron waves produced by the neutron generator and then transport them to the external port of the tank where the graphite medium was placed. This was accomplished by placing light water, steel bricks, lead, and graphite in the tank and facing the tank with a poured-paraffin section. By systematically varying the dimensions of the various materials and carving out a 8 cm. by 8 cm. square hole in the center of the paraffin section, the

---

* It should be mentioned that the attainment of such a high-quality source was due primarily to the efforts of Robert H. Hartley and George W. Fogle.

uncovered-to-covered count rate of a 1 atm. He^3 detector was optimized at 50 to 1 at the source interface of the graphite. The initial thinking associated with this thermalizing tank is presented in Reference (8). The unwanted, but ever present, fast background emitted from the tank was eliminated experimentally as discussed below and in the section dealing with the data analysis.

The Accumulation of Data

It is fitting at this point to indicate precisely what data are to be presented and how it was recorded. The main objective of the neutron wave experiment is to measure the frequency dependent complex inverse relaxation length, ρ, of the fundamental space and energy mode. The most obvious method to accomplish this objective is to modulate sinusoidally the neutron current which enters one boundary, $z=0$, of the medium under investigation and to measure the amplitude and phase of this neutron wave as it propagates from this source. The slope of the semilog plot of amplitude versus z is the real part of ρ, or the attenuation factor, α; while a plot of the phase of the wave versus z is linear with a slope equal to the imaginary part of ρ, or the phase shift factor, ξ. The source is modulated for as many frequencies as desired by the experimenter. The process outlined above was used to obtain the wave data presented in

this work. Still another way of obtaining the same information is to record the dispersion of a pulse of thermal neutrons as it propagates from the source boundary. The amplitude and phase of any frequency component of this pulse at a particular z position is obtained by numerically performing a Fourier transform of the measured, time response at that position. These methods are not new. The analogy in electrical theory to the discussion above is that the frequency characteristics of a "black box" can be determined by either directly measuring its response at various frequencies or by performing a Fourier transform of its unit impulse response. One method is not necessarily superior to the other for all applications, but in this measurement it was found convenient to obtain most of the data by exciting the neutron waves with thermal pulses.

The pulse propagation data were collected by Hartley, and first appeared in his master's thesis (14). The purpose of his investigation was accomplished by considering data in the time domain only. In this work the analysis of Hartley's data is extended beyond that which he completed since Fourier transforms are performed under the guidance of Reference (16) and the complex inverse relaxation length is obtained. Actually, in the final comparison with the theory, the wave data and pulse propagation data are combined as discussed in the next section.

From the above discussion it is evident that it will be necessary to discuss two data accumulation systems, that associated with a sine wave input and the one used by Hartley in his pulse propagation experiment. Before considering these systems individually, however, it is convenient to present those characteristics which were common to both experimental set-ups.

In each of the experiments use was made of a movable detector which could be located at several z positions, and a stationary, standard detector placed in the thermalizing tank. To facilitate accurate placement of the movable detector and cause as little perturbation as possible, length-wise holes were bored in several of the graphite stringers to accomodate the detector and its preamplifier. For measurements at a particular z position, a detector-filled stringer was inserted into the graphite pile so that its center was aligned with the transverse center of the pile and its length was in the transverse plane. By using several of these stringers with holes bored at different distances from their front face, the detector could be moved from the source in about 1 cm. increments from 1 cm. to 72 cm. Two measurements were made at each position of the movable detector; one where both epicadmium and thermal neutrons entered the moderating medium, the uncovered run, and a second where thermal neutron penetration was blocked with a cadmium shutter, the covered run. The standard detector was used to correct

for source variations and to facilitate subtraction of the epicadmium background from the movable detector data of the uncovered run, thereby obtaining the thermal wave. The same source (i.e., neutron generator and thermalizing tank) was used in both experiments, and changing from the wave experiment to the pulse experiment was accomplished by changing accordingly the mode of operation of the neutron generator. The same detector systems were also common to both measurements. They consisted of He^3 detectors and Nuclear-Chicago Corporation preamplifiers and scalers. The system dead time was about 3 microseconds, which was found to be adequate for our purposes. The arrangement of electronics beyond the scalers was unique for each of the two experiments and they will now be discussed separately.

Electronic Equipment Associated with the Wave Experiment

A block diagram of the electronics used in the wave experiment is shown in Figure 11. The main component of this system is the multi-channel analyzer manufactured by Technical Measurement Corporation. A modified 212 plug-in-unit is used in the multi-channel analyzer so that it stores the input pulses in a channel corresponding to their time of arrival after an initial trigger. The analysis time of each of the channels is stepwise variable from 10 to 2,560 microseconds so that the accumulation may cover a wide range in frequency. The remaining circuitry is arranged so

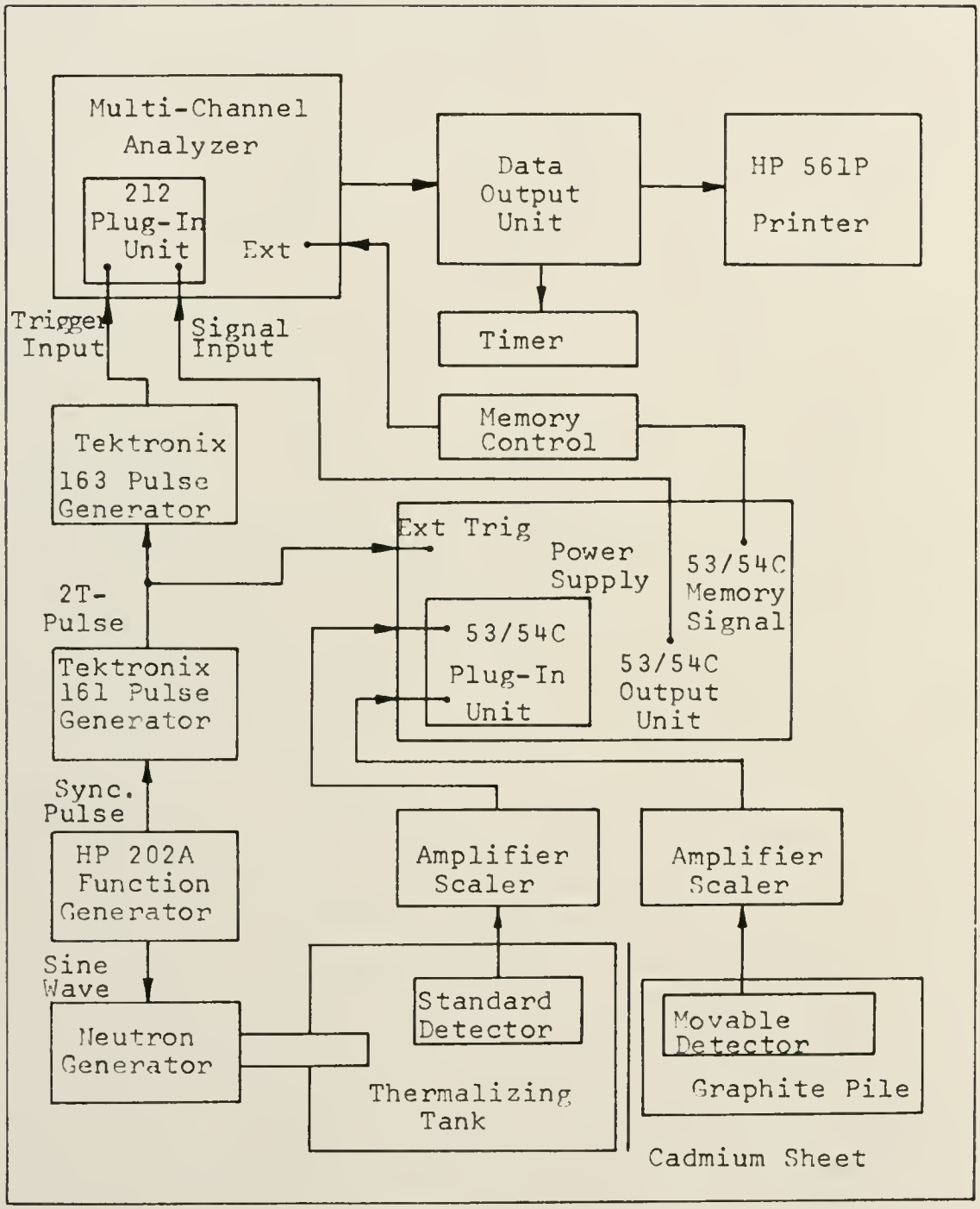

Fig. 11. A Block Diagram of the Electronic Equipment Used in the Wave Experiment.

that for two periods of the input sine wave the output of the standard detector and that of the movable detector are recorded, respectively, in the first half-memory and second half-memory of the multi-channel analyzer. This is accomplished by alternately allowing the pulses from each detector to reach the 212 plug-in-unit, controlling their storage in the multi-channel analyzer, and adjusting its channel width so that the total sweep time is slightly less than four periods of the input frequency.

A time-sequence diagram for the system is shown in Figure 12. The HP202A function generator provides a pulse at the positive peak of its sine wave output to the neutron generator. This pulse train is fed to a Tektronix type 161 pulse generator which, when triggered by a sync. pulse, produces another pulse whose width is almost as long as two periods of the input sine wave. This output pulse from the Tektronix type 161 pulse generator, which is triggered by every other sync. pulse, serves two purposes. It is used as a trigger for a Tektronix type 163 pulse generator whose output, connected to the trigger input of the 212 plug-in-unit, initiates the sweep of the multi-channel analyzer. Thus the analyzer sweep always begins at the same point in the cycle of the input wave. The pulse train is also connected to the external trigger input of the Tektronix type 53/54C plug-in-unit, and it controls the switching of this gate circuit. Other inputs to the Tektronix type 53/54C plug-in-unit are the pulses from the

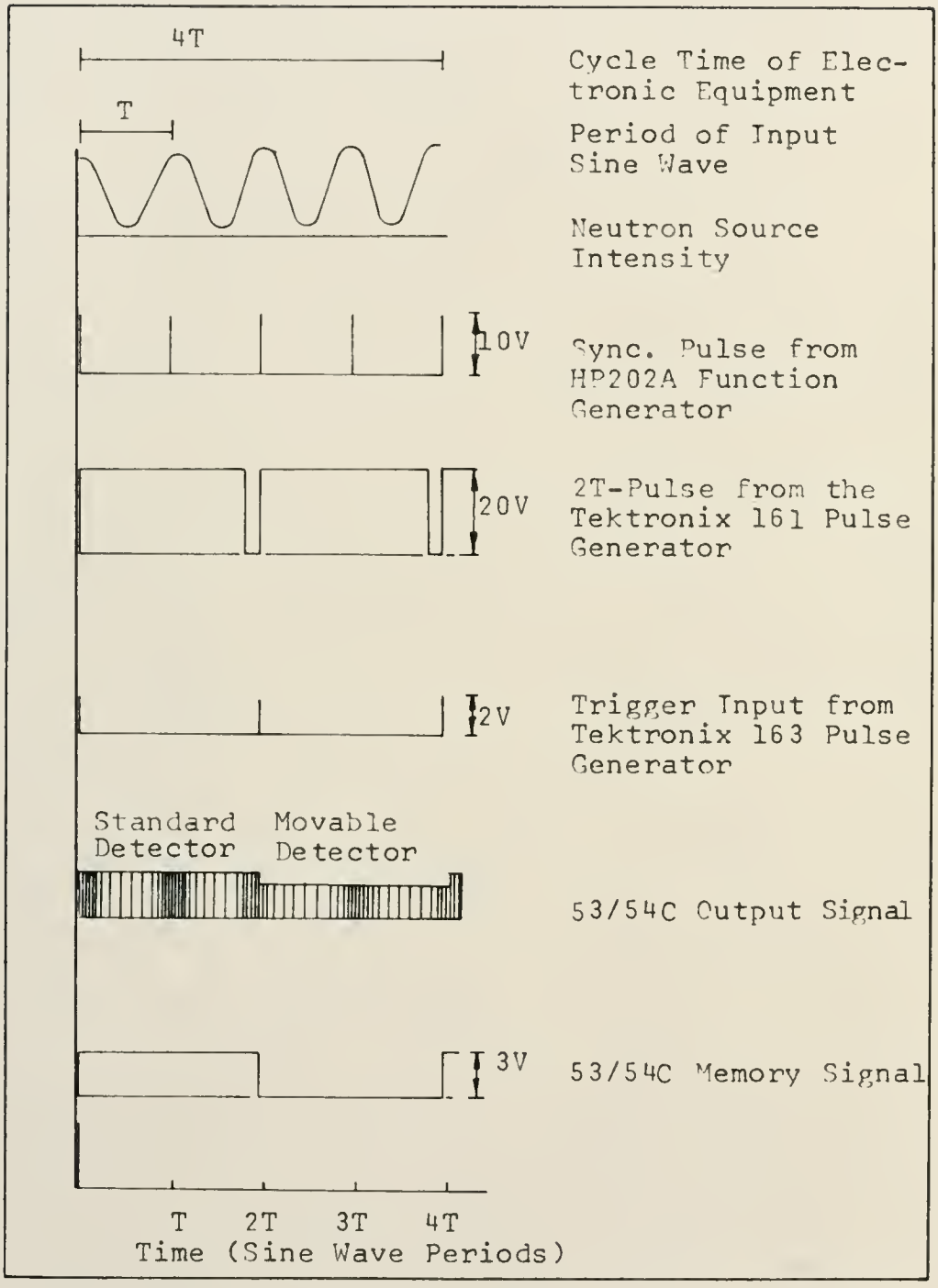

Fig. 12. Time Sequence of Electrical Signals Associated with the Electronic Equipment Used in the Wave Experiment.

standard detector and those from the movable detector. The Tektronix 53/54C plug-in-unit contains two identical amplifier channels; and it is usually used with a dual trace oscilloscope so that two signals, one connected to input A and the other to input B, appear on alternate sweeps of the oscilloscope. In this application the pulses from the two detectors are allowed to pass alternately to the input of the 212 plug-in-unit. An alternate output from the 53/54C plug-in-unit is connected to the EXT input of the multi-channel analyzer, and it is used to control the half-memory in which the detector pulses are being stored. Thus the 53/54C plug-in-unit controls which detector pulses are being recorded by the multi-channel analyzer and also controls the half-memory in which the pulses are being stored. This eliminates the possibility of the storage locations for the two detectors being interchanged during the accumulation of data.

Referring again to Figure 12, the functioning of the detection system during one analysis sweep of the multi-channel analyzer is as follows:

1. A trigger from the Tektronix type 163 pulse generator starts the multi-channel analyzer on its analysis sweep. The pulses from the standard detector will be stored in its first half-memory, and then it will stop and wait for another trigger.

2. The next trigger will start the multi-channel analyzer again, but now the Tektronix type 53/54C plug-in-unit is passing only the movable detector signal and holding the multi-channel analyzer in the second half of its memory.

3. The next trigger will again start the cycle, which is repeated until enough statistics have been obtained.

Electronic Equipment Associated with the Thermal Neutron Pulse Propagation Experiment

A block diagram of the circuitry used by Hartley is shown in Figure 13. For his experiment, only the integral counts of the standard detector were needed. The output of the movable detector was recorded in the multi-channel analyzer after shaping in a Tektronix type 163 pulse generator. The sweep of the multi-channel analyzer was initiated by a signal synchronized with the start of the neutron burst from the neutron generator.

The Data Analysis

Introduction

The focal point in the analysis of neutron wave data is the counts per channel recorded for the movable detector by the multi-channel analyzer. To indicate the typical appearance of these data, the 200 cps thermal wave is shown in Figure 14 for three of the positions used in the wave experiment; and the thermal pulse at several

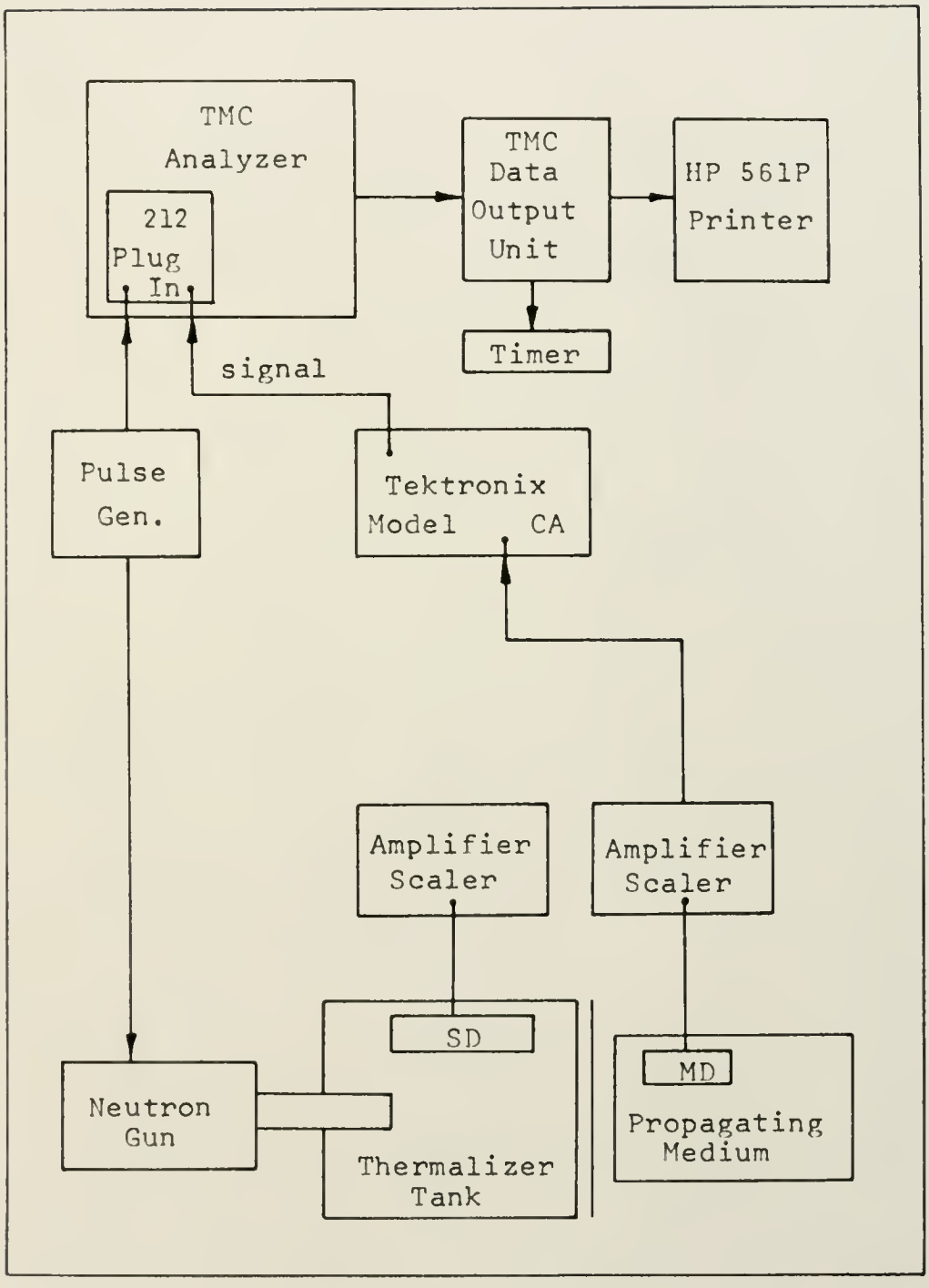

Fig. 13. A Block Diagram of the Electronic Equipment Used in the Pulse Propagation Experiment (from Reference 14).

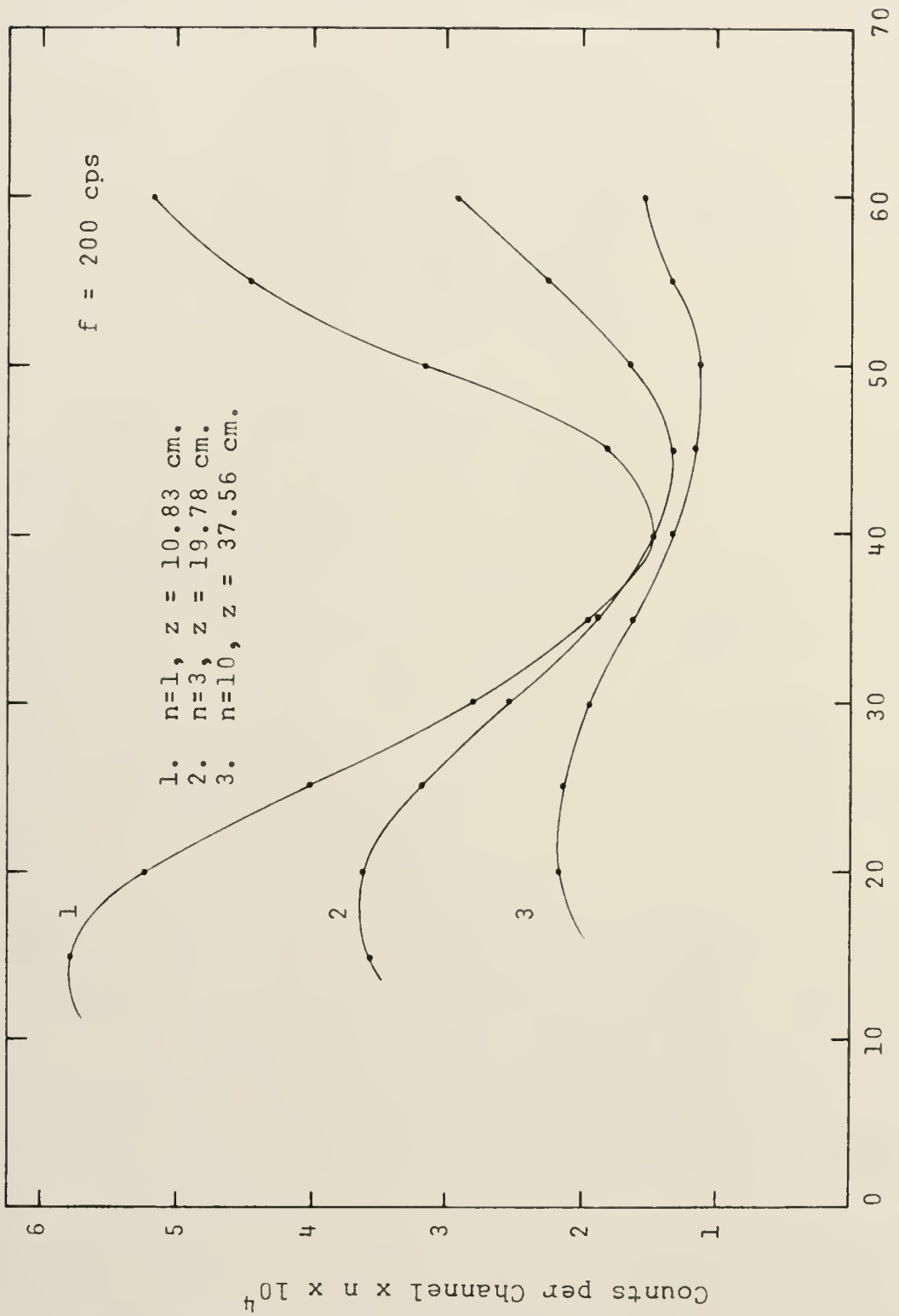

Fig. 14. Thermal Wave of the 200 cps Wave Experiment for Several z Positions.

positions is shown in Figure 15. In the wave experiment these data are composed of a fundamental sine wave contaminated by harmonic distortion, and a Fourier series expansion yields the amplitude and phase of the fundamental thermal wave. The thermal pulse, on the other hand, was considered to be composed of neutron waves in a continuous spectrum from zero frequency up to a high frequency cutoff. Thus the amplitude and phase of a particular frequency was obtained by numerically Fourier transforming the pulse at the frequency of interest. After the attainment of the amplitude and phase points versus z position for several frequencies, the data analysis and comparison with theory can proceed in an identical manner for both the wave and pulse propagation experiments. In fact, in this work the amplitude and phase curves obtained by the pulse propagation experiment and those from the wave experiment are normalized together before determining their slope. In this way the complex inverse relaxation length, ρ, arises from measurements in both the time domain and the frequency domain. The fact that these two sets of data can be normalized together effectively before proceeding with the evaluation of ρ is significant since it indicates that the basic assumptions associated with their analysis were correct and also points out the fundamental equivalence in these two methods of excitation of neutron waves.

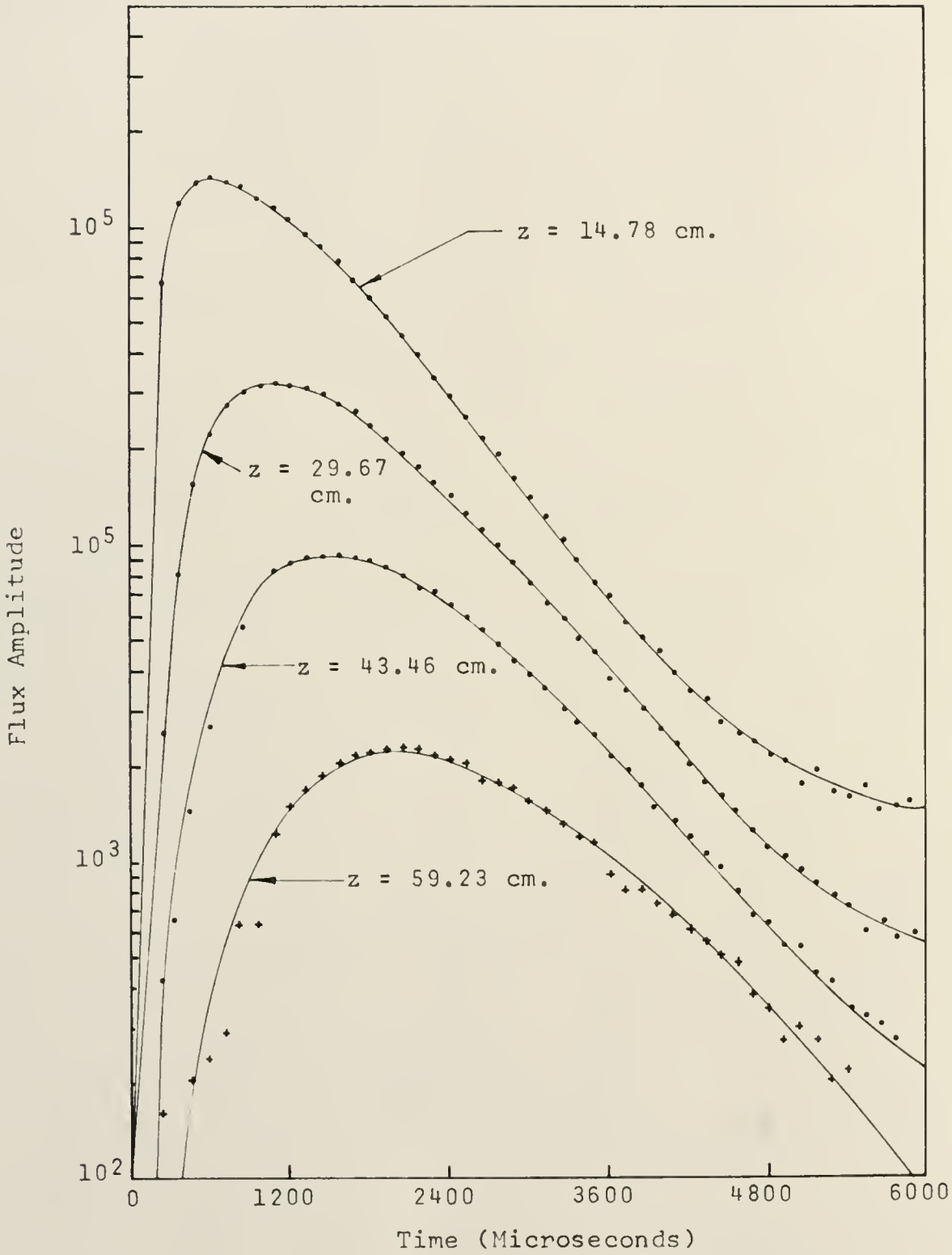

Fig. 15. Thermal Pulse for the Pulse Propagation Experiment for Several z Positions (from Reference 14).

In the discussion which follows in this section, the data evaluation will be carried through the calculation of the real and imaginary components of the complex inverse relaxation length. The data acquired from wave experiments will be considered separately from those of the pulse propagation experiment in obtaining the amplitude and phase as a function of position and frequency. Then these data will be normalized together for the evaluation of ρ.

The data presented here has been taken over a period of two years in two separate wave experiments and in Hartley's pulse propagation experiment. The curves of amplitude and phase versus z position have been determined for 65 frequencies ranging from zero to 1450 cps. For each of these curves a minimum of 14 z positons have been taken; and in many, where all three experiments have been normalized together, up to 40 z positions are considered. Moreover, to obtain each of the 14 to 40 points on the 130 amplitude and phase curves either a Fourier transform was performed over the 256 channel output of the multi-channel analyzer or a Fourier series expansion was made with between 50 and 120 channels per cycle.

The complex inverse relaxation lengths, obtained from least-squares fits of the amplitude and phase curves, were derived from a careful examination of from 2 to 8 fits of each of these curves in which points with largest error were systematically eliminated. The presentation of all

of these data would be impractical. One can, however, present some of the data which are indicative of the results obtained and show sample calculations to indicate the method of data analysis.

Determination of the Amplitude and Phase of the Fundamental Thermal Wave of the Wave Data

For the initial analysis of the wave data use was made of the University of Florida Non-Linear Least Squares (UF-NLLS) code (28). Several new subroutines were written for this code, and it was incorporated into another main program to facilitate a Fourier series expansion up to ten harmonics of the thermal neutron wave. The bulk of the numerical calculations were performed in the WAVE-ESTPAR subroutines which provided estimates of the parameters to the UF-NLLS code. The WAVE-ESTPAR subroutine will now be discussed.

Information was first read into the code which allowed it to calculate the period and number of channels per cycle of the fundamental sine wave variation. The code then read in the counts per channel recorded in the multichannel analyzer for the standard detector with no cadmium placed between the source and the graphite pile (bare standard data), for the standard detector with the cadmium sheet in place so that only neutrons of epicadmium energy entered the graphite (covered standard data), and for the movable-detector counts per channel for the latter situation

(covered movable data). The data of interest, that arising only from the thermal content of the source, are contained in the movable detector counts per channel for the bare run (bare movable data); but this information is contaminated by counts arising from the epicadmium content of the source. The fundamental amplitude, phase, and harmonic content up to the tenth harmonic of the former three sets of data were then calculated. From the two sets of standard data the source variation from the covered to the uncovered runs for each of the frequencies analyzed could be determined. This information was then used to generate correction factors to be applied to each of the frequency components of the covered movable data. A set of data was generated which represented the contribution of epicadmium neutrons from the source to the bare movable data. This was accomplished by individually multiplying the fundamental and each of the harmonics of the covered movable data by the ratio of the standards content of the same frequency for the covered and uncovered runs and by using a subroutine NEWCOV which synthesized the generated waves. This generated epicadmium content of the bare movable data was then subtracted from it to obtain the thermal neutron wave arising only from the thermal neutron content of the source. Note that this background subtraction has been made individually for each frequency; therefore, changes in the harmonic content of the source from one run to the next should not

affect the result. This elaborate method of background subtraction was necessary because of the instability of the neutron generator.

The fundamental component of the thermal wave and as many of its first ten harmonics as desired were then determined, and the results were normalized to the bare standard data. Corrections were also made for changes in the constant component of the source as determined from the total counts of the detectors for both runs. The data were normalized so that the channel width of the multichannel analyzer, its total number of sweeps, counting time, dead time between channels, and channels per cycle could be varied without affecting the results. The printout of WAVE-ESTPAR included the normalized amplitude and phase of the frequencies analyzed for the two detectors for both runs so that any variation in the source was recorded.

The numerical methods used in WAVE-ESTPAR were rather crude compared to those which could have been applied. The correction for dead time between channels was made by calculating the average of the counts accumulated in two consecutive channels, multiplying this by the dead time between channels, and adding the result to the counts of the first of these two channels.* The numerical integrations associated

---

* The 212 plug-in-unit used for this experiment requires 10 microseconds to store the counts accumulated in a channel before moving to the next channel. During this storage time no input pulses are counted.

with the calculation of the Fourier coefficients were approximated by a summation. The method can, however, be justified for these data. The operation of the multi-channel analyzer is such that it will store in each channel all of the counts accumulated during the count-time of that channel. In effect, the counts recorded in a channel are the integral of the detector count rate over the time interval allotted to the channel. If exact adjustment could be made for the dead time between channels, the summation of the counts accumulated in all the channels would be identical to the integral of the count rate over the total sweep of the multi-channel analyzer. The weighted summation performed by the code approximates the exact integral over a period of the fundamental sinusoidal variation by a weighted summation of integrals over each channel. In each of these "channel integrals" the sinusoidal function has been effectively moved outside the integral, and the integrated count rate for the time interval of the channel is multiplied by the value of the sinusoidal function at the center of the time interval. This approximation is mathematically expressed by

$$\int_0^T \sin n\omega t \; y(t)dt \approx \sum_{j=1}^{N} \sin n\omega(t_j + \tau/2) \int_{tj}^{tj+\tau} y(t)dt \tag{65}$$

where T is the period of the fundamental sinusoidal variation of the count rate, y(t), τ is the channel width,

t_j is the time when the jth channel is opened; and it has been assumed that the dead time was zero and that there were exactly N channels per cycle. The accuracy of the above expression is based primarily upon the value of N, which varied between 50 and 120 for this work.

To prevent inaccuracies in the data, the harmonic distortion, fast neutron content, and D.C. component of the source were all held at as low a value as possible; and every attempt was made to hold the neutron generator in stable operation during all of the runs of a particular frequency. These objectives were well realized, especially for the second wave experiment; and for these data the elaborate corrections seemed somewhat extreme. The original purpose of WAVE-ESTPAR was to extract the thermal wave from the bare movable data, keep track of variations in the source, and provide estimates to the UF-NLLS code of the amplitude and phase of the fundamental thermal wave. The UF-NLLS code was then to be used to modify these initial estimates to values which yielded the best fit to the experimental results. Actually, WAVE-ESTPAR did such a good job of estimating the parameters that changes in them by the UF-NLLS code were made only in the third and fourth decimal places. In the interest of saving computer time, the parameters calculated by WAVE-ESTPAR were accepted for the majority of the data considered.

To indicate the accuracy achieved by this technique, Figures 16 and 17 show the amplitude and phase versus z position of the 400 cycle data obtained from runs made when the fundamental sinusoidal variation was 200 cps and then 400 cps. For the 200 cps runs, the magnitude of the 400 cps distortion was about 3 per cent. As shown in the Figures, the 400 cps results obtained from this small percentage of the thermal source agree quite well with that for the 400 cps data. In fact, plotting the first harmonic of a particular frequency became a very useful way to determine if any mistakes had been made in the data input since this small component of the measured signal was very sensitive to inaccuracies or inconsistencies.

Analysis of the Pulse Data by Moore's Method*

Some enlightening derivations by Moore (16,17) provide the guidelines for the analysis of data obtained from the pulse propagation experiment. Moore expressed Fourier moments, $\psi_n(\vec{q},\nu)$, of the measured data as

$$\psi_n(\vec{q},\nu) = \int_{-\infty}^{\infty} dt\, t^n\, e^{-2\pi i\nu t}\, \psi(\vec{q},t) \qquad (66)$$

---

* The author is indebted to Dr. M. N. Moore for several stimulating discussions concerning the analysis of pulse propagation data.

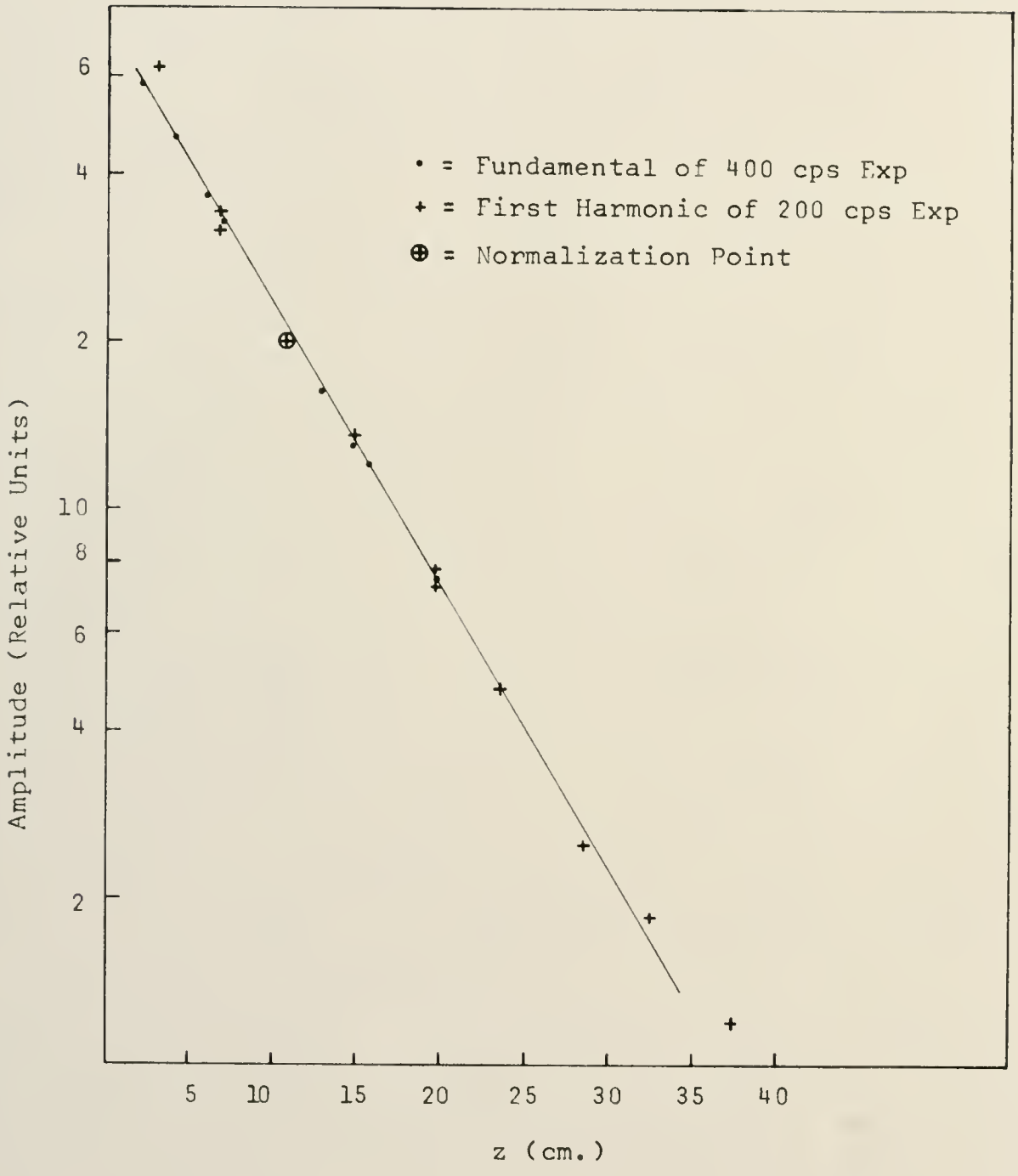

Fig. 16. Amplitude of the 400 cps Wave as Obtained from the First Harmonic of the 200 cps Wave Data and the Fundamental of the 400 cps Wave Data.

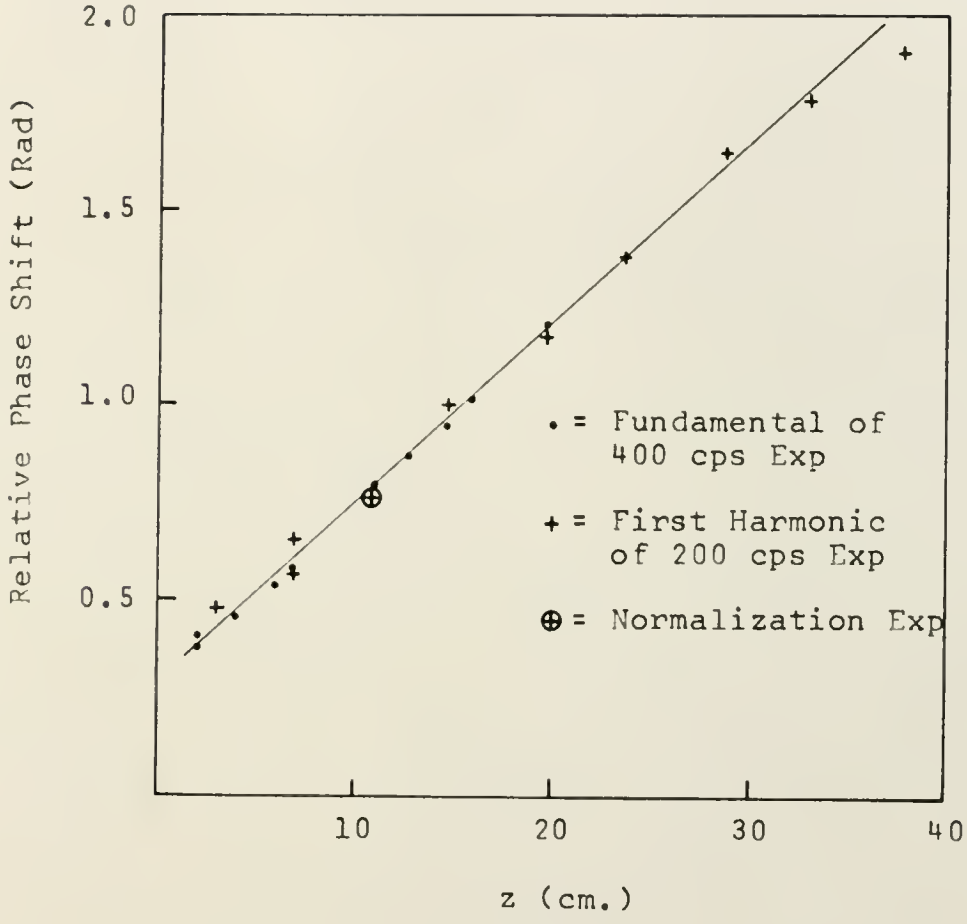

Fig. 17. Phase of the 400 cps Wave as Obtained from the First Harmonic of the 200 cps Wave Data and the Fundamental of the 400 cps Wave Data.

where $\psi(\vec{q},t)$ is the experimentally measured pulse at space point $\vec{q}$ as a function of time, t, and ν is the frequency in cycles per second. He then defined Fourier widths, $W_n(\vec{q},\nu)$, by the expression

$$W_n(\vec{q},\nu) = [\int_{-\infty}^{\infty} dt(t-\bar{t})^n e^{-2\pi i\nu t} \psi(\vec{q},t)]/\psi_o(\vec{q},\nu) \tag{67}$$

where

$$\bar{t} = \psi_1(\vec{q},\nu)/\psi_o(\vec{q},\nu) \tag{68}$$

and proved that, neglecting higher space and energy mode contamination, these widths are related to the frequency derivatives of the system dispersion law by the expression

$$W_n(\vec{q},\nu) = \left(\frac{i}{2\pi}\right)^n \{ G_n(\nu,q_2,q_3,B_1^2) + \frac{d^n}{d\nu^n} [-\alpha_1(\nu,B_1^2) + i\xi_1(\nu,B_1^2)]z \} \quad n > 1 \tag{69}$$

where

$$G_n = \frac{\partial^n}{\partial\nu^n} \log A_{10}Q_{23}(q_2,q_3,B_1^2) \tag{70}$$

and

$$\psi_o(\vec{q},\nu) = A_{10}(\nu)Q_{23}(q_2,q_3,B_1^2)\exp\{[-\alpha_1(\nu,B_1^2) + i\xi_1(\nu,B_1^2)]z\}$$

In the above expression, $\psi_o(\vec{q},\nu)$ is the fundamental space and energy mode which propagates through the system. The source condition is specified through A_{10}, and the transverse space dependence is expressed by $Q_{23}(q_2,q_3,B_1^2)$. Also α_1 and ξ_1 are, respectively, the real and imaginary parts of the fundamental complex inverse relaxation length.

The significance of these expressions is that they form the link between the pulse propagation experiment performed in the time domain and the theory derived in the frequency domain. If, for example, a unit impulse were introduced at z=0, $\psi(\vec{q},t)$ would be the unit impulse response whose Fourier transform, $\psi_o(\vec{q},\nu)$, is the transfer function of the system. Herein lies the key to the normalization of data from the pulse propagation experiment and from the wave experiment. These expressions indicate that the amplitude and phase curves measured directly by the wave experiment can also be obtained by numerically Fourier transforming the data obtained from the pulse propagation experiment. However, much more than this is evident from a careful inspection of the equations. Not only are α and ξ readily obtainable from the raw data of the pulse propagation experiment, but their derivatives with respect to frequency can also be calculated by the use of $\bar{t}$ and the Fourier widths. Expressing $\bar{t}$ in the form

$$\bar{t}(\nu,B_1^2) = \frac{i}{2\pi}\left\{ G_1 + \frac{d}{d\nu}\left[-\alpha_1(\nu,B^2) + i\xi_1(\nu,B^2)\right]z \right\} \tag{71}$$

indicates that plots of the imaginary and real parts of $\bar{t}$ versus z, numerically evaluated for a particular frequency by the use of equations (66) and (68), should yield linear curves with slopes equal to α' and ξ', respectively. The same calculation performed at several frequencies yields the frequency dependence of the first derivative of the complex inverse relaxation length. Similarly, an inspection of equation (69) shows that the Fourier width, W_n, calculated numerically from equation (67) can be used to determine experimentally the nth derivative of α and ξ as a function of frequency. Thus one can not only compare the theoretically derived α and ξ in the frequency domain to those obtained in the experiment; but one can also perform the more demanding comparison of the theoretically and experimentally determined derivatives of α and ξ.

Moore has also shown that this comparison is especially applicable when the perturbation expansion method is used to determine the complex eigenvalue ρ^2. In fact, a direct determination of the coefficients of this expansion is possible through application of his suggested procedure for data analysis. This is easily illustrated by considering the ρ^2 expansion, which for convenience is expressed in the form

$$\rho^2{}_T(\omega) = \sum_{\substack{n=0 \\ (\text{even})}}^{N} \frac{B^{(n)}{}_\omega{}^n}{n!} + i \sum_{\substack{n=1 \\ (\text{odd})}}^{N+1} \frac{B^{(n)}{}_\omega{}^n}{n!} \tag{72}$$

where $B^{(n)}$ is, as before, the nth coefficient of the power series expansion; and the T subscript of ρ^2 indicates that this is a theoretical prediction. Since

$$\rho = \alpha + i\xi \tag{73}$$

and α and ξ are what one obtains experimentally, the contrast between theory and experiment is expressed by

$$\rho_E^2 = \alpha_E^2 - \xi_E^2 + i2\alpha_E\xi_E \leftrightarrow \sum_{\substack{n=0 \\ (\text{even})}}^{N} \frac{B^{(n)}{}_\omega{}^n}{n!} + i \sum_{\substack{n=1 \\ (\text{odd})}}^{N+1} \frac{B^{(n)}{}_\omega{}^n}{n!} \tag{74}$$

The double arrow above indicates reciprocal correspondence, and the E subscript stands for experimental quantities. Thus a power series fit in the frequency variables $\alpha_E^2 - \xi_E^2$ and $2\alpha_E\xi_E$ yields coefficients which should be equal to the theoretically determined coefficients of the perturbation expansion. If α_E' and ξ_E' were also calculated, one could contrast theory and experiment through the relationship

$$\frac{d}{d\omega}\rho_E^2 = 2(\alpha_E'\alpha_E - \xi_E'\xi_E) + 2i(\alpha_E'\xi_E + \xi_E'\alpha_E) \leftrightarrow$$

$$\leftrightarrow \sum_{\substack{n=2 \\ (\text{even})}}^{N} \frac{B^{(n)}{}_{n\omega^{n-1}}}{n!} + i \sum_{\substack{n=1 \\ (\text{odd})}}^{N+1} \frac{B^{(n)}{}_{n\omega^{n-1}}}{n!} \qquad (75)$$

Allowing ω to approach zero in the above relationship indicates that the zero intercept of the experimental curve $2(\alpha_E'\xi_E + \xi_E'\alpha_E)$ yields a value to be compared with the theoretically determined $B^{(1)}$. Likewise, if the second derivatives of α and ξ could be determined, the experimental curve arising from the derivative of the real part of equation (75) would, when extrapolated to $\omega=0$, have a value to be compared to $B^{(2)}$ of the theory. Moreover, one could also fit equation (75), and others derived from it using higher derivatives of α and ξ, to power series expansions in still another attempt to determine these coefficients. The above discussion illustrates that the analysis of pulse propagation data by the method suggested by Moore can be visualized as the experimental equivalent to the perturbation expansion developed by Perez.

Moore has also derived a very elegant method by which the derivatives of α and ξ can be calculated. As indicated previously, one calculates the Fourier width, W_n, of the thermal pulse at several z positions and fits their real

and imaginary components to a linear function of z. From equation (69) it is evident that the slopes of these curves yield α^n and ξ^n. One does not have to take pulse propagation data to be able to determine these derivatives, however. If only wave data were available, one could arrive at a set of points on the curves of α and ξ versus frequency and then apply numerical differentiation techniques for the determination of the derivatives. This latter method, though mathematically equivalent to that suggested by Moore, is quite different experimentally. Using Fourier widths, the derivatives are obtained almost directly from the raw data, that is, from $\psi(\vec{q},t)$. For the other method, α' and ξ', for example, are obtained through the intermediate step of calculating α and ξ; and the errors accumulated in the latter two will surely propagate to their derivatives.

One further comment concerning the Fourier widths will be made before proceeding to the discussion of the computer code used to analyze the pulse propagation data. An inspection of equation (67) reveals that $W_o = 1$ and $W_1 = 0$. These relationships can be used to check the correctness of the method of data analysis, the accuracy of the numerical methods, and the consistency of the data.

The MOORE MOMENTS code, though complicated by the fact that the integrands contain complex numbers, is simple in terms of its overall sequence of operations. One reason

for this was that the subtraction of the signal caused by source neutrons with energies above cadmium cutoff was able to be based only upon the total counts accumulated in the standard detector during both the covered and the uncovered runs. As shown by Hartley (14), the fast pulse was localized in the first few channels of the multi-channel analyzer while the thermal pulse extended over most of the 256 channels. Thus extraction of the thermal pulse from the bare movable data by taking the source corrected difference between it and the covered movable data was accepted as adequate for these data.

For the numerical approximation to equations (66) and (67), the same method was used as has been explained in connection with the WAVE-ESTPAR subroutine. Some difficulty arose in justifying the fact that theory called for an integral over an infinite range and the data extended over a finite interval of time. However, Hartley's exacting experimental technique reduced this problem to an academic one. He accumulated the data on one long run of about 30 hours during which time the neutron generator was held within narrow operating limits. The ratio of maximum to minimum value of the thermal pulse was maintained well above 1000 to 1 and showed only a slight drift over the course of the experiment. Enough channels were allotted to times after the complete decay of the pulse so that the D.C. contribution,

which was due to the constant drift current, could be determined. Thus the contributions to the integral beyond the counting range on the multi-channel analyzer was held to a negligible amount and could be subtracted from the thermal pulse before performing the numerical integrations.

The MOORE MOMENTS code was set up to evaluate numerically for any desired frequency the Fourier moments, equation (66); $\bar{t}$, equation (68); and Fourier widths for any value of n, equation (67). Corrections were made for the dead time between channels and the drift current contribution. The numerical integration scheme could be either a direct summation or Simpson's rule. The results were normalized, printed out, and plotted. Little difference (less than 1 per cent) was obtained when Simpson's rule was applied rather than the direct summation. This was because 256 points were available in the numerical integration. This difference increased with frequency but was never more than 1 per cent for the range of frequency considered. The value of W_1, which should be zero, was quite dependent upon the value of the argument selected for the sinusoidal functions used in the formation of the integrand. It was found that the smallest W_1 values were obtained when these arguments corresponded to times at the center of the counting interval of the channels. Values of about 10^{-12} were obtained at the low frequencies, but they increased to about 10^{-8} at the high frequencies.

The Fit of the Combined Amplitude and Phase Curves to Obtain the Real and Imaginary Components of the Complex Inverse Relaxation Length

As previously mentioned, the curves of amplitude and phase versus z position for a particular frequency are obtained from the Fourier series analysis of the wave data and from the zero moment, $\psi_o(q,\nu)$ of equation (66), of the pulse propagation data. The slope of the semilog plot of the amplitude curves is α, and the slope of the linear phase curve is ξ. To obtain these components of the complex inverse relaxation length, the amplitude and phase curves from both wave experiment and from the pulse propagation experiment were combined; and the UF-NLLS code was used to obtain the slope of the result. It would be impractical to present plots of each of the 130 amplitude and phase curves. However, all of the data points of these curves have been tabulated in the Appendix, and several of them are shown in Figure 18 and Figure 19 to indicate the agreement obtained between the wave data and pulse propagation data. One point which is clear from an inspection of these curves is that data were able to be obtained at larger z values with the pulse propagation experiment than with the wave experiment. This is because in the wave experiment the D.C. component of the source must be at least equal in magnitude to the sinusoidal component. The D.C. component suffers less attenuation with distance from

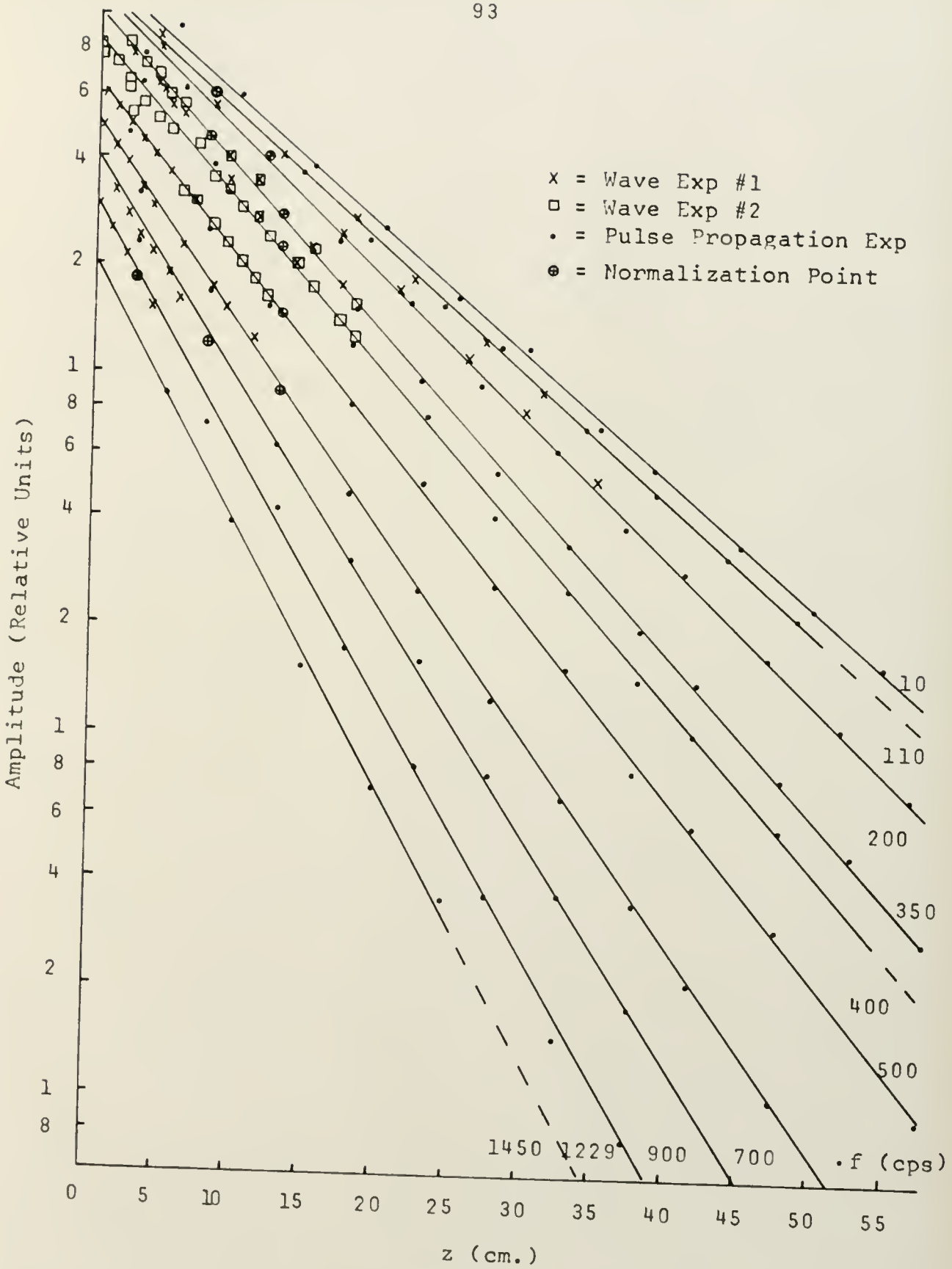

Fig. 18. Combined Amplitude Curves for Several Frequencies.

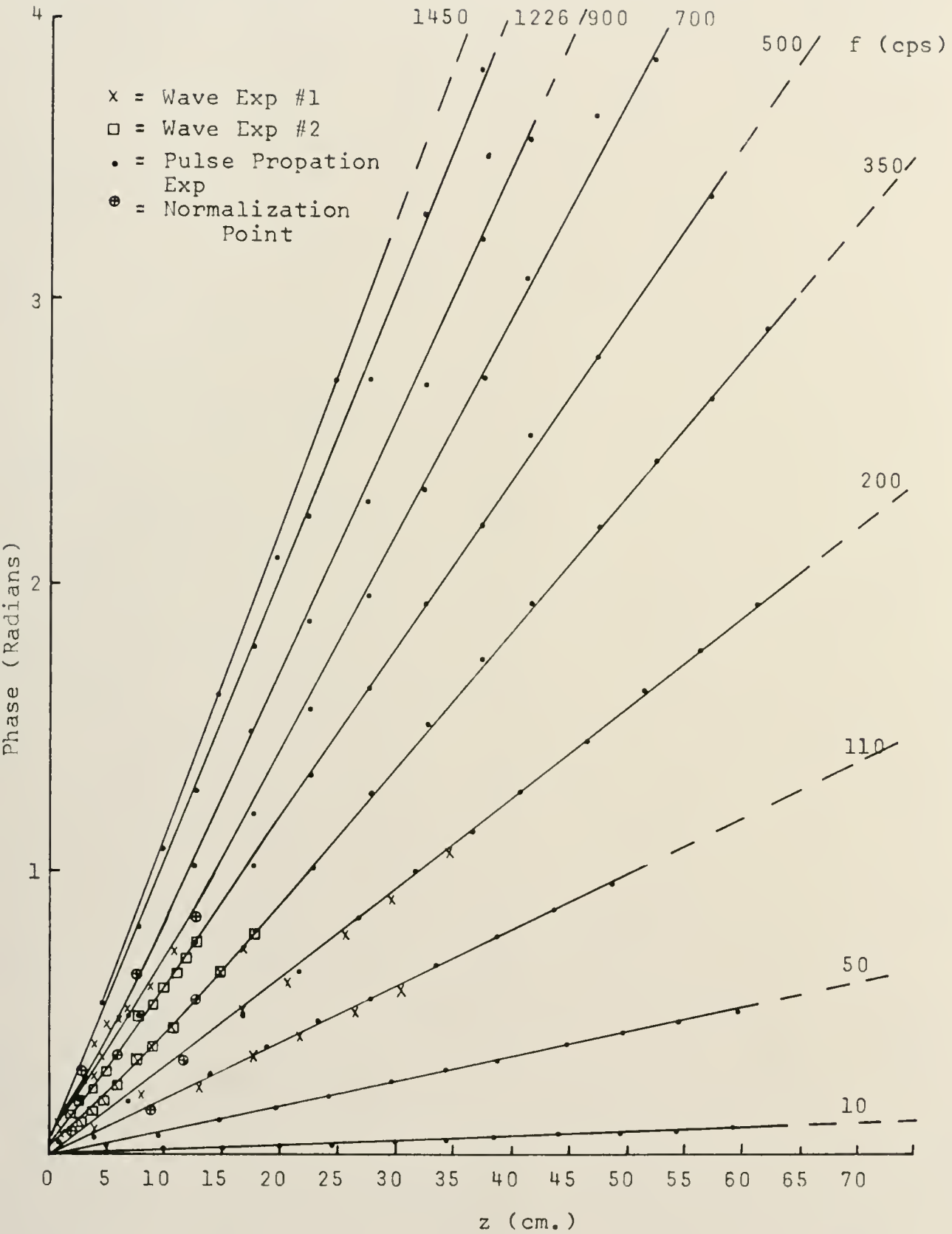

Fig. 19. Combined Phase Curves for Several of the Frequencies.

the source. After a decade or so of decay of the wave, its contribution to the movable detector count rate is swamped by the D.C. component. In this circumstance, cross correlation techniques could be applied to extract the sinusoidal component of the signal but this was not attempted. For the pulse propagation experiment, on the other hand, the D.C. component of the source is determined only by the on-off ratio of the neutron generator, which for this data was about 1000 to 1.

The amplitude curves were normalized to a value of unity at the first z position at which data were obtained, and their logarithms were least-squares fit to a linear function of z with a slope of α and a zero intercept. The phase curves were normalized to a value of zero at the closest z position, and they were least-squares fit to a straight line with slope ξ and zero intercept. Only one parameter, the slope, was varied through the iterative process of the code. It is important to note that for the calculation of α and ξ only the relative amplitude and phase of the neutron wave at various z positions were required. Thus the frequency spectrum of the source did not need to be determined. The interest here was how the wave of a particular frequency was attenuated with distance from the source, not with how its amplitude and phase compared with that of another frequency at a certain point in the medium. The ability to adequately analyze the data without

knowledge of the frequency dependency of the source was found to be very fortunate, especially when an attempt was made to obtain this knowledge in connection with the reflection experiment (13).

The final determination of α and ξ resulted from several fits of each of the amplitude and phase curves in which points were systematically eliminated from both their high z values and low z values. The points for large z were poor because of statistical errors. The thermal pulse was detected over an attenuation of nearly 3 decades, but for the same range of z values the pulse resulting from the epicadmium energy source neutrons was only slightly attenuated. Thus the ratio of useful signal to background decreased rapidly with increasing z because of the rapid attenuation of the useful signal. The points obtained at small z values were contaminated by space and energy modes and were, therefore, not as useful. The first fit of the data included all of the points. The channel-chop option of the UF-NLLS code was then used to eliminate the smaller z data in sets of 3 to 8 points at a time, depending on the total number of points and their z values. For this first sequence of channel chops, the points fit covered the approximate ranges of 4 through 69 centimeters, 10 through 69 centimeters, 15 through 69 centimeters, and 20 through 69 centimeters. The highest z points, those with largest error, were then eliminated from each curve. The number of points eliminated

increased slowly with frequency from zero to 3 or 4 at around 1000 cps, and then more rapidly to 6 to 8 at the high frequency limit of 1450 cps. The channel-chop sequence was then applied to these depleted curves in the same fashion as before.

The results obtained from this procedure were very gratifying. At the lower frequencies (10 to 300 cps), the variation of the slopes with the number of points chopped clearly approached an asymptotic value in a fashion which indicated the progressive elimination of contributions from higher space and energy modes. For this frequency range, values of the slope versus the number of points chopped were plotted and a smooth curve drawn through them. All of these curves tended towards an asymptotic value which was taken to be that of the fundamental space and energy mode. The change in slope observed over these curves was about 5 per cent. For the rest of the frequency range, no such trend was observed; and up to about 1000 cps, the final slopes were obtained from a simple averaging of the various values obtained. The percentage variation of these slopes was slightly less than for the lower frequencies except between the range of about 700 cps to 900 cps where the points appeared to exhibit more scatter. Only one or two chops were made and fewer points were available above 1000 cps so the final values of these slopes are less accurate.

With the attainment of α and ξ from the amplitude and phase curves, the first stage of the data analysis is complete. It is hoped that these experimentally determined values are, in fact, the real and imaginary parts of the fundamental complex inverse relaxation length. The presentation of α and ξ versus frequency is left to the next chapter.

CHAPTER V

COMPARISON OF THE THEORY WITH THE EXPERIMENT

Presentation of the Measured Complex Inverse Relaxation Length

It has been proposed by Beckurts (29) that it is more useful to contrast the experimentally obtained eigenvalues with the ones computed theoretically than to compare parameters extracted from the data to their values as predicted by the theory. Consistent with this idea, Figures 20 and 21 show the real and imaginary components of the experimentally determined complex inverse relaxation length versus frequency, along with those curves from the theory using both the SUMMIT kernel and the MASSMK kernel. From an inspection of these figures, it appears that both theoretical models predict the experiment quite well up to about 300 cps. For higher frequencies, the theory and experiment diverge slightly, with the discrepancy of the MASSMK kernel exceeding that of the SUMMIT kernel by a noticeable amount. In the frequency range between 400 cps and 1000 cps, the deviation between the SUMMIT kernel and the experiment rises from 4 per cent to about 10 per cent, while in this same frequency range, the MASSMK deviation

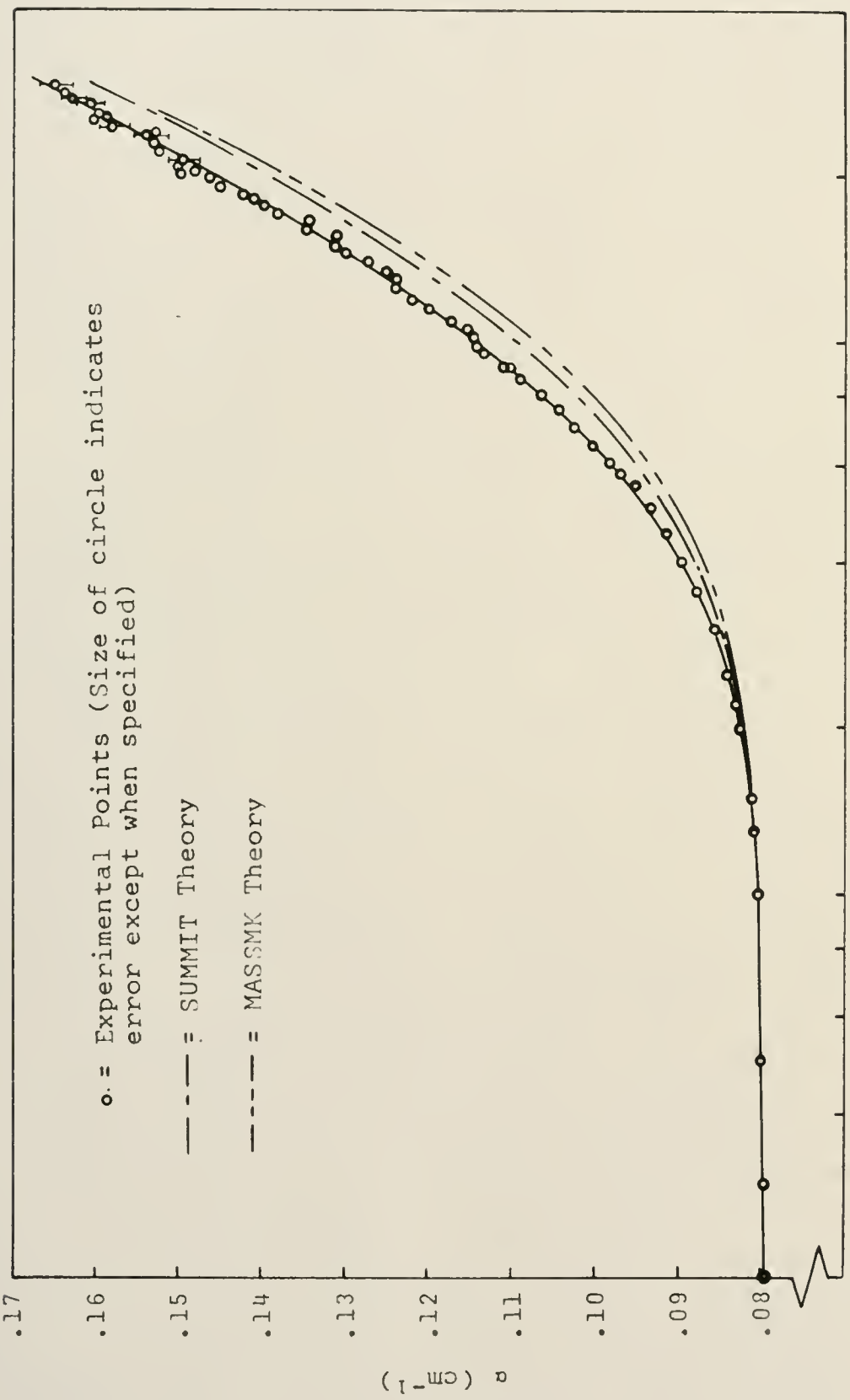

Fig. 20. Comparison of the Theoretically Derived α to the Experimental Results.

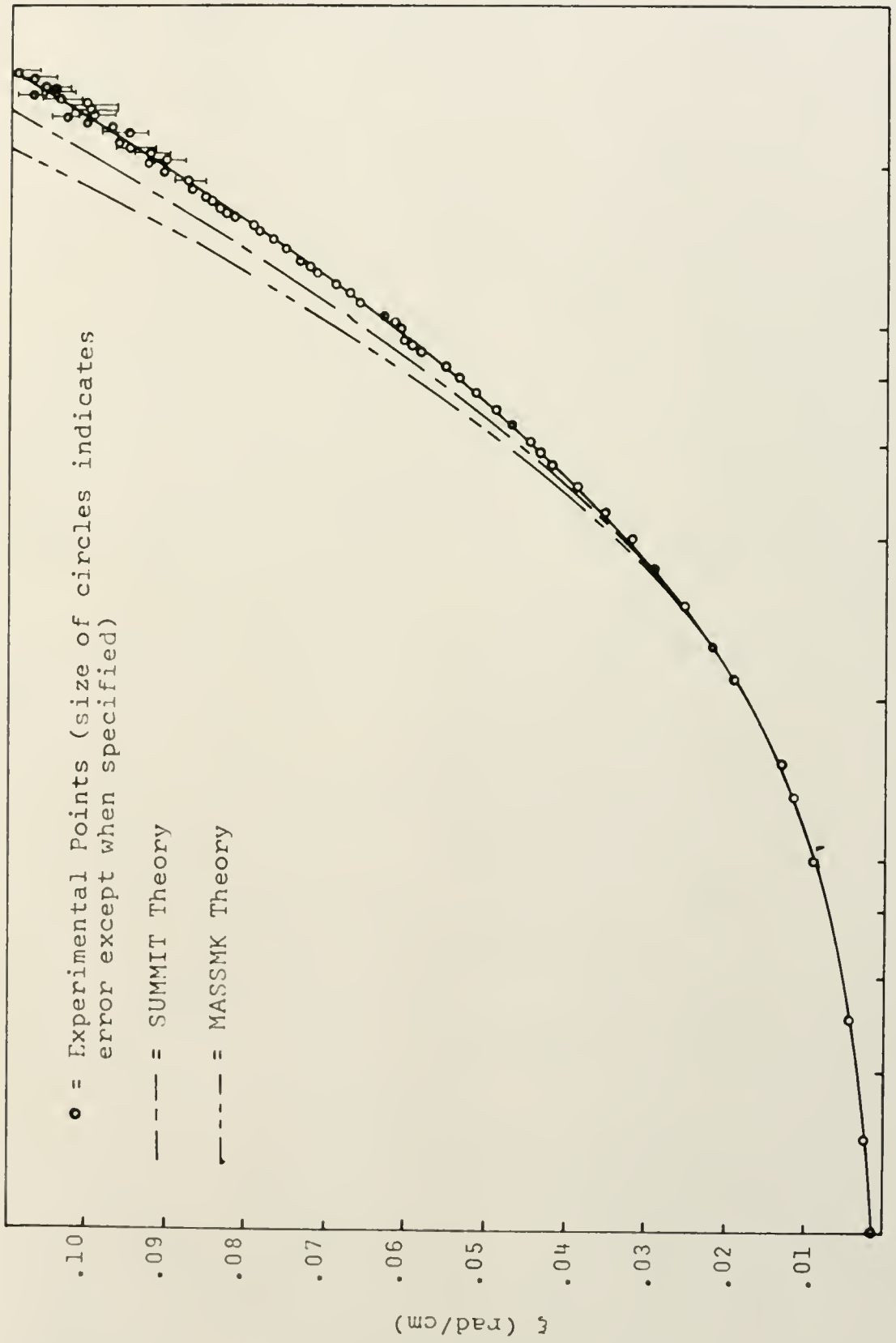

Fig. 21. Comparison of the Theoretically Derived ξ to the Experimental Results.

ranges between 8 and 15 per cent. Both theories tend to underestimate the damping coefficient, α, and to overestimate the phase shift factor, ξ, especially at higher frequencies.

One could conclude from this direct comparison that the disagreement between theory and experiment exists only for frequencies higher than 300 cps. However, an ambiguity exists in that this disagreement can be attributed to one or more of the following facts: (1) higher energy mode contamination, (2) higher spatial mode contamination, (3) transport effects, (4) inadequacy of the particular kernels which were used to describe the thermalization effects. Consideration will now be given to each of these possibilities in the same order as they were listed.

Both scattering kernels were used to generate the complex inverse relaxation lengths associated with higher energy modes. It was found (see Figure 6) that the damping coefficients for these higher energy modes are significantly larger for low frequencies but become, in general, smaller than the fundamental α beyond the first crossing point of 300 cps. This result agrees with the observation by Starr and Price (11) that for large bucklings waiting times on the order of two milliseconds were needed to obtain the asymptotic behavior in die-away experiments in graphite. In terms of the neutron wave experiment, this is equivalent

to the prediction that higher energy modes will become prevalent for frequencies larger than 500 cps.

As frequency increases, all of the spatial modes associated with the fundamental energy mode approach the same values for their damping and phase shift coefficients. This is because they differ only by the transverse leakage term, $B^2_{\perp,\ell,m}$, which becomes progressively less significant compared to the frequency dependent terms of ρ^2 as the frequency increases. At low frequencies these higher spatial modes can be easily discriminated against by obtaining data only at points far from the source boundary and by applying the channel-chop technique previously discussed. At higher frequencies, however, one cannot be sure that higher spatial modes are not contributing to the data since their attenuation and phase shift factors will be nearly equal to those of the fundamental spatial mode. Perez and Uhrig (9) estimated that for a point source in the assembly whose transverse buckling is 1.65×10^{-2} cm^{-2} higher spatial mode contamination could become as large as 5 per cent in the upper frequency range.

Another source of difficulty arises from the fact that transport theory should be introduced when the time between two collisions becomes of the same order of magnitude as the inverse of the frequency. This effect is less important than the thermalization effects, and it has been estimated by Kunaish (18) to be on the order of 2 per cent.

Hence the direct comparison test without additional information can both preclude any firm conclusion about the disagreement between theory and experiment at the higher frequencies and lead one to assume that since there was agreement over a reasonable range of frequencies the diffusion and thermalization parameters derived from the theory are adequate. From this fact the question arises as to how sensitive the direct comparison test is to thermalization phenomena. Still another example of the difficulty in deriving firm conclusions concerning thermalization effects by the direct comparison of eigenvalue curves can be obtained by applying the reasoning presented thus far to typical die-away experiments. By doing this, one could conclude that diffusion theory gives adequate theoretical predictions except in the range of bucklings where the experimental data can be affected by higher energy and spatial modes as well as by transport corrections. The inadequacy of the direct comparison test is confirmed by the fact that the MASSMK kernel, which is much less sophisticated from a thermalization viewpoint than the SUMMIT kernel, gives results which appear very similar to those of the SUMMIT kernel.

The difficulties encountered in the direct comparison test for both the die-away and the neutron wave experiments arise because the thermalization parameters enter as second-order effects in the frequency range in which the asymptotic

mode is more easily measured. In order to perform a meaningful comparison between the theory and the experimental results, one should be able to isolate thermalization effects from diffusion effects.

In the conventional die-away experiment this is not possible because only one quantity, the decay constant, is measured. In the neutron wave experiment, however, two independent parameters, α and ξ, are measured; and they can be combined to yield two frequency dependent functions, $2\alpha\xi$ and $\alpha^2 - \xi^2$. The former is primarily dependent upon diffusion parameters; and the latter, except for the zero-frequency intercept, is exclusively a function of thermalization parameters.

Figure 22 shows a plot of $2\alpha\xi$ as a function of frequency. Since the fundamental dependence of this function is upon diffusion parameters, the agreement between the SUMMIT theory and the experimental results appears within the experimental error over the full frequency range considered. The MASSMK kernel also represents the data well in a reasonably large range of frequencies. Note that the above is especially true for frequencies less than 300 cps, where no problems associated with modal contamination and transport corrections are expected to occur.

The $\alpha^2 - \xi^2$ versus ω^2 function, shown in Figure 23 for the frequency range from 10 cps to 1400 cps and in Figure 24 for the frequency range below 400 cps, indicates that sizeable

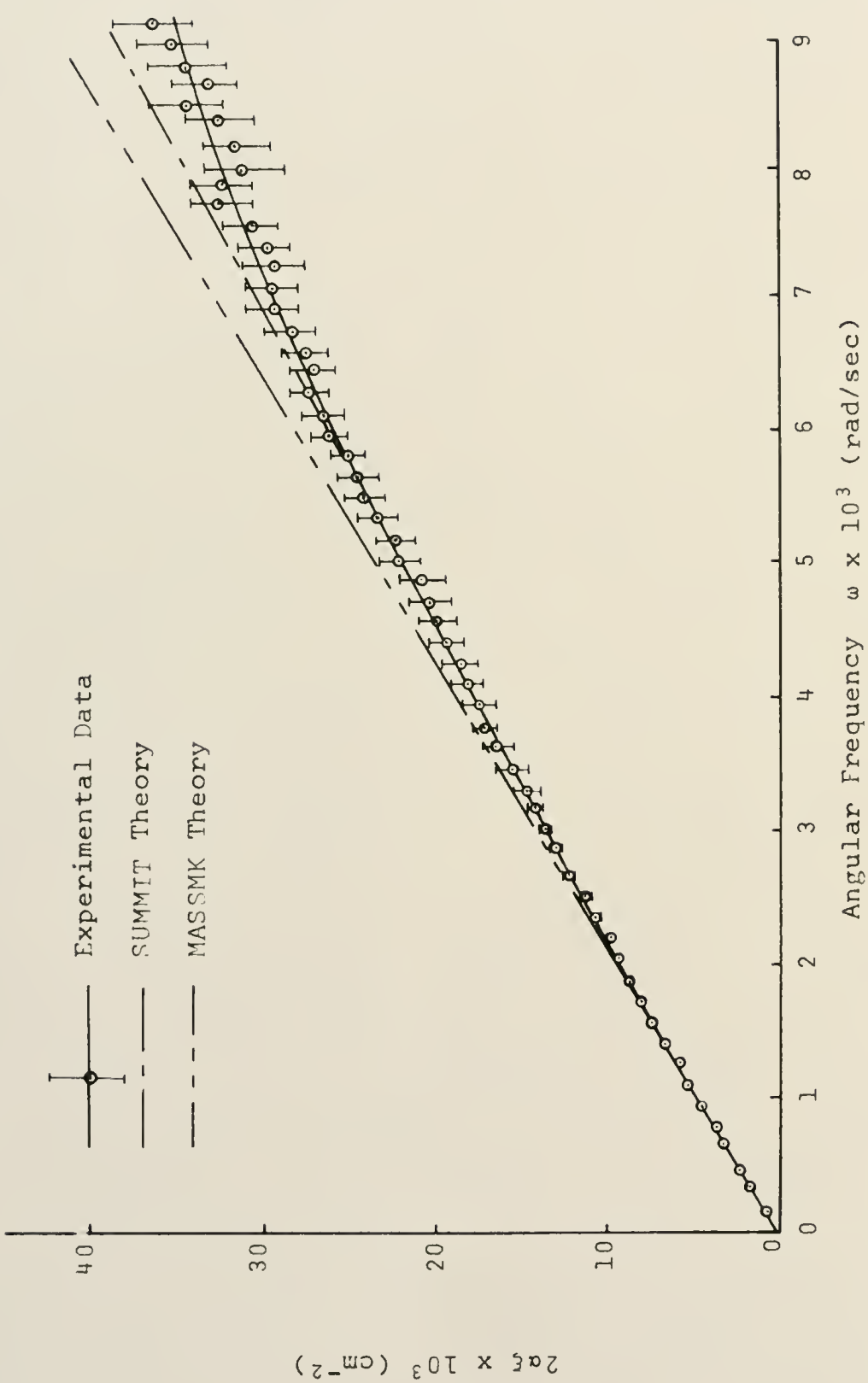

Fig. 22. Comparison of the Theoretically Derived $2\alpha\xi$ to the Experimental Results.

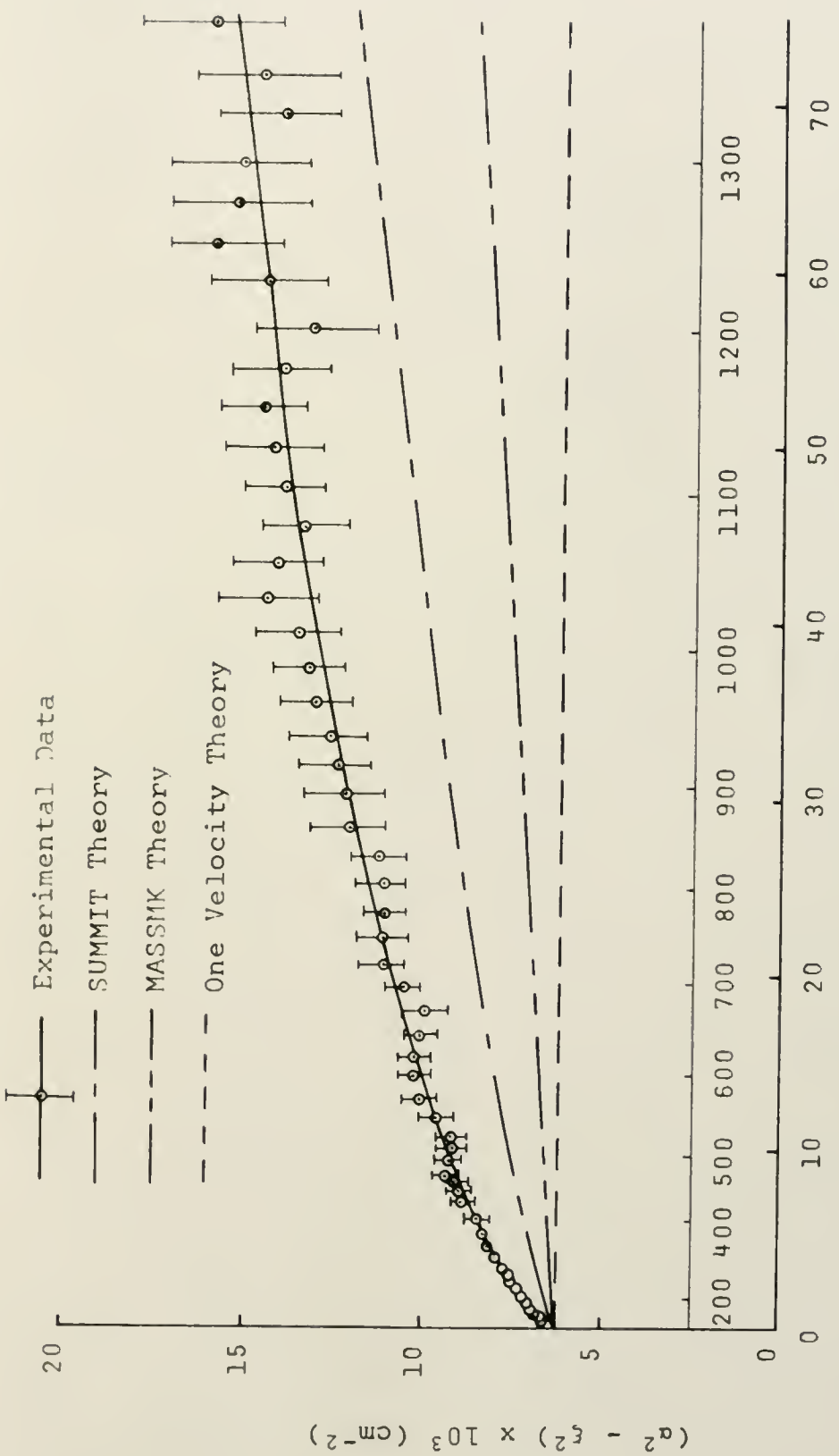

Fig. 23. Comparison of the Theoretically Derived $\alpha^2 - \xi^2$ to the Experimental Results for Frequencies up to 1,400 cps.

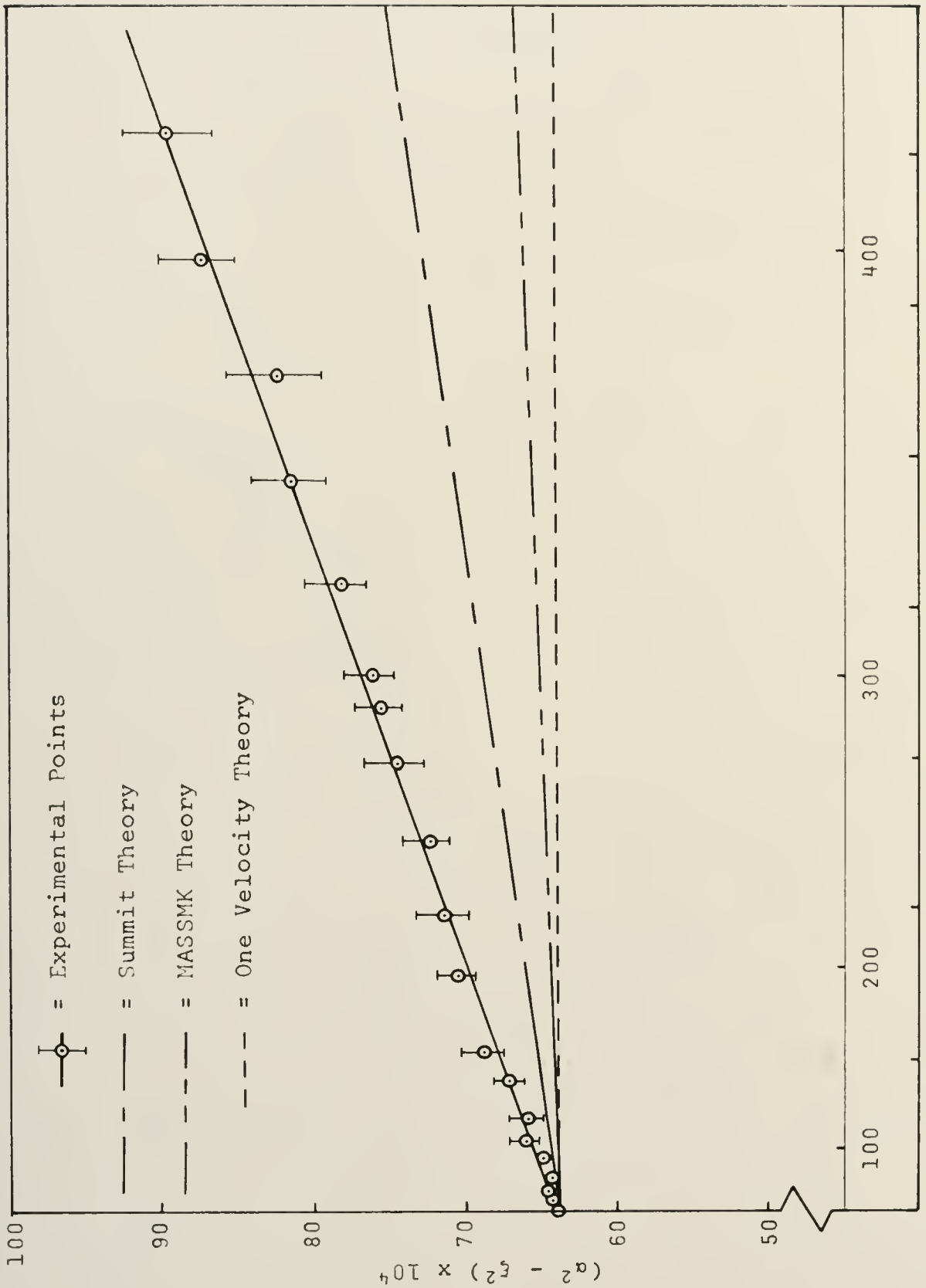

Fig. 24. Comparison of the Theoretically Derived $\alpha^2 - \xi^2$ to the Experimental Results for Frequencies up to 400 cps.

differences exist among the MASSMK kernel, SUMMIT kernel, and the experimental results over the full frequency range. Note that the one-velocity diffusion theory model predicts a constant behavior of $\alpha^2 - \xi^2$. This is the only curve thus far presented in which noticeable differences exist between the two theories and the experimental results in the zero to 300 cps frequency range. Therefore, this is the first instance in which the various thermalization models can be compared with the experimental results in the frequency interval where the experimental data are most accurate and reliable and with no interference arising from diffusion phenomena. In other words, the small differences in the theoretically and experimentally determined α and ξ, which are mainly due to thermalization effects, tend to compensate in the $2\alpha\xi$ curve and to be amplified in the $\alpha^2 - \xi^2$ curve.

An inspection of Figures 23 and 24 clearly indicates that although the trend of the SUMMIT theory correctly describes that of the experimental results the coefficient associated with the linear rise at low frequency will be about twice as large in the experimental curve as the one for the theory. The evaluation of this coefficient and the others to be compared with the theory are discussed in the next section.

Least-Squares Fits of the Squared Complex Inverse Relaxation Length

The real and imaginary components of ρ^2, $\alpha^2-\xi^2$, and $2\alpha\xi$, respectively, were least-squares fit to polynomials of the form

$$\alpha^2 - \xi^2 = \sum_{\substack{n=0 \\ (\text{EVEN})}}^{N} P^{(n)}{}_{\omega} n \tag{76}$$

$$2\alpha\xi = \sum_{\substack{n=1 \\ (\text{ODD})}}^{N-1} P^{(n)}{}_{\omega} n \tag{77}$$

so that the $P^{(n)}$ thereby determined could be compared with the coefficients, $B^{(n)}/n!$, obtained for the perturbation expansion of the theory. A STEP-WISE MULTIPLE REGRESSION code* was used for these least-squares fits. Each data point was weighted by the inverse of its variance as determined by the error analysis. The code added one term of the above expressions at a time in the order of their importance to the "goodness of fit" of the power series to the experimental data. Terms were added as long as, and only if, their inclusion increased the "goodness of fit" by a statistically significant amount as determined by both the F-test and the specific level of significance specified by the input. By analyzing the data in this way,

---

* This code was obtained from the University of Florida Computer Center.

the answer to the difficult question of how many terms to include in the expansions was based upon dependable, statistical tests and not left to intuition.

It was found that for the $2\alpha\xi$ curve experimentally determined in this work only the $P^{(1)}$ and $P^{(3)}$ coefficients were statistically significant enough to be evaluated. In the $\alpha^2 - \xi^2$ curve the $P^{(0)}$, $P^{(2)}$, and $P^{(4)}$ coefficients were important enough to be determined. As a test of the accuracy of this method for the extraction of the $P^{(n)}$, the highest frequency points were progressively chopped from the data, 5 at a time; and the depleted data re-analyzed. The results of this procedure are shown in Figure 25 along with the theoretical predictions for their values as derived from the perturbation expansion. This very small variation of these $P^{(n)}$ can be interpreted in two ways:

(1) No space or energy mode contamination was present in the experimentally determined α and ξ.

(2) Space and energy mode contamination were present but combined in such a way that cancellation of their contamination occurred.

Although one would like for the actual situation to be correctly described by possibility (1), above, there is strong theoretical evidence, previously presented, to indicate the contrary. More realistically, one should

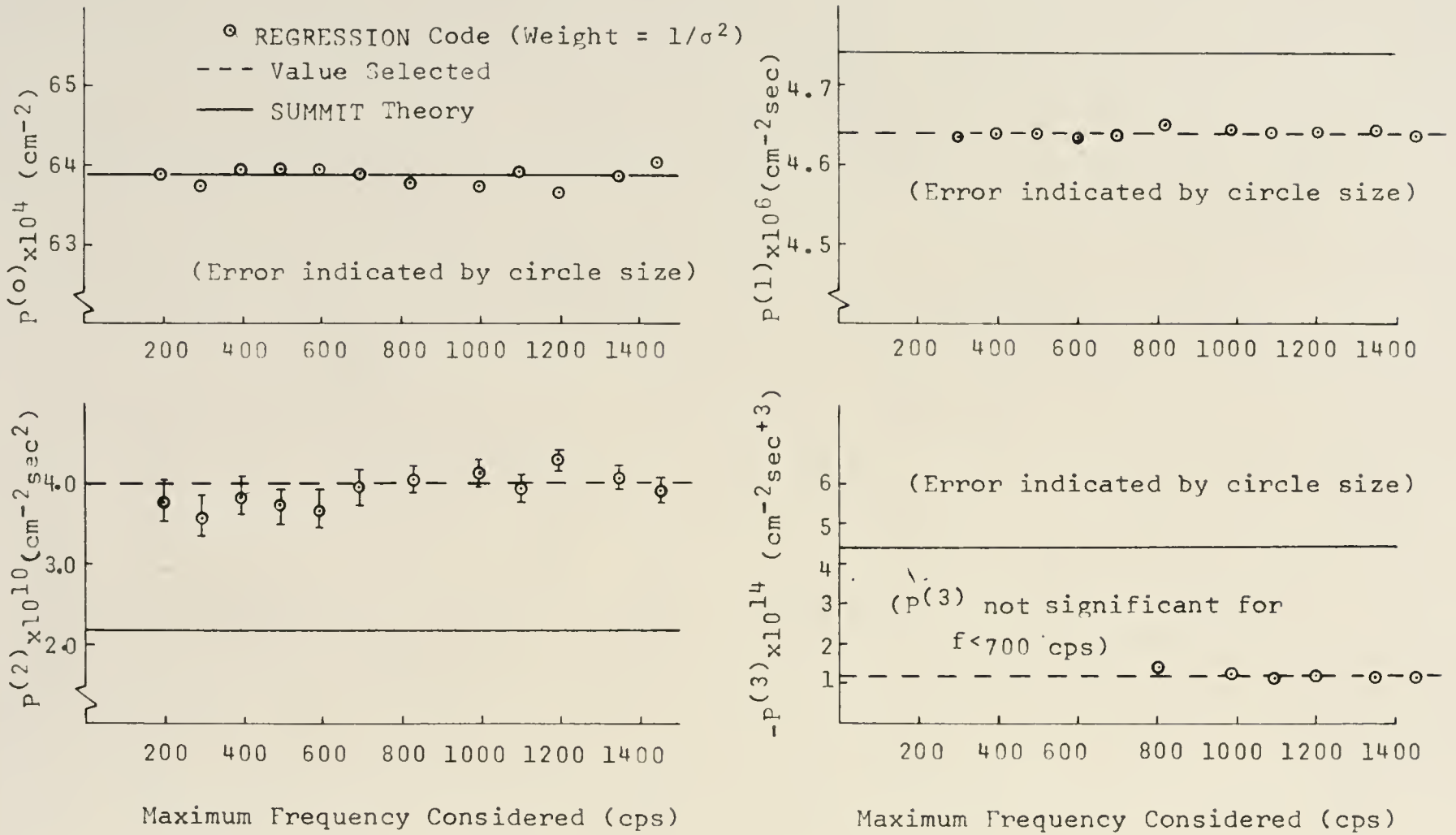

Fig. 25. The $P^{(n)}$ as a Function of the Maximum Frequency Included in the Least-Squares Fit.

expect that some modal contamination will exist in any neutron wave experiment. The main point of concern, therefore, is focused upon whether this contamination affected the final results.

Kunaish (18) has shown that for the heavy-gas kernel theoretical calculations confirm the fact that the higher spatial and energy modes can combine in such a way that the total flux propagates with a complex inverse relaxation length which is nearly equal to the one associated with the fundamental complex eigenvalue. Also, if higher mode contamination were present, the $P^{(n)}$ would be frequency dependent unless cancellation occurred. The above considerations have led the author to postulate that modal contamination was present in the measured data; but enough cancellation occurred so that it did not affect, or would not be detected by, the data analysis procedure.

From the information presented in Figure 25 and similar considerations associated with $P^{(4)}$, the best estimates for the values of the several $P^{(n)}$ determined are:

$$P^{(0)} = (63.86 \mp .09) \times 10^{-4} \text{ cm}^{-2}$$

$$P^{(1)} = (4.64 \mp .01) \times 10^{-6} \text{ sec cm}^{-2}$$

$$P^{(2)} = (3.92 \mp .09) \times 10^{-10} \text{ sec}^2\text{cm}^{-2}$$

$$P^{(3)} = -(1.02 \mp .07) \times 10^{-14} \text{ sec}^3\text{cm}^{-2}$$

$$P^{(4)} = -(11. \mp 1.) \times 10^{-18} \text{ sec}^4\text{cm}^{-2}$$

Application of Moore's Method to the Analysis of the Pulse Propagation Data

The MOORE MOMENTS code was used to determine the Fourier moments and widths of the pulse propagation data. Shown in Figures 26 and 27 are the real and imaginary components of $\bar{t}$ versus z for several of the frequencies analyzed. Consistent with Moore's prediction, these curves vary linearly with distance from the source. The slopes of these straight lines, ξ'* and α', were determined and are shown in Figure 28. Also shown are values of the derivatives as determined from numerical differentiation, using six order differences, of the α and ξ curves. It appears that at these lower frequencies the Fourier moments allow for a more accurate determination of the derivatives. From the four quantities α, ξ, α', and ξ', one can construct the first frequency derivatives of $\alpha^2-\xi^2$ and $2\alpha\xi$. The former should increase linearly with frequency with a slope of $2P^{(2)}$ until the $P^{(4)}$ term becomes significant, and the latter should be a constant at low frequencies with the value $P^{(1)}$. These quantities are shown in Figure 29, where it is evident that success in the determination of the first derivative of ρ^2 was limited to its imaginary component. The zero intercept of this curve yields a $P^{(1)}$ value of

---

* The prime as used here indicates derivative with respect to ω.

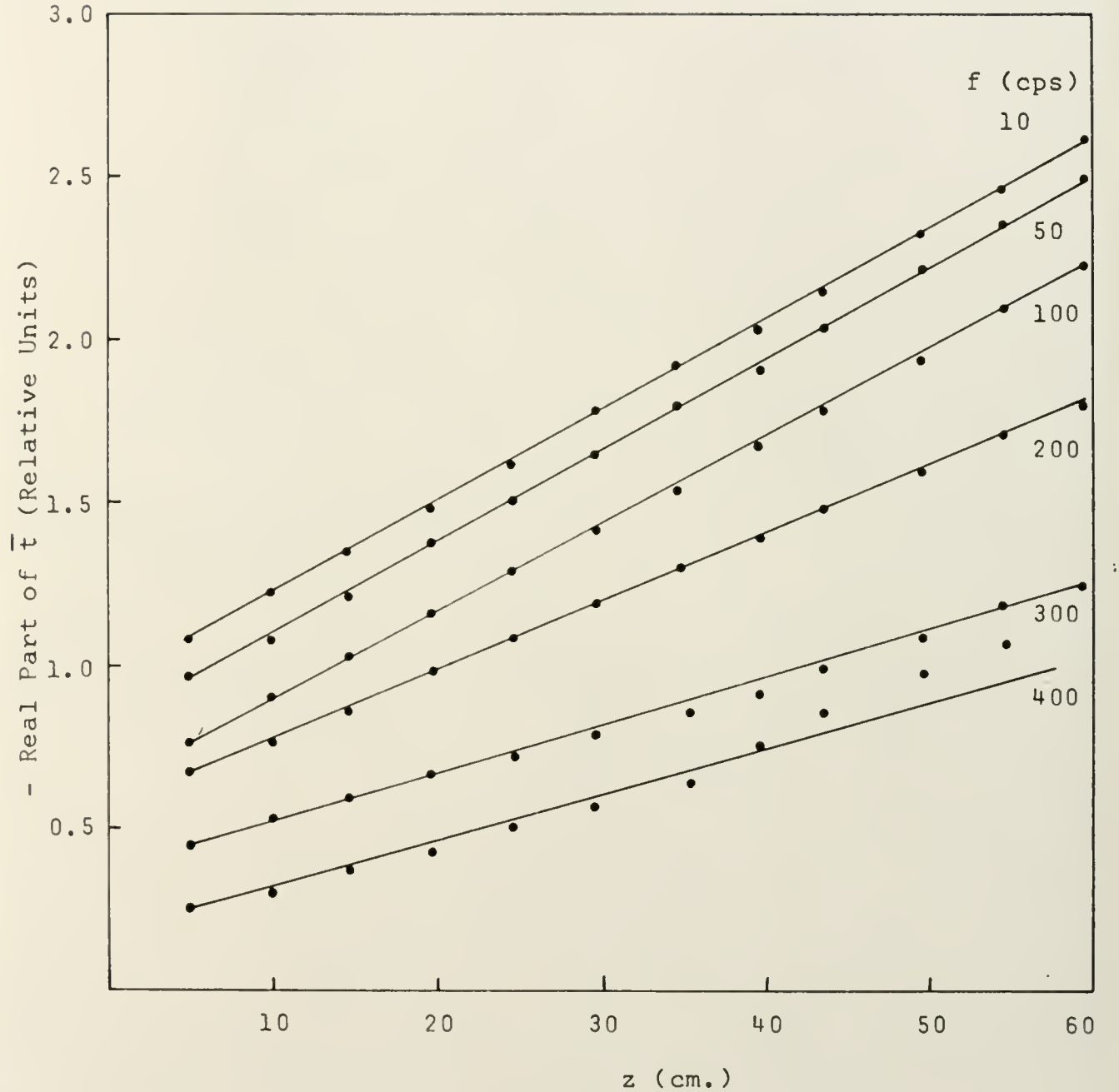

Fig. 26. The Experimentally Determined Real Part of $\bar{t}$ versus Distance from the Source.

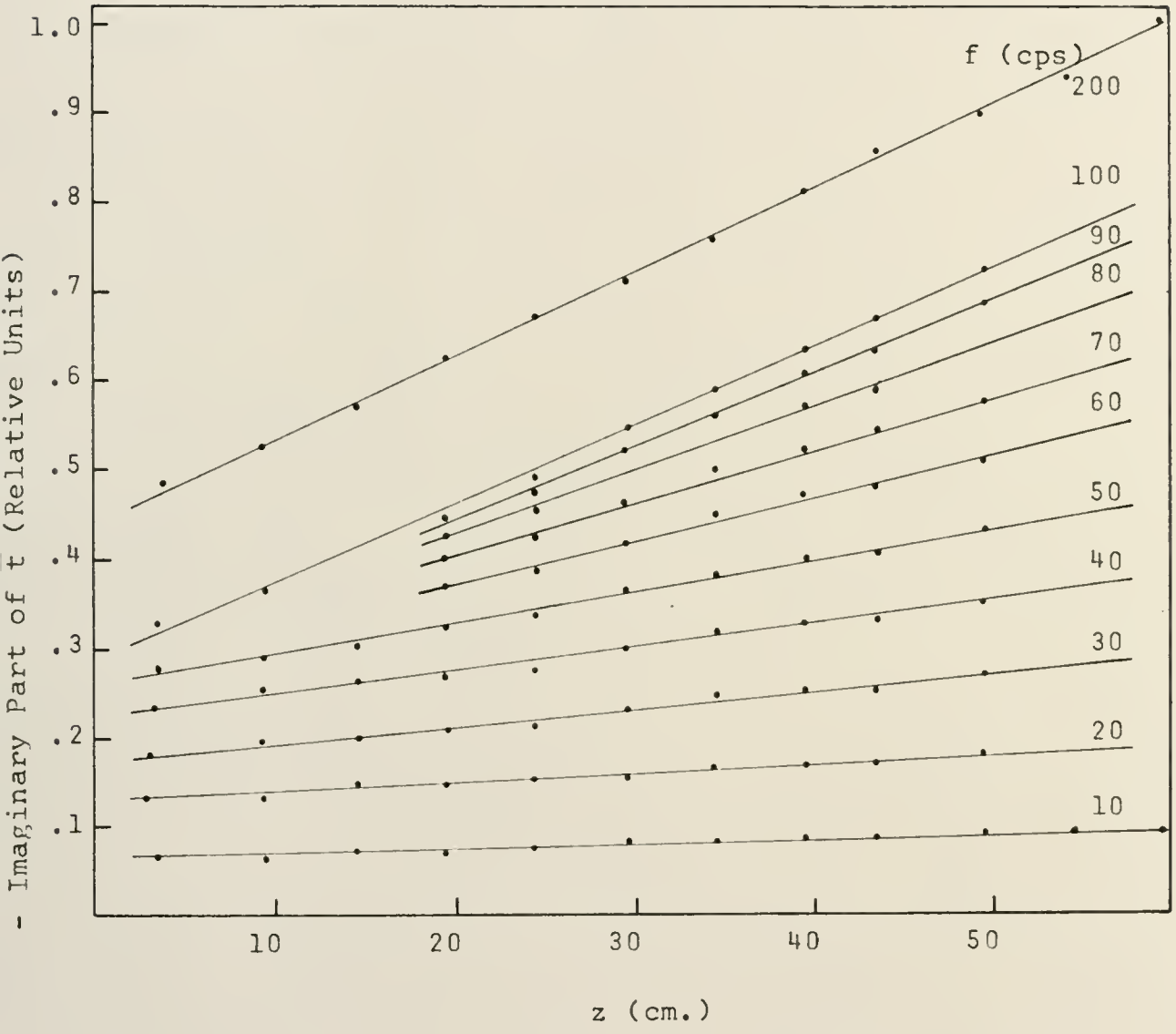

Fig. 27. The Experimentally Determined Imaginary Part of $\bar{t}$ versus Distance from the Source.

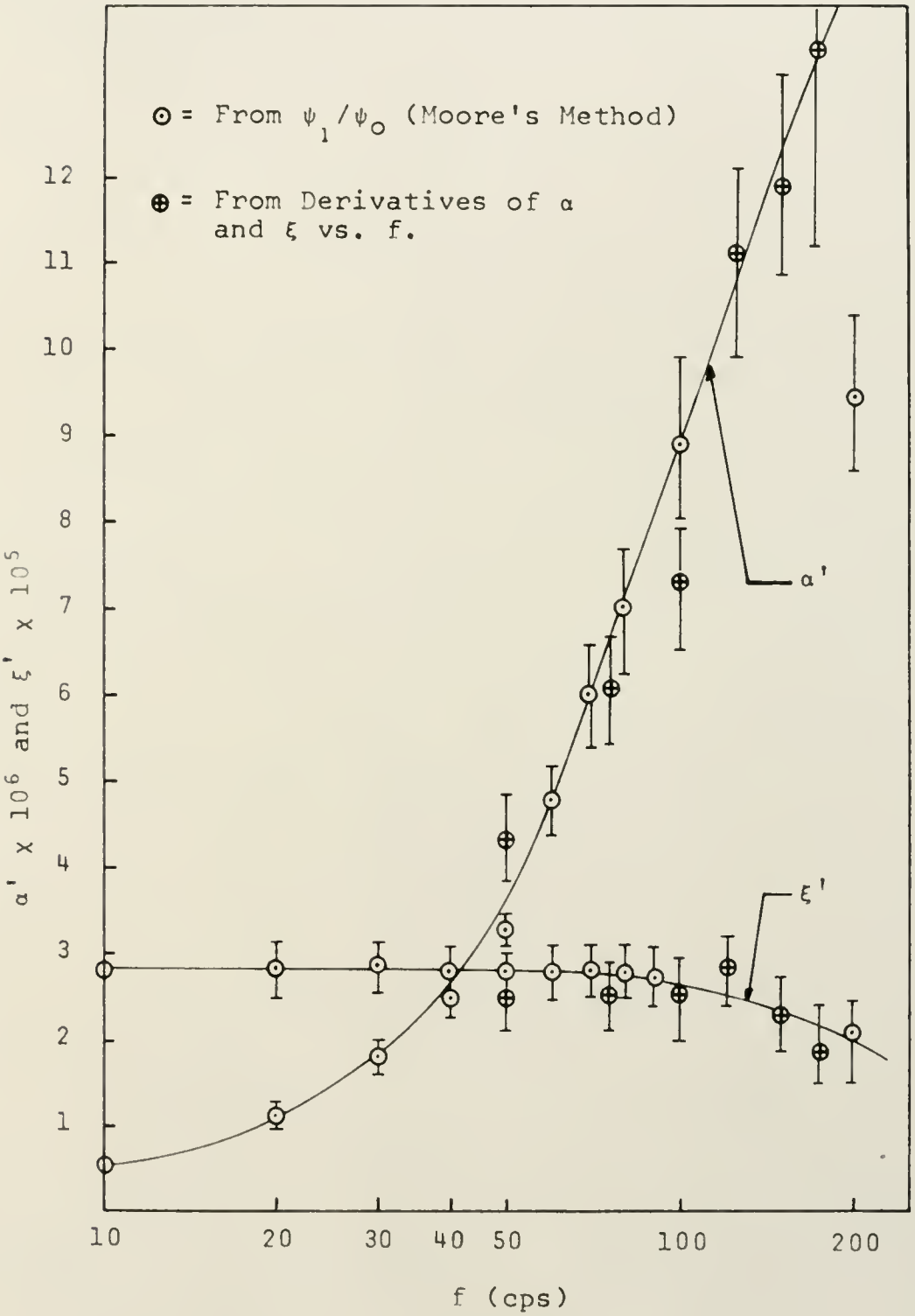

Fig. 28. The Experimentally Determined α' amd ξ' as a Function of Frequency.

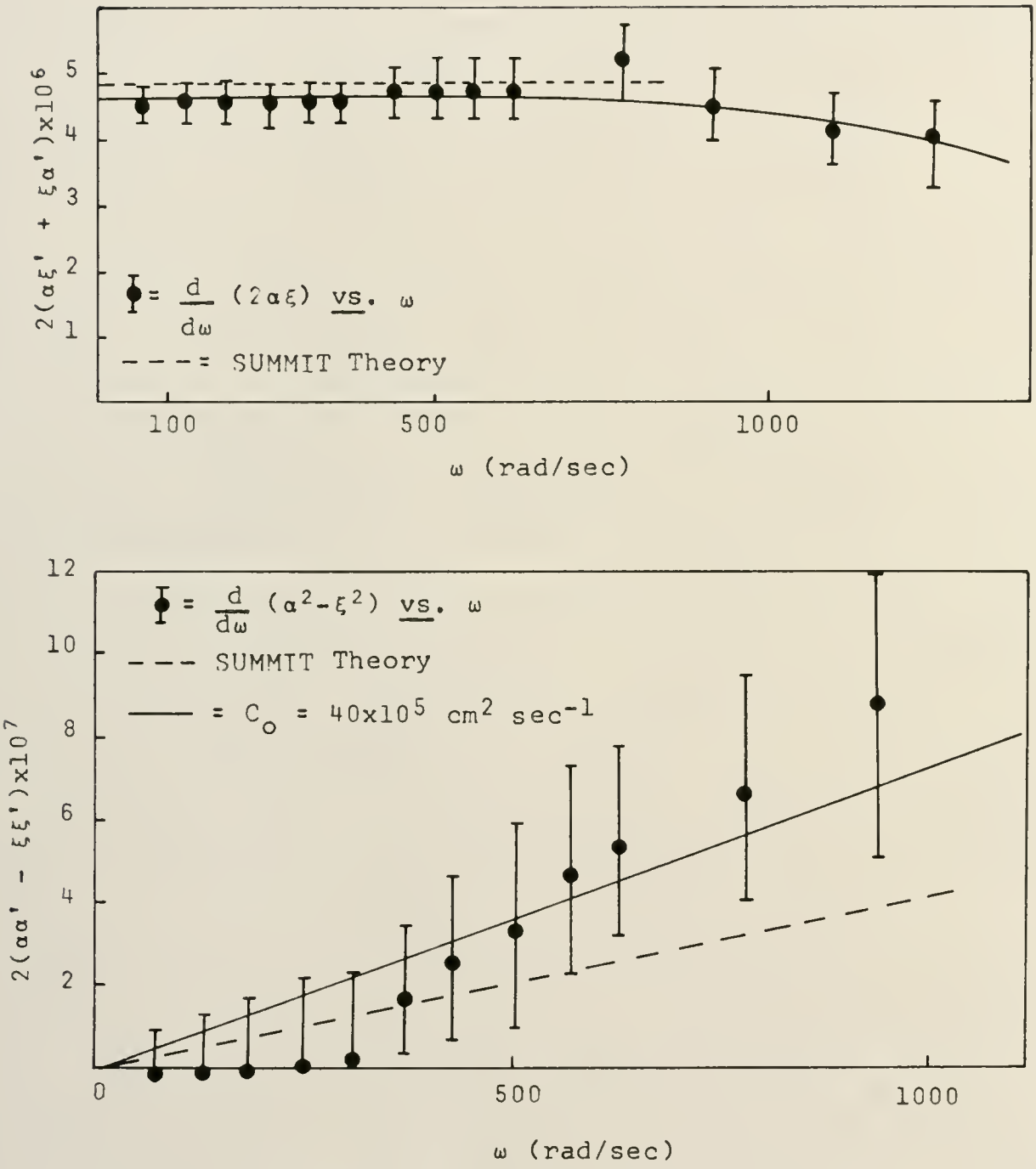

Fig. 29. First Frequency Derivatives of $2\alpha\xi$ and $\alpha^2 - \xi^2$ versus ω.

$(4.65 \pm .02) \times 10^{-6}$ sec cm^{-2}, which is in good agreement with the value obtained from the power series fit of $2\alpha\xi$. As in the case of the power series analysis, the curve from which $P^{(2)}$ is calculated, $2(\alpha\alpha' - \xi\xi')$, results from the difference of two nearly equal quantities. The error propagation associated with this calculation was more severe than the ones encountered in the determination of $P^{(1)}$ from the curve $2(\alpha'\xi + \xi'\alpha)$. An inspection of the relative magnitude of the parameters indicated that at these low frequencies $\alpha_o >> \xi_o$ and $\xi' >> \alpha'$. Thus the $(2\alpha\xi)'$ curve is dominated by the term $\alpha\xi'$, both of whose components are nearly constant in the frequency range considered. On the other hand, both the terms $\alpha\alpha'$ and $\xi\xi'$ from which the $(\alpha^2-\xi^2)'$ curve is formed are significant; and they contain terms which vary comparatively rapidly with frequency. It appears that difficulties are self-compensating for the $P^{(1)}$ calculation and amplified when $P^{(2)}$ is to be determined. Although this curve of $(\alpha^2-\xi^2)'$ shows the correct trend and agrees with reasonable values for $P^{(2)}$, it cannot be used for an accurate determination of this parameter. Similar results were obtained when the second derivative of ρ_R^2 (i.e., $(\alpha^2-\xi^2)''$) was calculated from α, α', α'', ξ, ξ' and ξ''. These second derivatives, α'' and ζ'', were determined from the linear variation of W_2 with frequency. The zero intercept of the

experimentally determined ρ_R'' yielded a value only within a factor of 2 of the expected value, with an error roughly equal to its magnitude.

The results of the analysis, however, appear encouraging. The experimental results confirm the validity of Moore's method of data analysis. It was found that the accuracy of the higher moments is strongly dependent upon the number of time channels used to describe the pulse and its foreground to background ratio. In this experiment, channel widths of 30 microseconds yielding 256 channels per pulse and ratios of about 1000 to 1 were used. Presently available techniques allow for significant improvements in both of these quantities, which would hopefully result in more accurate points for curves of ρ_R' and ρ_R'' from which $P^{(2)}$ could be calculated.

Coefficients of the Power Series Expansion Through Zero Frequency Extrapolation

Though not as sophisticated as the methods previously presented, the $P^{(0)}$, $P^{(1)}$, and $P^{(2)}$ coefficients can be calculated, respectively, from the zero frequency intercept of the curves α versus ω (intercept $[P^{(0)}]^{1/2}$), $\alpha^2-\xi^2$ (intercept $P^{(0)}$), $2\alpha\xi/\omega$ (intercept $P^{(1)}$), $(\alpha^2-\xi^2-P^0)/\omega^2$ (intercept $P^{(2)}$), and $[(\alpha^2+\xi^2)^2 - (P^{(0)})^2]/\omega^2$ (intercept $(P^{(1)})^2 + 2P^{(0)}P^{(2)}$). These curves were determined and

extrapolated to zero in an attempt to extract the coefficients. Use was first made of the α, $\alpha^2-\xi^2$, and $2\alpha\xi$ curves to determine $p^{(0)}$ and $p^{(1)}$. These values were then used in the determination of that value of $p^{(2)}$ which yielded the best intercepts for the latter two curves. $p^{(3)}$ was calculated from the slope of $2\alpha\xi/\omega$. Shown below are the $p^{(n)}$ as determined by this method.

$$p^{(0)} = (63.87 \pm .09) \times 10^{-4} \text{ cm}^{-2}$$

$$p^{(1)} = (4.64 \pm .05) \times 10^{-6} \text{ sec cm}^{-2}$$

$$p^{(2)} = +(3.8) \pm .3) \times 10^{-10} \text{ sec}^2\text{cm}^{-2}$$

$$p^{(3)} = -(1.0 \pm .3) \times 10^{-14} \text{ sec}^3\text{cm}^{-2}$$

Summary of the Experimental Results And Discussion Of the Error Analysis

Shown in Table 4 are theoretical values for the first four $p^{(n)}$ coefficients, along with the experimental values obtained by the various methods of data analysis presented in this chapter. It is clear from the table that consistent experimental values for the $p^{(n)}$ were obtained in every case and that theory and experiment began to diverge after $p^{(1)}$.

The determination of the errors associated with the α and ξ values was based upon the reproducibility of points on the amplitude and phase curves and the variation of α and ξ as the low z points were successively eliminated.

TABLE 4

THE EXPERIMENTAL AND THEORETICAL VALUES FOR THE $P^{(n)}$ COEFFICIENTS

Method	$P^{(n)}$ Coefficients				
	$10^4 \times P^{(0)}$ (cm^{-2})	$10^6 \times P^{(1)}$ ($sec\ cm^{-2}$)	$10^{10} \times P^{(2)}$ ($sec^2 cm^{-2}$)	$10^{14} P^{(3)}$ ($sec^3 cm^{-2}$)	$10^{18} \times P^{(4)}$ ($sec^4 cm^{-2}$)
Polynomial Fits of $2\alpha\xi$ and $\alpha^2 - \xi^2$	63.86 ±.09	4.64 ±.01	+3.92 ±.09	-1.02 ±.07	-11. ± 1.
Moore Moments	----	4.65 ±.02	----	----	---
Hand Extrapolations to $\omega=0$	63.87 ±.09	4.64 ±.05	+3.8 ±.3	-1.0 ±.3	---
SUMMIT Theory	63.884	4.7386	+2.1143	-4.4903	-28.969

These errors were found to be on the order of 1 per cent for the lower frequencies and about 5 per cent at the higher frequencies. A standard propagation of errors technique resulted in estimates of the errors associated with the experimental curves derived from α and ξ. The same procedure was used in the curves which were based upon the derivatives of α and ξ. Errors in the $P^{(n)}$ as listed are consistent with the ones calculated by the STEP-WISE MULTIPLE REGRESSION code.

CHAPTER VI

RELATIONSHIPS BETWEEN THE NEUTRON WAVE EXPERIMENT AND DIE-AWAY EXPERIMENT IN THE DETERMINATION OF DIFFUSION AND THERMALIZATION PARAMETERS

The main objective of this dissertation has been to demonstrate the effectiveness of the neutron wave technique for the determination of diffusion and thermalization parameters. In order to evaluate the fulfillment of this objective, the results obtained here for the experiment in graphite will be compared to published results of die-away experiments where the same parameters were measured. The various complementary relationships between the two experiments will also be investigated.

In the die-away experiment one measures the decay constant of the fundamental time and energy dependent eigenfunction of the Boltzmann operator associated with the fundamental spatial mode. The real eigenvalue, λ, is determined as a function of the system's lowest geometric buckling; and this λ versus B^2 curve yields the parameters of interest. Consistent with current terminology, this method will be referred to as a dynamic experiment. The neutron wave experiment, in contrast, is a static experiment (i.e., in the same class as the

poisoning experiment); and one measures the complex, fundamental eigenvalue, ρ, of the space and energy dependent Boltzmann operator as a function of frequency.

The complementary nature of the two experiments is expressed pictorially in Figure 30.* Shown in the first quadrant of the figure are results of a typical die-away experiment, and in the third quadrant the modulus of ρ^2 as determined in this work is plotted as a function of frequency up to 1000 cps. It is interesting to note that B^2, the independent variable of the die-away experiment, and $|\rho^2|$, the dependent variable of the neutron wave experiment, can be mathematically equated. This result is not surprising when one recalls that ρ is the complex eigenvalue associated with the space decay of the neutron wave and B^2 is the eigenvalue of the fundamental spatial dependence of the die-away experiment. One can also devise correlations between ω and time after the pulse in the die-away experiment. This is most easily explained if one considers the expansion of the energy dependence of the neutron wave experiment in the time-energy eigenvalues of the Boltzmann operator (i.e., the

---

* The die-away points were obtained from Reference (29).

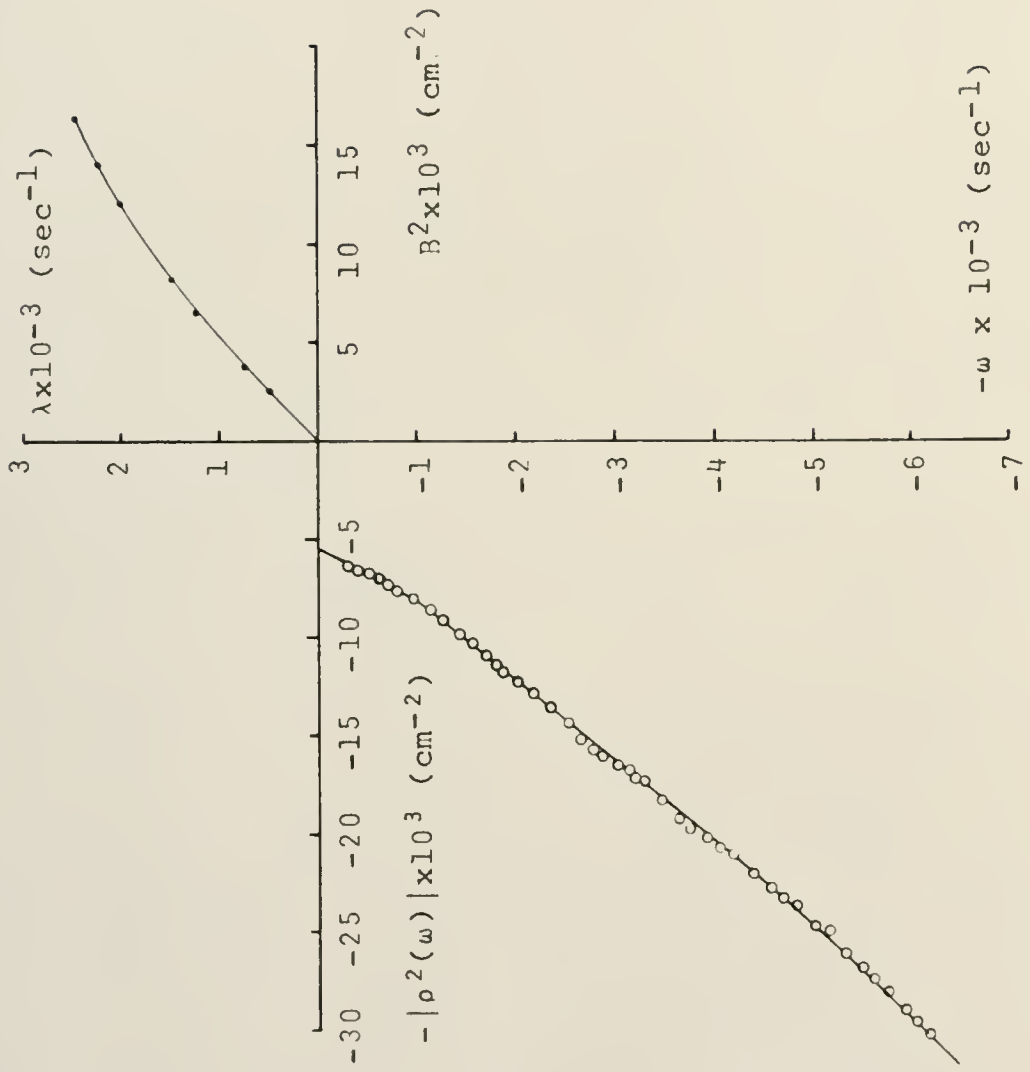

Fig. 30. A Pictorial Representation of the Die-Away and Neutron Wave Experiments.

energy modes of the die-away experiment).* If this expansion is used, very similar results to those previously presented are obtained. As frequency increases, the higher energy modes begin to contribute proportionally more to the total energy dependence which is dominated at low f by the fundamental energy mode. This is exactly the situation that exists at short times after the pulse in the die-away experiment. Thus in terms of energy mode contamination, frequency in the neutron wave experiment and time after the pulse in the die-away experiment are inversely related.

One can also represent the poisoning experiment in Figure 30. A curve very similar to the one associated with the wave experiment would be obtained if the poisoning experiment's squared inverse relaxation length is plotted on the same axis as $|\rho^2|$ and $\Sigma_p v_o$, the added poison times v, plotted with ω. It is for this reason that the $j\omega/v$ term of the neutron wave experiment is sometimes equated to a complex 1/v poison. Note also that the point on the figure which represents the conventional exponential experiment is common to both the

---

* This was actually done by the author for the MASSMK kernel using 45 energy points. The fundamental complex inverse relaxation length thereby obtained was in excellent agreement with the one presented in this work. This result indicates that 33 energy points are adequate for theoretical results to be compared with the experiment and that the energy expansion as presented was valid.

poisoning and neutron wave experiment and that it is represented as the $\omega=0$ or $\Sigma_p v=0$ intercept. Herein lies the justification for the reference of the space-energy eigenfunctions of the Boltzmann operator, used in the energy expansion of this dissertation, as eigenfunctions of the exponential experiment.

Perez and Uhrig (9) have shown that the eigenvalues, λ^w and ρ^2, are mathematically related when ρ^2 is expressed in the form

$$\rho^2 = B_\perp^2 + \sum_{n=1}^{N} Q^{(n)} \left(\frac{\alpha_o + j\omega}{D_o}\right)^n \tag{78}$$

and use is made of the relationships

$$j\omega = -\lambda^w \tag{79}$$

where the w superscript indicates that λ^w is the eigenvalue that is to be obtained from the $Q^{(n)}$ in a neutron wave experiment and

$$-\rho = jB_z \tag{80}$$

Substitution of the above transformation into equation (78) yields

$$-B^2 = -(B_z^2 + B_\perp^2) \sum_{n=1}^{N} Q^{(n)} \left(\frac{\alpha_o - \lambda^w}{v_o} \right)^n \qquad (81)$$

By inverting the series in $\left(\frac{\alpha_o - \lambda^w}{v_o}\right)$ to one in B^2, one obtains for N = 3

$$\lambda^w = \alpha_o + D_o^w B^2 - C_o^w B^4 + F_o^w B^6 \qquad (82)$$

where

$$\alpha_o = v_o \Sigma_{ao} \qquad (83)$$

$$D_o^w = v_o / Q^{(1)} \qquad (84)$$

$$C_o^w = -v_o Q^{(2)} / (Q^{(1)})^3 \qquad (85)$$

$$F_o^w = v_o / (Q^{(1)})^5 [2(Q^{(2)})^2 - Q^{(1)} Q^{(3)}] \qquad (86)$$

The coefficients as defined above differ slightly from the ones measured in the dynamic die-away experiment because they were derived from the static, wave experiment expressions.*

---

* In this context the difference between static and dynamic experiments is related to the effect upon the energy dependence of a 1/v absorber in the medium. In the die-away experiment a 1/v absorber does not affect the energy dependence of the fundamental eigenfunction (19) which, for zero buckling, is a Maxwellian. The fundamental eigenvalue of the exponential experiment is a Maxwellian distribution only in the zero absorption case. Thus the static and dynamic experiments are equivalent only when $\alpha_o = 0$ in the expressions for the static experiment.

In the analysis of data presented in the previous chapter, ρ^2 was expressed in the form

$$\rho^2 = \underset{\substack{n=0 \\ (\text{EVEN})}}{\sum^{N-1}} P^{(n)}\omega^n + j \underset{\substack{n=1 \\ (\text{ODD})}}{\sum^{N}} P^{(n)}\omega^n \tag{87}$$

From equations (78) and (87) the following connection between the $Q^{(n)}$ and $P^{(n)}$ coefficients is obtained with N=3

$$P^{(0)} = B_1^2 + \sum_{n=1}^{N} Q^{(n)}\left(\frac{\alpha_o}{v_o}\right)^n \tag{88}$$

$$P^{(1)} = \frac{1}{v_o}\left\{Q^{(1)} + 2\left(\frac{\alpha_o}{v_o}\right)Q^{(2)} + 3\left(\frac{\alpha_o}{v_o}\right)^2 Q^{(3)}\right\} \tag{89}$$

$$P^{(2)} = -\frac{1}{v_o^2}\left\{Q^{(2)} + 3\left(\frac{\alpha_o}{v_o}\right)Q^{(3)}\right\} \tag{90}$$

$$P^{(3)} = -\frac{1}{v_o^3} Q^{(3)} \tag{91}$$

The $Q^{(n)}$ and $\frac{\alpha_o}{v_o}$ obtained from the $P^{(n)}$ by the iterative use of these expresions can be used to determine D_o^w, C_o^w, and F_o^w. For the determination of these same parameters for comparison to die-away experiments by use of expressions (84), (85), and (86), the above expressions with $\alpha_o=0$ should be used to determine the $Q^{(n)}$.

Table 5(a) shows the values of α_o, $Q^{(1)}$, $Q^{(2)}$, and $Q^{(3)}$ obtained from the experimental data as well as theoretical results obtained by use of the SUMMIT kernel. In Table 5(b) these same parameters derived by the use of equations (89), (90), and (91) with α_o=0 are presented. From these two tables and equations (83), (84), (85), and (86), the values of both the static and dynamic α_o, D_o, C_o, and F_o parameters were calculated and are shown in Table 6. In Table 7 the values for the various diffusion and thermalization parameters that are to be compared with the die-away results are listed along with the results from several die-away experiments.* From an inspection of these tables one can conclude the following:

(1) The static and dynamic parameters differ by less than 5 per cent with most differences on the order of 1 per cent.

(2) The experimentally obtained diffusion

---

* D_o and C_o were also calculated using the SUMMIT kernel by Ohanian's method with both 33 points and 45 points in the discrete energy representation. The values obtained were: $D_o = (2.092) \times 10^5)$ cm sec^{-1}, $C_o = (20.9014 \times 10^5)$ $cm^2 sec^{-1}$, 33 points; $D_o = (2.1435 \times 10^5)$ cm sec^{-1}, $C_o = (21.128 \times 10^5)$ $cm^2 sec^{-1}$, 45 points. These values agree very well with the ones in Table 6 especially when one recalls that the time-energy eigenfunctions were used in the Ohanian method and the space-energy eigenfunctions were used in this work.

TABLE 5

THE EXPERIMENTAL AND THEORETICAL VALUES
FOR THE $Q^{(n)}$ COEFFICIENTS

	α_o/v_o	$Q^{(1)}$	$Q^{(2)}$	$Q^{(3)}_{\times 10^{-2}}$
EXPERIMENT (ρ = 1.60 gm/cm^3)	4.14 ± .03	1.036 ± .005	-19.1 ± .9	1.09 ± .05
THEORY (ρ = 1.60 gm/cm^3)	4.0965	1.0505	-10.9455	4.7682

(a) $\alpha_o \neq 0$

EXPERIMENT (ρ = 1.60 gm/cm^3)	----	1.020 ± .005	-19.0 ± .9	1.09 ± .05
THEORY	----	1.0415	-10.3595	4.7682

(b) α_o Set Equal to Zero to Calculate $Q^{(n)}$

TABLE 6

THE STATIC AND DYNAMIC PARAMETERS

	α_o sec^{-1}	$D_o \times 10^{-5}$ $cm^2 sec^{-1}$	$C_o \times 10^{-5}$ $cm^4 sec^{-1}$	$F_o \times 10^{-7}$ $cm^6 sec^{-1}$
EXPERIMENT (ρ = 1.60 gm/cm^3)	91. ± 1	2.12 ± .01	38. ± 2	12. ± 2
	Made zero to obtain $Q(n)$	2.16 ± .01	39. ± 2	12. ± 2
THEORY (ρ = 1.60 gm/cm^3)	90.04	2.0838	20.9110	-4.4891
	Made zero to obtain $Q(n)$	2.1104	20.1553	-5.0574

TABLE 7

PARAMETERS AS DETERMINED FROM VARIOUS DIE-AWAY EXPERIMENTS COMPARED WITH THE RESULTS OF THIS WORK

Year	Authors	$\alpha_o(sec^{-1})$	$D_o \times 10^{-5}$ $cm^2 sec^{-1}$	$C_o \times 10^{-5}$ $cm^4 sec^{-1}$	$F_o \times 10^{-7}$ $cm^8 sec^{-1}$
1961	Lalande	79.5±3*	2.07±.04	25.8±2	----
	Starr & Price				
1962	type GBF	74.6±.06	2.14±.01	34±3	----
	type AA	68.1±.08	2.19±.03	41±4	----
1962	Starr & de Villiers			38±5	----
1962	Klose et al.†	88.3±1.2	2.13±.02	26±5	----
		88.6±1.6	2.11±.02	16±5	-20±10
1963	Sagot et al. (30)	74.1±3	2.19±.03	37.9±4	----
1965	This work	91. ±1	2.16±.01	39. ±2	12.±2

* All values listed in the table have been corrected to a density of 1.60 gm/cm^3.

† Both the three and four parameter fits are included.

coefficient agrees quite well with those of pulsed experiments and with the theory.

(3) The value obtained in this work for the cooling coefficient, C_o, is about a factor of two higher than the one predicted by use of the SUMMIT kernel but is in very good agreement with the more recent die-away results. However, this result is still somewhat lower than the lower bound of 45 x 10^5 $cm^4 sec^{-1}$ predicted for C_o by de Saussure (31).

(4) The value of F_o obtained experimentally differs both in sign and magnitude from the one predicted here by the use of the SUMMIT kernel. It also disagrees both in sign and magnitude with the value obtained by Klose, et al. (32). Honeck (33) used the SUMMIT kernel and obtained a value of of -7.44 x 10^7 $cm^6 sec^{-1}$ for F_o. However, Nelkin (34) predicts a positive coefficient of the order of C_o^2/D_o which is consistent with equation (86) if one neglects the contribution of $Q^{(3)}$. An inspection of equation (86) indicates that the sign of F_o is determined by the magnitude of $2(Q^{(2)})^2$ compared to $Q^{(1)}Q^{(3)}$. The solution to this contradiction awaits more exacting theoretical and experimental work.

CHAPTER VII

CONCLUSIONS AND RECOMMENDATIONS

The space, energy, and time or frequency dependent Boltzmann equation in the diffusion approximation has been used within the framework of neutron thermalization theory to predict thermal neutron wave propagation in a moderating medium. This theory was then compared with the experiment conducted on a graphite pile.

In the theoretical section the energy dependence was expanded in the space-energy eigenfunctions of the Boltzmann operator, and the transverse-space dependence was expanded in the orthogonal solutions to the Helmholtz equation with homogeneous boundary conditions. It was then shown that each of these space and energy modes thus formed propagates with characteristic complex inverse relaxation lengths. The perturbation method developed by Perez was used to expand these complex eigenvalues in a Maclaurin's series of the frequency variable. In cases where this series did not rapidly converge, a direct solution of the complex secular determinant was obtained. Two scattering kernels were selected for implementation into the theory, the MASSMK kernel and the SUMMIT kernel, which is based primarily upon derivations by

Parks (22). The numerical calculations of the theory were performed on an IBM 709 digital computer and founded upon the previous work of Ohanian (19).

In the experimental section an accurate technique for conducting neutron wave experiments in multiplying or diffusing media was presented along with the results of the graphite experiment. The excitation of neutron waves, both by modulated and pulsed sources, and the electronic systems associated with their detection were discussed. Special attention was given to the analysis of data for which several computer codes were developed.

In the comparison of theory and experiment it was shown that the neutron wave technique allows for the separation of diffusion and thermalization effects, thereby yielding a more exacting comparison of theoretical and experimental results. Polynomial fits of functions formed from the experimental results yielded coefficients to be compared with the theoretically derived terms of the perturbation expansion. The results of the thermal pulse propagation experiment were also analyzed by a method suggested by Moore, and confirmation of his predictions was established.

The diffusion and thermalization parameters determined from the data analysis were then compared with results of several die-away experiments and with the theory. The

complementary relationships between the neutron wave and die-away experiments were also presented.

The more significant results of this dissertation are listed below:

A. It was demonstrated that the neutron wave technique is a very powerful method for the determination of thermalization and diffusion parameters.

B. The numerical methods developed by Ohanian for the determination of the time-energy eigenfunctions of the Boltzmann operator and investigation of the die-away experiment were successfully applied to the determination of the space-energy eigenfunctions of the Boltzmann operator. It was shown that these latter eigenfunctions are especially well suited for theoretical studies of the neutron wave experiment.

C. Higher energy mode contamination of the fundamental complex inverse relaxation length is predicted by the SUMMIT scattering kernel for frequencies above 300 cps when the transverse buckling is on the order of 6×10^{-4} cm^{-2}. The frequency at which this contamination becomes significant is dependent upon the transverse buckling, and its severity is not predicted by less accurate scattering kernels than the one incorporated into the SUMMIT code.

D. The experimental equivalence of excitation of neutron waves by either modulated or pulsed sources

has been confirmed. It was found that, in general, the thermal pulse propagation technique is more useful; but it is recommended that the results thereby obtained be always "spot checked" by the use of a modulated source. The advantages inherent in these two methods are listed below:

(1) Advantages of the modulated source.

(a) It is much simpler to check the accuracy of the experimental results and the accuracy of the method of data analysis.

(b) Hand calculations and integral count methods can be used to analyze the data.

(c) Resonance phenomena can be more easily detected. One could, for example, set the input to the resonance point through hand calculations of the output at several frequencies or, perhaps, by analog circuits connected to a continuous representation of the sinusoidally varying count rate.

(d) A sinusoidal source is very useful when crosscorrelation techniques are to be applied. In some measurements one cannot, or does not want to, perturb the flux to any significant degree. For this situation a sinusoidal input together with cross-correlation methods of data analysis may prove to be useful.

(e) The data analysis is not complicated by the approximation of a Fourier transform with a finite numerical integration.

(2) Advantages of the thermal pulsed source.

(a) One is able to extract many frequency points on the system's transfer function from a single measurement in the system.

(b) The system's response to thermal pulses can be used as suggested by Moore to determine derivatives of the complex inverse relaxation length directly from the experimental results.

(c) The epicadmium background and room return are present only at the beginning of the thermal pulse. Therefore, less elaborate methods are needed for the subtraction of these unwanted effects.

(d) The D.C. background can be made as small as the neutron generator will allow. Ratios of 1000 to 1 have been obtained here while with a modulated source the maximum ratio is 1 to 1. For this reason one can generally detect more decades of decay of frequencies excited by a thermal pulse source than those from a modulated source.

(e) Reflection of thermal pulses at an interface may prove to be a very useful way for testing various interface boundary conditions.

E. The predictions by Moore in his suggested method of analysis of thermal pulse propagation data have been experimentally verified.

F. The relationships between the die-away and neutron wave experiments and, in general, between dynamic and static experiments have been more clearly defined through the theoretical work presented here combined with the previous work of Ohanian (19).

G. In connection with the comparison of experimental work previously done in neutron wave propagation in moderating media, the following extensions have been made.

1. A neutron generator has been used with an electronically varied source intensity rather than mechanical sources. This increases the frequency range where data can be obtained and allows for simpler expressions for the spatial dependence of the source.

2. The data analysis is based upon Fourier series expansions of Fourier transforms rather than upon the area method. The Fourier method used here allows for more accurate source normalizations (independent of frequency harmonic distortion) and more exacting extraction of the amplitude and phase values.

3. The experiment, because of the above extensions, has been applied to the thermalization problem. Previous experimentalists concentrated upon diffusion effects.

It is evident from the results presented in this dissertation and from those summarized in the Review of the Literature that much more can still be done in the area of neutron wave experimentation. A logical extension of the theory presented here is to make the more exacting comparison between theory and experiment by generating a "theoretical experiment." That is, to synthesize the frequency, space, and energy dependent flux predicted by the theory for several ω and z values and compare this result to the experimental measurements. It was assumed here that the behavior of the complex eigenvalue associated with the measured flux was well represented by the fundamental eigenvalue. This assumption was shown to be valid for low frequencies for the experiment presented but of questionable validity at high frequencies.

The experiment could be improved in several ways. First, it is expected that less energy mode contamination

would be present if a larger system were investigated. In the experiment presented, the transverse leakage was much larger than the zero intercepts of the complex inverse relaxation lengths associated with the various energy modes. If the opposite were true, differences in these intercepts would cause a proportionally wider spread in the various ρ's at low frequency, thereby causing cross-over points of the α curves versus frequency to occur at higher frequencies. Improvements can also be made in the error analysis which, for this work, could have been biased by the lack of consistent statistical techniques. The fact that little variation was observed in the ρ's as determined by the variance-weighted, STEP-WISE MULTIPLE REGRESSION code could have been fortuitous. More confidence could have been placed in this result if the weights had been more rigorously determined.

Significant improvements can be made in the attainment of pulse propagation data to be analyzed by the method suggested by Moore. The refinements which appear to be most profitable are decreasing the channel width of the multi-channel analyzer, increasing the peak to background ratio of the pulse, and decreasing the pulse width.

Much can also be done to improve the source used for the experiment. A thermal source of a single energy, as can be obtained by use of a Van de Graaff accelerator,

is surely more desirable than the neutron generator and thermalizing tank used for this work. Also, the elimination of higher spatial modes by use of a source which contains only the fundamental spatial mode is of unquestionable value.

The extension of the neutron wave technique to other areas of application has already begun. Some of these areas are listed for completeness:

(1) The data analysis and experimental technique discussed here could be applied to fast waves and fast systems. In fact, a good starting point for this investigation could be the analysis of the epicadmium pulse propagation data as detected in the experiment done by Hartley.

(2) Some work has been done with respect to the propagation of neutron waves in heterogeneous assemblies. It is hoped that neutron waves will be sensitive to the lattice parameters associated with these assemblies.

(3) The most obvious extension of this work has been applied by several experimentalists. It is the investigation of thermal multiplying systems by the neutron wave technique. Still, much can and surely will be done in this area in the future.

LIST OF REFERENCES

1. A. M. Weinberg and H. C. Schweinler, "Theory of Oscillating Absorber in a Chain Reactor," Physical Review, 74, 851-863 (1948).

2. A. M. Weinberg and E. P. Wigner, The Physical Theory of Neutron Chain Reactors, University of Chicago Press, Chicago (1958).

3. V. Raievski and J. Horowitz, "Determination of the Mean Transfer Free Path of Thermal Neutrons by Measurement of the Complex Diffusion Length," Proceedings of the International Conference on the Peaceful Uses of Atomic Energy - Geneva. 1955, 5, 42-51, United Nations, New York (1956).

4. R. E. Uhrig, "Neutron Waves in a Subcritical Assembly," Transactions of the American Nuclear Society, 2, 71-80 (1959).

5. R. E. Uhrig, "Oscillating Techniques in a Subcritical Assembly," Proceedings of the University Subcritical Assemblies Conference, 1961, TID-7619, 161-182 (1962).

6. R. E. Uhrig, "Operating Characteristics of a Graphite Moderated Subcritical Assembly," Nuclear Science and Engineering, 5, 120-126 (1959).

7. H. L. Hussmann, "Characteristics of Neutron Waves in a Subcritical Assembly," Master's Thesis, Iowa State University of Science and Technology (1960).

8. R. S. Booth, "Neutron Wave Propagation in a Subcritical Assembly," Master's Thesis, University of Florida (1962).

9. R. B. Perez and R. E. Uhrig, "Propagation of Neutron Waves in Moderating Media," Nuclear Science and Engineering, 17, 90-100 (1963).

10. R. B. Perez, R. S. Booth, and R. H. Hartley, "Experimentation with Thermal Neutron Wave Propagation," Transactions of the American Nuclear Society, 6, 287-288 (1963).

11. E. Starr and G. A. Price, "Measurement of the Diffusion Parameters of Graphite and Graphite-Bismuth by Pulsed Neutron Methods," Proceedings of the Brookhaven Conference on Neutron Thermalization, BNL 715 (C-32), 1034-1073 (1962).

12. R. B. Perez, R. S. Booth, R. S. Denning, and R. H. Hartley, "Propagation of Neutron Waves in Subcritical Assemblies," Transactions of the American Nuclear Society, 7, 49-50 (1964).

13. R. S. Denning, R. S. Booth, and R. B. Perez, "The Demonstration of Thermalization Effects by the Reflection of Neutron Waves," Transactions of the American Nuclear Society, 7, 229-230 (1964).

14. R. H. Hartley, "Propagation and Detection of Pulses of Thermal Neutrons," Master's Thesis, University of Florida (1964).

15. G. H. Miley and P. K. Doshi, "Reactor-Pulse Propagation through Graphite," Transactions of the American Nuclear Society, 7, 45-46 (1964).

16. M. N. Moore, "The Propagation of Neutron Bursts and the Determination of the System Dispersion Law," Transactions of the American Nuclear Society, 7, 278-279 (1964).

17. M. N. Moore, "The Dispersion of Thermal Neutron Pulses in Neutronic Systems," to be published in Nuclear Science and Engineering.

18. H. H. Kunaish, "Time-, Energy-, and Space-Dependent Neutron Thermalization Theory," Ph.D. Dissertation, University of Florida (1964).

19. M. J. Ohanian, "Eigenfunction Analysis of Hydrogenous Neutron Spectra," Ph.D. Dissertation, Rensselaer Polytechnic Institute (1963).

20. M. J. Ohanian and P. B. Daitch, "Eigenfunction Analysis of Thermal-Neutron Spectra," Nuclear Science and Engineering, 19, 343-352 (1964).

21. S. G. Mikhlin, Integral Equations and Their Applications to Certain Problems in Mechanics, Mathematical Physics, and Technology, Pergamon Press, New York (1957).

22. D. E. Parks, The Calculation of Thermal-Neutron Scattering Kernels in Graphite, GA-2438, OTI-131 (1962).

23. N. F. Wikner, G. D. Joanou, and D. E. Parks, "Neutron Thermalization in Graphite," Nuclear Science and Engineering, 19, 108-129 (1964).

24. J. Bell, SUMMIT, an IBM-7090 Program for the Computation of Crystalline Scattering Kernels, GA-2492, (1962).

25. M. J. Ohanian, Private Communication (1964).

26. R. B. Razminas, "The Application of Variational Methods to Neutron Thermalization Problems," Ph.D. Dissertation, University of Florida (1965).

27. J. B. Scarborough, Numerical Mathematical Analysis, Johns Hopkins Press, Baltimore (1950).

28. R. G. Cockrell, "A Description of the UF-NLLS University of Florida Non-Linear Least Squares Code," Nuclear Engineering Department Internal Report (1963).

29. K. H. Beckurts, "Transient Effects in Space, Time, and Energy," Proceedings of the Brookhaven Conference on Neutron Thermalization, BNL 719 (C-32), RE-1-RE-62 (1962).

30. M. Sagot et al., "Technique des Neutrons Pulsés Appliquée aux Assemblages Critiques et Sous-Critiques," Proceedings of the Symposium on Exponential and Critical Experiments Held by the International Atomic Energy Agency in Amsterdam, Netherlands, 2-6 September 1963, 3, 163-189 (1964).

31. G. de Saussure, "The Neutron Asymptotic Decay Constant in a Small Crystalline Moderator Assembly," Proceedings of the Brookhaven Conference on Neutron Thermalization, BNL 719 (C-32), 1158-1174 (1962).

32. H. Klose, M. Kuchle, and W. Reichardt, "Pulsed Neutron Measurements on Graphite," Proceedings of the Brookhaven Conference on Neutron Thermalization, BNL 719 (C-32), 935-945 (1962).

33. H. C. Honeck, "On the Calculation of Thermal Neutron Diffusion Parameters," Proceedings of the Brookhaven Conference on Neutron Thermalization, BNL 719 (C-32), 1186-1210 (1962).

34. M. Nelkin, "The Diffusion Cooling of Neutrons in a Finite Moderator," Journal of Nuclear Energy, 8, 48-58 (1958).

APPENDIX

RESULTS OF THE DATA ANALYSIS

This Appendix is divided into three parts. In Part 1 the amplitude and phase of the neutron wave versus distance from the source is listed for all of the frequencies analyzed. The error associated with these data has been estimated to be about 1 per cent. Generally, results of the wave experiments are listed first and followed by points obtained from the pulse propagation experiment. These data were used on the final channel chop sequence from which the real and imaginary components of the complex inverse relaxation length were determined. The data have been normalized to the first z position at which measurements were made which was always within five and usually about two centimeters from the source boundary.

In Part 2 the real and imaginary components of the complex inverse relaxation length (slopes of the curves of Part 1) are shown along with their error estimates for each of the frequencies analyzed. The squared complex inverse relaxation length is shown in Part 3 for each frequency analyzed. Error estimates are also shown.

PART I AMPLITUDE AND PHASE CURVES

RESULTS OF 10. CPS. DATA ANALYSIS

POSITION	AMPLITUDE	PHASE
0.	0.1000E 01	0.
0.5010E 01	0.6208E 00	0.7600E-02
0.9890E 01	0.4114E-00	0.1550E-01
0.1489E 02	0.2539E-00	0.2440E-01
0.1978E 02	0.1770E-00	0.3240E-01
0.2478E 02	0.1092E-00	0.4240E-01
0.2968E 02	0.7470E-01	0.5170E-01
0.3467E 02	0.4901E-01	0.5970E-01
0.3857E 02	0.3845E-01	0.6580E-01
0.4445E 02	0.2366E-01	0.7670E-01
0.4946E 02	0.1588E-01	0.8510E-01
0.5434E 02	0.1088E-01	0.9460E-01
0.5934E 02	0.7392E-02	0.1022E-00

RESULTS OF 15. CPS. DATA ANALYSIS

PUSITION	AMPLITUDE	PHASE
0.	0.1000E 01	0.
0.5010E 01	0.6208E 00	0.1141E-01
0.9890E 01	0.4113E-00	0.2336E-01
0.1489E 02	0.2539E-00	0.3672E-01
0.1978E 02	0.1770E-00	0.4870E-01
0.2478E 02	0.1092E-00	0.6371E-01
0.2968E 02	0.7464E-01	0.7758E-01
0.3467E 02	0.4898E-01	0.8956E-01
0.3857E 02	0.3842E-01	0.9883E-01
0.4445E 02	0.2364E-01	0.1152E-00
0.4946E 02	0.1586E-01	0.1277E-00
0.5434E 02	0.1087E-01	0.1420E-00
0.5934E 02	0.7383E-02	0.1533E-00

RESULTS OF 25. CPS. DATA ANALYSIS

PUSITION	AMPLITUDE	PHASE
0.	0.1000E 01	0.
0.5010E 01	0.6156E 00	0.1909E-01
0.9890E 01	0.4078E-00	0.3909E-01
0.1489E 02	0.2516E-00	0.6139E-01
0.1978E 02	0.1753E-00	0.8139E-01
0.2478E 02	0.1081E-00	0.1064E-00
0.2968E 02	0.7386E-01	0.1295E-00
0.3467E 02	0.4845E-01	0.1495E-00

0.3857E 02	0.3800E-01	0.1651E-00
0.4445E 02	0.2337E-01	0.1924E-00
0.4946E 02	0.1568E-01	0.2134E-00
0.5434E 02	0.1074E-01	0.2370E-00
0.5934E 02	0.7291E-02	0.2560E-00

RESULTS OF 50. CPS. DATA ANALYSIS

POSITION	AMPLITUDE	PHASE
0.	0.1000E 01	0.
0.5010E 01	0.6199E 00	0.3830E-01
0.9890E 01	0.4099E-00	0.7840E-01
0.1489E 02	0.2524E-00	0.1232E-00
0.1978E 02	0.1757E-00	0.1637E-00
0.2478E 02	0.1080E-00	0.2134E-00
0.2968E 02	0.7356E-01	0.2594E-00
0.3467E 02	0.4820E-01	0.3001E-00
0.3857E 02	0.3780E-01	0.3318E-00
0.4445E 02	0.2316E-01	0.3862E-00
0.4946E 02	0.1556E-01	0.4291E-00
0.5434E 02	0.1061E-01	0.4761E-00
0.5934E 02	0.7186E-02	0.5147E 00

RESULTS OF 65. CPS. DATA ANALYSIS

POSITION	AMPLITUDE	PHASE
0.	0.1000E 01	0.
0.5010E 01	0.6190E 00	0.5047E-01
0.9890E 01	0.4086E-00	0.1028E-00
0.1489E 02	0.2510E-00	0.1611E-00
0.1978E 02	0.1744E-00	0.2140E-00
0.2478E 02	0.1069E-00	0.2783E-00
0.2968E 02	0.7264E-01	0.3376E-00
0.3467E 02	0.4752E-01	0.3912E-00
0.3857E 02	0.3724E-01	0.4331E-00
0.4445E 02	0.2275E-01	0.5035E 00
0.4946E 02	0.1528E-01	0.5603E 00
0.5434E 02	0.1039E-01	0.6209E 00
0.5934E 02	0.7017E-02	0.6716E 00

RESULTS OF 75. CPS. DATA ANALYSIS

POSITION	AMPLITUDE	PHASE
0.	0.1000E 01	0.
0.5010E 01	0.6181E 00	0.5840E-01
0.9890E 01	0.4073E-00	0.1187E-00
0.1489E 02	0.2498E-00	0.1859E-00
0.1978E 02	0.1733E-00	0.2480E-00
0.2478E 02	0.1060E-00	0.3209E-00

0.2968E 02	0.7185E-01	0.3890E-00
0.3467E 02	0.4694E-01	0.4512E-00
0.3857E 02	0.3676E-01	0.5002E 00
0.4445E 02	0.2240E-01	0.5810E 00
0.4946E 02	0.1504E-01	0.6473E 00
0.5434E 02	0.1019E-01	0.7179E 00
0.5934E 02	0.6873E-02	0.7758E 00

RESULTS OF 100. CPS. DATA ANALYSIS

POSITION	AMPLITUDE	PHASE
0.	0.1000E 01	0.
0.5010E 01	0.6150E 00	0.7745E-01
0.9890E 01	0.4031E-00	0.1572E-00
0.1489E 02	0.2457E-00	0.2460E-00
0.1978E 02	0.1696E-00	0.3277E-00
0.2478E 02	0.1030E-00	0.4236E-00
0.2968E 02	0.6933E-01	0.5124E 00
0.3467E 02	0.4504E-01	0.5964E 00
0.3857E 02	0.3516E-01	0.6633E 00
0.4445E 02	0.2124E-01	0.7690E 00
0.4946E 02	0.1425E-01	0.8602E 00
0.5434E 02	0.9561E-02	0.9506E 00
0.5934E 02	0.6401E-02	0.1030E 01

RESULTS OF 110. CPS. DATA ANALYSIS

POSITION	AMPLITUDE	PHASE
0.	0.1000E 01	0.
0.4000E 01	0.7123E 00	0.8506E-01
0.8890E 01	0.4779E-00	0.1788E-00
0.1289E 02	0.3337E-00	0.2535E-00
0.1778E 02	0.2194E-00	0.3622E-00
0.2667E 02	0.1001E-00	0.5001E 00
0.2178E 02	0.1446E-00	0.4134E-00
0.3067E 02	0.6564E-01	0.5902E 00
-0.1089E 02	-0.2848E 01	-0.1794E-00
-0.5880E 01	-0.1747E 01	-0.9476E-01
-0.1000E 01	-0.1142E 01	-0.7700E-02
0.4000E 01	0.6942E 00	0.8920E-01
0.8890E 01	0.4779E-00	0.1788E-00
0.1389E 02	0.2893E-00	0.2830E-00
0.1879E 02	0.1941E-00	0.3795E-00
0.2378E 02	0.1257E-00	0.4719E-00
0.2768E 02	0.9796E-01	0.5460E 00
0.3356E 02	0.5897E-01	0.6610E 00
0.3857E 02	0.3948E-01	0.7623E 00
0.4345E 02	0.2638E-01	0.8604E 00
0.4845E 02	0.1759E-01	0.9486E 00

RESULTS OF 125. CPS. DATA ANALYSIS

POSITION	AMPLITUDE	PHASE
0.	0.1000E 01	0.
0.5010E 01	0.6112E 00	0.9480E-01
0.9890E 01	0.3979E-00	0.1923E-00
0.1489E 02	0.2407E-00	0.3007E-00
0.1978E 02	0.1650E-00	0.4014E-00
0.2478E 02	0.9940E-01	0.5174E 00
0.2968E 02	0.6637E-01	0.6247E 00
0.3467E 02	0.4276E-01	0.7292E 00
0.3857E 02	0.3319E-01	0.8143E 00
0.4445E 02	0.1986E-01	0.9419E 00
0.4946E 02	0.1325E-01	0.1058E 01
0.5434E 02	0.8792E-02	0.1167E 01
0.5934E 02	0.5825E-02	0.1267E 01

RESULTS OF 150. CPS. DATA ANALYSIS

POSITION	AMPLITUDE	PHASE
0.	0.1000E 01	0.
0.5010E 01	0.6074E 00	0.1104E-00
0.9890E 01	0.3926E-00	0.2240E-00
0.1489E 02	0.2356E-00	0.3502E-00
0.1978E 02	0.1602E-00	0.4678E-00
0.2478E 02	0.9583E-01	0.6013E 00
0.2968E 02	0.6350E-01	0.7260E 00
0.3467E 02	0.4049E-01	0.8487E 00
0.3857E 02	0.3118E-01	0.9493E 00
0.4445E 02	0.1847E-01	0.1097E 01
0.4946E 02	0.1223E-01	0.1236E 01
0.5434E 02	0.8017E-02	0.1360E 01
0.5934E 02	0.5244E-02	0.1480E 01

RESULTS OF 175. CPS. DATA ANALYSIS

POSITION	AMPLITUDE	PHASE
0.	0.1000E 01	0.
0.5010E 01	0.6039E 00	0.1252E-00
0.9890E 01	0.3878E-00	0.2541E-00
0.1489E 02	0.2310E-00	0.3971E-00
0.1978E 02	0.1559E-00	0.5303E 00
0.2478E 02	0.9264E-01	0.6822E 00
0.2968E 02	0.6096E-01	0.8222E 00
0.3467E 02	0.3849E-01	0.9609E 00
0.3857E 02	0.2937E-01	0.1075E 01
0.4445E 02	0.1727E-01	0.1240E 01
0.4946E 02	0.1133E-01	0.1400E 01
0.5434E 02	0.7340E-02	0.1537E 01

0.5934E 02	0.4738E-02	0.1673E 01

RESULTS OF 200. CPS. DATA ANALYSIS

POSITION	AMPLITUDE	PHASE
0.	0.1000E 01	0.
0.3890E 01	0.7105E 00	0.6277E-01
0.7890E 01	0.4723E-00	0.9343E-01
0.1178E 02	0.3359E-00	0.2030E-00
0.1678E 02	0.2144E-00	0.2297E-00
0.2067E 02	0.1493E-00	0.3471E-00
0.2567E 02	0.9416E-01	0.3471E-00
0.2956E 02	0.6749E-01	0.5120E 00
0.3456E 02	0.4256E-01	0.5071E 00
0.1890E 01	0.8773E 00	0.6160E 00
0.6900E 01	0.5269E 00	0.6554E 00
0.1178E 02	0.3359E-00	0.7845E 00
0.1678E 02	0.1987E-00	0.8256E 00
0.2167E 02	0.1331E-00	0.9024E 00
0.2667E 02	0.7861E-01	0.9821E 00
0.3157E 02	0.5138E-01	0.1070E 01
0.3656E 02	0.3214E-01	0.1136E 01
0.4046E 02	0.2435E-01	0.1262E 01
0.4634E 02	0.1422E-01	0.1446E 01
0.5135E 02	0.9255E-02	0.1623E 01
0.5623E 02	0.5932E-02	0.1772E 01
0.6123E 02	0.3786E-02	0.1924E 01

RESULTS OF 225. CPS. DATA ANALYSIS

POSITION	AMPLITUDE	PHASE
0.	0.1000E 01	0.
0.5010E 01	0.5966E 00	0.1555E-00
0.9890E 01	0.3774E-00	0.3145E-00
0.1489E 02	0.2214E-00	0.4915E-00
0.1978E 02	0.1471E-00	0.6553E 00
0.2478E 02	0.8623E-01	0.8445E 00
0.2968E 02	0.5591E-01	0.1018E 01
0.3467E 02	0.3465E-01	0.1188E 01
0.3857E 02	0.2609E-01	0.1326E 01
0.4445E 02	0.1513E-01	0.1531E 01
0.4946E 02	0.9795E-02	0.1724E 01
0.5434E 02	0.6210E-02	0.1886E 01
0.5934E 02	0.3929E-02	0.2054E 01

RESULTS OF 250. CPS. DATA ANALYSIS

POSITION	AMPLITUDE	PHASE
0.	0.1000E 01	0.

0.5010E 01	0.5918E 00	0.1698E-00
0.9890E 01	0.3710E-00	0.3422E-00
0.1489E 02	0.2154E-00	0.5355E 00
0.1978E 02	0.1418E-00	0.7139E 00
0.2478E 02	0.8231E-01	0.9211E 00
0.2968E 02	0.5281E-01	0.1111E 01
0.3467E 02	0.3237E-01	0.1298E 01
0.3857E 02	0.2420E-01	0.1450E 01
0.4445E 02	0.1392E-01	0.1676E 01
0.4946E 02	0.8962E-02	0.1887E 01
0.5434E 02	0.5611E-02	0.2063E 01
0.5934E 02	0.3525E-02	0.2250E 01

RESULTS OF 275. CPS. DATA ANALYSIS

POSITION	AMPLITUDE	PHASE
0.	0.1000E 01	0.
0.5010E 01	0.5868E 00	0.1820E-00
0.9890E 01	0.3646E-00	0.3659E-00
0.1489E 02	0.2094E-00	0.5731E 00
0.1978E 02	0.1364E-00	0.7639E 00
0.2478E 02	0.7830E-01	0.9862E 00
0.2968E 02	0.4964E-01	0.1190E 01
0.3467E 02	0.3000E-01	0.1392E 01
0.3857E 02	0.2226E-01	0.1559E 01
0.4445E 02	0.1263E-01	0.1806E 01
0.4946E 02	0.8088E-02	0.2035E 01
0.5434E 02	0.4975E-02	0.2224E 01
0.5934E 02	0.3103E-02	0.2433E 01

RESULTS OF 290. CPS. DATA ANALYSIS

POSITION	AMPLITUDE	PHASE
0.	0.1000E 01	0.
0.1890E 01	0.8215E 00	0.7499E-01
0.3890E 01	0.6711E 00	0.1279E-00
0.7840E 01	0.4273E-00	0.2957E-00
0.9890E 01	0.3542E-00	0.3704E-00
0.1178E 02	0.3177E-00	0.4632E-00
0.1678E 02	0.1723E-00	0.6743E 00
0.1878E 02	0.1438E-00	0.7390E 00
0.2067E 02	0.1175E-00	0.8041E 00
0.2567E 02	0.7189E-01	0.1032E 01
0.1890E 01	0.8796E 00	0.8481E-01
0.6900E 01	0.5138E 00	0.2732E-00
0.1178E 02	0.3177E-00	0.4632E-00
0.1678E 02	0.1813E-00	0.6776E 00
0.2167E 02	0.1174E-00	0.8747E 00
0.2667E 02	0.6700E-01	0.1104E 01
0.3157E 02	0.4218E-01	0.1315E 01

0.3656E 02	0.2527E-01	0.1525E 01
0.4046E 02	0.1862E-01	0.1699E 01
0.4634E 02	0.1047E-01	0.1956E 01
0.5135E 02	0.6673E-02	0.2198E 01
0.5623E 02	0.4059E-02	0.2392E 01
0.6123E 02	0.2519E-02	0.2614E 01

RESULTS OF 300. CPS. DATA ANALYSIS

POSITION	AMPLITUDE	PHASE
0.	0.1000E 01	0.
0.5010E 01	0.5827E 00	0.1927E-00
0.9890E 01	0.3592E-00	0.3866E-00
0.1489E 02	0.2043E-00	0.6055E 00
0.1978E 02	0.1318E-00	0.8064E 00
0.2478E 02	0.7494E-01	0.1041E 01
0.2968E 02	0.4698E-01	0.1255E 01
0.3467E 02	0.2799E-01	0.1469E 01
0.3857E 02	0.2052E-01	0.1648E 01
0.4445E 02	0.1148E-01	0.1911E 01
0.4946E 02	0.7283E-02	0.2160E 01
0.5434E 02	0.4398E-02	0.2357E 01
0.5934E 02	0.2721E-02	0.2587E 01

RESULTS OF 325. CPS. DATA ANALYSIS

POSITION	AMPLITUDE	PHASE
0.	0.1000E 01	0.
0.5010E 01	0.5793E 00	0.2037E-00
0.9890E 01	0.3549E-00	0.4080E-00
0.1489E 02	0.2002E-00	0.6385E 00
0.1978E 02	0.1283E-00	0.8488E 00
0.2478E 02	0.7241E-01	0.1095E 01
0.2968E 02	0.4503E-01	0.1319E 01
0.3467E 02	0.2652E-01	0.1541E 01
0.3857E 02	0.1922E-01	0.1730E 01
0.4445E 02	0.1063E-01	0.2006E 01
0.4946E 02	0.6664E-02	0.2268E 01
0.5434E 02	0.3965E-02	0.2470E 01
0.5934E 02	0.2439E-02	0.2718E 01

RESULTS OF 350. CPS. DATA ANALYSIS

POSITION	AMPLITUDE	PHASE
0.	0.1000E 01	0.
0.2000E 01	0.7901E 00	0.1532E-01
0.3890E 01	0.6492E 00	0.2546E-01
0.5900E 01	0.5592E 00	0.6960E-01
0.7900E 01	0.4501E-00	0.8690E-01

0.8890E 01	0.4210E-00	0.1095E-00
0.1089E 02	0.3433E-00	0.1157E-00
0.1278E 02	0.2766E-00	0.1605E-00
0.1479E 02	0.2229E-00	0.1604E-00
0.1679E 02	0.1804E-00	0.1893E-00
0.	0.1016E 01	0.2398E-00
0.2000E 01	0.8581E 00	0.2449E-00
0.3890E 01	0.7085E 00	0.3363E-00
0.5900E 01	0.5909E 00	0.3277E-00
0.8890E 01	0.4292E-00	0.3316E-00
0.1089E 02	0.3532E-00	0.3779E-00
0.1278E 02	0.2766E-00	0.3799E-00
0.1478E 02	0.2223E-00	0.4543E-00
0.1778E 02	0.1598E-00	0.4558E-00
0.1000E 01	0.1045E 01	0.5474E 00
0.2890E 01	0.7551E 00	0.5474E 00
0.4890E 01	0.6199E 00	0.5474E 00
0.7900E 01	0.4410E-00	0.6454E 00
0.2890E 01	0.7892E 00	0.6374E 00
0.7900E 01	0.4544E-00	0.7302E 00
0.1278E 02	0.2767E-00	0.7843E 00
0.1778E 02	0.1548E-00	0.7908E 00
0.2267E 02	0.9863E-01	0.1012E 01
0.2767E 02	0.5536E-01	0.1272E 01
0.3257E 02	0.3419E-01	0.1508E 01
0.3756E 02	0.2000E-01	0.1740E 01
0.4146E 02	0.1437E-01	0.1937E 01
0.4734E 02	0.7886E-02	0.2226E 01
0.5235E 02	0.4900E-02	0.2498E 01
0.5723E 02	0.2887E-02	0.2706E 01
0.6223E 02	0.1781E-02	0.2972E 01

RESULTS OF 375. CPS. DATA ANALYSIS

POSITION	AMPLITUDE	PHASE
0.	0.1000E 01	0.
0.5010E 01	0.5714E 00	0.2280E-00
0.9890E 01	0.3452E-00	0.4555E-00
0.1489E 02	0.1912E-00	0.7122E 00
0.1978E 02	0.1210E-00	0.9456E 00
0.2478E 02	0.6739E-01	0.1222E 01
0.2968E 02	0.4126E-01	0.1472E 01
0.3467E 02	0.2398E-01	0.1719E 01
0.3857E 02	0.1713E-01	0.1924E 01
0.4445E 02	0.9336E-02	0.2231E 01
0.4946E 02	0.5784E-02	0.2511E 01
0.5434E 02	0.3372E-02	0.2737E 01
0.5934E 02	0.2108E-02	0.3025E 01

RESULTS OF 400. CPS. DATA ANALYSIS

POSITION	AMPLITUDE	PHASE
0.	0.1000E 01	0.
0.2000E 01	0.8042E 00	-0.5217E-01
0.3890E 01	0.6286E 00	0.4326E-01
0.4890E 01	0.5639E 00	-0.1174E-01
0.8890E 01	0.3472E-00	0.6108E-01
0.1089E 02	0.2772E-00	0.2606E-01
0.1278E 02	0.2237E-00	0.3680E-00
0.1378E 02	0.2060E-00	0.6496E-01
0.1778E 02	0.1303E-00	-0.4567E-01
0.	0.8268E 00	0.1525E-00
0.1000E 01	0.7333E 00	0.1150E-00
0.2000E 01	0.6580E 00	0.1802E-00
0.2890E 01	0.5797E 00	0.1317E-00
0.3890E 01	0.5207E 00	0.1783E-00
0.3890E 01	0.5403E 00	0.2367E-00
0.4890E 01	0.4940E-00	0.8283E-01
0.5900E 01	0.4455E-00	0.3862E-00
0.7900E 01	0.3651E-00	0.3298E-00
0.8890E 01	0.3297E-00	0.8058E 00
0.9890E 01	0.2980E-00	0.3741E-00
0.1089E 02	0.2831E-00	0.4785E-00
0.1178E 02	0.2461E-00	0.4171E-00
0.1278E 02	0.2237E-00	0.4443E-00
0.1378E 02	0.2042E-00	0.5587E 00
0.1478E 02	0.1769E-00	0.5138E 00
0.1678E 02	0.1454E-00	0.3206E-00
0.1778E 02	0.1259E-00	0.6180E 00
0.8890E 01	0.3160E-00	0.5587E 00
0.2000E 01	0.6408E 00	0.5930E 00
0.	0.7659E 00	0.6618E 00
0.2890E 01	0.6600E 00	0.8280E 00
0.7900E 01	0.3737E-00	0.7686E 00
0.1278E 02	0.2237E-00	0.5583E 00
0.1778E 02	0.1225E-00	0.8259E 00
0.2267E 02	0.7682E-01	0.1071E 01
0.2767E 02	0.4227E-01	0.1363E 01
0.3257E 02	0.2556E-01	0.1626E 01
0.3756E 02	0.1470E-01	0.1892E 01
0.4146E 02	0.1041E-01	0.2109E 01
0.4734E 02	0.5622E-02	0.

RESULTS OF 425. CPS. DATA ANALYSIS

POSITION	AMPLITUDE	PHASE
0.	0.1000E 01	0.
0.5010E 01	0.5620E 00	0.2449E-00
0.9890E 01	0.3337E-00	0.4904E-00
0.1489E 02	0.1806E-00	0.7653E 00
0.1978E 02	0.1122E-00	0.1020E 01

0.2478E 02	0.6094E-01	0.1322E 01
0.2968E 02	0.3635E-01	0.1593E 01
0.3467E 02	0.2053E-01	0.1875E 01
0.3857E 02	0.1441E-01	0.2106E 01
0.4445E 02	0.7648E-02	0.2449E 01
0.4946E 02	0.4716E-02	0.2762E 01
0.5434E 02	0.2588E-02	0.3033E 01

RESULTS OF 450. CPS. DATA ANALYSIS

POSITION	AMPLITUDE	PHASE
0.	0.1000E 01	0.
0.1000E 01	0.9075E 00	0.3930E-01
0.2000E 01	0.8010E 00	0.7820E-01
0.2890E 01	0.7275E 00	0.2575E-01
0.3890E 01	0.6750E 00	0.1361E-00
0.4890E 01	0.5934E 00	0.1458E-00
0.5900E 01	0.5170E 00	0.1640E-00
0.7900E 01	0.4075E-00	0.2206E-00
0.8890E 01	0.3556E-00	0.2817E-00
0.9890E 01	0.3230E-00	0.3977E-00
0.1000E 01	0.9110E 00	0.3977E-00
0.2890E 01	0.7282E 00	0.4243E-00
0.7900E 01	0.4075E-00	0.4840E-00
0.1278E 02	0.2405E-00	0.6505E 00
0.1778E 02	0.1292E-00	0.9314E 00
0.2267E 02	0.7975E-01	0.1194E 01
0.2767E 02	0.4286E-01	0.1502E 01
0.3257E 02	0.2533E-01	0.1777E 01
0.3756E 02	0.1401E-01	0.2068E 01
0.4146E 02	0.9718E-02	0.2306E 01
0.4734E 02	0.5086E-02	0.2659E 01
0.5235E 02	0.3090E-02	0.2989E 01
0.5723E 02	0.1616E-02	0.3258E 01

RESULTS OF 451. CPS. DATA ANALYSIS

POSITION	AMPLITUDE	PHASE
0.	0.1000E 01	0.
0.2000E 01	0.7897E 00	0.8557E-01
0.3890E 01	0.6108E 00	0.1056E-00
0.5900E 01	0.4768E-00	0.1762E-00
0.7900E 01	0.3724E-00	0.3260E-00
0.8890E 01	0.3262E-00	0.3578E-00
0.1089E 02	0.2617E-00	0.3578E-00
0.2890E 01	0.6657E 00	0.3376E-00
0.7900E 01	0.3724E-00	0.5307E 00
0.1278E 02	0.2197E-00	0.6109E 00
0.1778E 02	0.1180E-00	0.8921E 00
0.2267E 02	0.7284E-01	0.1155E 01

0.2767E 02	0.3913E-01	0.1463E 01
0.3257E 02	0.2313E-01	0.1738E 01
0.3756E 02	0.1278E-01	0.2030E 01
0.4146E 02	0.8855E-02	0.2269E 01
0.4734E 02	0.4636E-02	0.2621E 01
0.5235E 02	0.2814E-02	0.2952E 01
0.5723E 02	0.1469E-02	0.3220E 01

RESULTS OF 475. CPS. DATA ANALYSIS

POSITION	AMPLITUDE	PHASE
0.	0.1000E 01	0.
0.5010E 01	0.5580E 00	0.2613E-00
0.9890E 01	0.3276E-00	0.5230E 00
0.1489E 02	0.1752E-00	0.8121E 00
0.1978E 02	0.1076E-00	0.1085E 01
0.2478E 02	0.5754E-01	0.1399E 01
0.2968E 02	0.3388E-01	0.1681E 01
0.3467E 02	0.1848E-01	0.1975E 01
0.3857E 02	0.1269E-01	0.2218E 01
0.4445E 02	0.6635E-02	0.2577E 01
0.4946E 02	0.3951E-02	0.2913E 01
0.5434E 02	0.2008E-02	0.3155E 01

RESULTS OF 500. CPS. DATA ANALYSIS

POSITION	AMPLITUDE	PHASE
0.	0.1000E 01	0.
0.1000E 01	0.9222E 00	0.4976E-01
0.2000E 01	0.8432E 00	0.1464E-00
0.2890E 01	0.7665E 00	0.8940E-01
0.3890E 01	0.6862E 00	0.1559E-00
0.4890E 01	0.6081E 00	0.1709E-00
0.5900E 01	0.5374E 00	0.2050E-00
0.5900E 01	0.5323E 00	0.2710E-00
0.7900E 01	0.4229E-00	0.3154E-00
0.8890E 01	0.3882E-00	0.3240E-00
0.9890E 01	0.3459E-00	0.3390E-00
0.1089E 02	0.3140E-00	0.4395E-00
0.1178E 02	0.2805E-00	0.4443E-00
0.1278E 02	0.2530E-00	0.4767E-00
0.5900E 01	0.5653E 00	0.5461E 00
0.2000E 01	0.9109E 00	0.5911E 00
0.2890E 01	0.7804E 00	0.6472E 00
0.7900E 01	0.4336E-00	0.7157E 00
0.1278E 02	0.2530E-00	0.7157E 00
0.1778E 02	0.1345E-00	0.1016E 01
0.2267E 02	0.8217E-01	0.1303E 01
0.2767E 02	0.4375E-01	0.1627E 01
0.3257E 02	0.2566E-01	0.1923E 01

0.3756E 02	0.1390E-01	0.2221E 01
0.4146E 02	0.9546E-02	0.2474E 01
0.4734E 02	0.5014E-02	0.2848E 01
0.5723E 02	0.1507E-02	0.3403E 01

RESULTS OF 510. CPS. DATA ANALYSIS

POSITION	AMPLITUDE	PHASE
0.	0.1000E 01	0.
0.2000E 01	0.7790E 00	0.1041E-00
0.3890E 01	0.6276E 00	0.1180E-00
0.5900E 01	0.4718E-00	0.1790E-00
0.7900E 01	0.3669E-00	0.2981E-00
0.8890E 01	0.3255E-00	0.4131E-00
0.1089E 02	0.2599E-00	0.3963E-00
0.1278E 02	0.2067E-00	0.4534E-00
0.1479E 02	0.1653E-00	0.5661E 00
0.1679E 02	0.1268E-00	0.6715E 00
0.2890E 01	0.6411E 00	0.6715E 00
0.7900E 01	0.3553E-00	0.8031E 00
0.1278E 02	0.2067E-00	0.8895E 00
0.1778E 02	0.1095E-00	0.9768E 00
0.2267E 02	0.6666E-01	0.1270E 01
0.2767E 02	0.3541E-01	0.1598E 01
0.3257E 02	0.2070E-01	0.1901E 01
0.3756E 02	0.1119E-01	0.2204E 01
0.4146E 02	0.7685E-02	0.2459E 01
0.4734E 02	0.4046E-02	0.2847E 01
0.5235E 02	0.2372E-02	0.3176E 01
0.5723E 02	0.1223E-02	0.3401E 01

RESULTS OF 525. CPS. DATA ANALYSIS

POSITION	AMPLITUDE	PHASE
0.	0.1000E 01	0.
0.5010E 01	0.5516E 00	0.2851E-00
0.9890E 01	0.3194E-00	0.5652E 00
0.1489E 02	0.1682E-00	0.8772E 00
0.1978E 02	0.1016E-00	0.1180E 01
0.2478E 02	0.5375E-01	0.1515E 01
0.2968E 02	0.3118E-01	0.1827E 01
0.3467E 02	0.1680E-01	0.2138E 01
0.3857E 02	0.1154E-01	0.2404E 01
0.4445E 02	0.6067E-02	0.2813E 01
0.4946E 02	0.3551E-02	0.3141E 01
0.5434E 02	0.1854E-02	0.3377E 01

RESULTS OF 550. CPS. DATA ANALYSIS

POSITION	AMPLITUDE	PHASE
0.	0.1000E 01	0.
0.5010E 01	0.5469E 00	0.2938E-00
0.9890E 01	0.3146E-00	0.5801E 00
0.1489E 02	0.1639E-00	0.9001E 00
0.1978E 02	0.9752E-01	0.1213E 01
0.2478E 02	0.5109E-01	0.1557E 01
0.2968E 02	0.2909E-01	0.1881E 01
0.3467E 02	0.1549E-01	0.2207E 01
0.3857E 02	0.1054E-01	0.2500E 01
0.4445E 02	0.5463E-02	0.2947E 01
0.4946E 02	0.3186E-02	0.3276E 01
0.5434E 02	0.1679E-02	0.3553E 01

RESULTS OF 575. CPS. DATA ANALYSIS

POSITION	AMPLITUDE	PHASE
0.	0.1000E 01	0.
0.5010E 01	0.5434E 00	0.3002E-00
0.9890E 01	0.3116E-00	0.5929E 00
0.1489E 02	0.1610E-00	0.9177E 00
0.1978E 02	0.9444E-01	0.1235E 01
0.2478E 02	0.4915E-01	0.1583E 01
0.2968E 02	0.2750E-01	0.1908E 01
0.3467E 02	0.1440E-01	0.2242E 01
0.3857E 02	0.9630E-02	0.2561E 01
0.4445E 02	0.4799E-02	0.3033E 01
0.4946E 02	0.2757E-02	0.3362E 01
0.5434E 02	0.1436E-02	0.3692E 01

RESULTS OF 600. CPS. DATA ANALYSIS

POSITION	AMPLITUDE	PHASE
0.	0.1000E 01	0.
0.5010E 01	0.5413E 00	0.3075E-00
0.9890E 01	0.3098E-00	0.6100E 00
0.1489E 02	0.1594E-00	0.9403E 00
0.1978E 02	0.9278E-01	0.1260E 01
0.2478E 02	0.4824E-01	0.1613E 01
0.2968E 02	0.2682E-01	0.1936E 01
0.3467E 02	0.1389E-01	0.2271E 01
0.3857E 02	0.9050E-02	0.2601E 01
0.4445E 02	0.4358E-02	0.3071E 01
0.4946E 02	0.2445E-02	0.3378E 01
0.5434E 02	0.1243E-02	0.3747E 01

RESULTS OF 625. CPS. DATA ANALYSIS

POSITION	AMPLITUDE	PHASE

0.	0.1000E 01	0.
0.5010E 01	0.5393E 00	0.3171E-00
0.9890E 01	0.3074E-00	0.6331E 00
0.1489E 02	0.1575E-00	0.9724E 00
0.1978E 02	0.9137E-01	0.1298E 01
0.2478E 02	0.4753E-01	0.1664E 01
0.2968E 02	0.2645E-01	0.1993E 01
0.3467E 02	0.1371E-01	0.2330E 01
0.3857E 02	0.8711E-02	0.2663E 01
0.4445E 02	0.4206E-02	0.3122E 01
0.4946E 02	0.2358E-02	0.3375E 01
0.5434E 02	0.1195E-02	0.3777E 01

RESULTS OF 650. CPS. DATA ANALYSIS

POSITION	AMPLITUDE	PHASE
0.	0.1000E 01	0.
0.5010E 01	0.5360E 00	0.3273E-00
0.9890E 01	0.3028E-00	0.6565E 00
0.1489E 02	0.1542E-00	0.1007E 01
0.1978E 02	0.8890E-01	0.1344E 01
0.2478E 02	0.4602E-01	0.1726E 01
0.2968E 02	0.2552E-01	0.2072E 01
0.3467E 02	0.1328E-01	0.2424E 01
0.3857E 02	0.8356E-02	0.2767E 01
0.4445E 02	0.4104E-02	0.3235E 01
0.4946E 02	0.2400E-02	0.3436E 01
0.5434E 02	0.1240E-02	0.3901E 01

RESULTS OF 675. CPS. DATA ANALYSIS

POSITION	AMPLITUDE	PHASE
0.	0.1000E 01	0.
0.5010E 01	0.5320E 00	0.3352E-00
0.9890E 01	0.2971E-00	0.6731E 00
0.1489E 02	0.1500E-00	0.1032E 01
0.1978E 02	0.8545E-01	0.1381E 01
0.2478E 02	0.4369E-01	0.1776E 01
0.2968E 02	0.2384E-01	0.2141E 01
0.3467E 02	0.1234E-01	0.2516E 01
0.3857E 02	0.7683E-02	0.2865E 01
0.4445E 02	0.3788E-02	0.3386E 01
0.4946E 02	0.2387E-02	0.3562E 01
0.5434E 02	0.1239E-02	0.4132E 01

RESULTS OF 700. CPS. DATA ANALYSIS

POSITION	AMPLITUDE	PHASE
0.	0.1000E 01	0.

0.2000E 01	0.7747E 00	0.1025E-00
0.3890E 01	0.5949E 00	0.1195E-00
0.5900E 01	0.4592E-00	0.1853E-00
0.7900E 01	0.3514E-00	0.1503E-00
0.8890E 01	0.3098E-00	0.2703E-00
0.1089E 02	0.2391E-00	0.3864E-00
0.1278E 02	0.1829E-00	0.5185E 00
0.2890E 01	0.6549E 00	0.4912E-00
0.1000E 01	0.8436E 00	0.5893E 00
0.2890E 01	0.6244E 00	0.7051E 00
0.7900E 01	0.3304E-00	0.8338E 00
0.1278E 02	0.1830E-00	0.8338E 00
0.1778E 02	0.9175E-01	0.1198E 01
0.2267E 02	0.5149E-01	0.1553E 01
0.2767E 02	0.2600E-01	0.1952E 01
0.3257E 02	0.1384E-01	0.2324E 01
0.3756E 02	0.7028E-02	0.2716E 01
0.4146E 02	0.4261E-02	0.3082E 01
0.4734E 02	0.2031E-02	0.3655E 01
0.5235E 02	0.1404E-02	0.3849E 01

RESULTS OF 725. CPS. DATA ANALYSIS

POSITION	AMPLITUDE	PHASE
0.	0.1000E 01	0.
0.5010E 01	0.5277E 00	0.3474E-00
0.9890E 01	0.2911E-00	0.6958E 00
0.1489E 02	0.1456E-00	0.1067E 01
0.1978E 02	0.8083E-01	0.1422E 01
0.2478E 02	0.4068E-01	0.1821E 01
0.2968E 02	0.2133E-01	0.2188E 01
0.3467E 02	0.1066E-01	0.2578E 01
0.3857E 02	0.6286E-02	0.2950E 01
0.4445E 02	0.2764E-02	0.3520E 01
0.4946E 02	0.2061E-02	0.3799E 01

RESULTS OF 750. CPS. DATA ANALYSIS

POSITION	AMPLITUDE	PHASE
0.	0.1000E 01	0.
0.5010E 01	0.5266E 00	0.3569E-00
0.9890E 01	0.2895E-00	0.7158E 00
0.1489E 02	0.1446E-00	0.1099E 01
0.1978E 02	0.7981E-01	0.1456E 01
0.2478E 02	0.4035E-01	0.1863E 01
0.2968E 02	0.2113E-01	0.2228E 01
0.3467E 02	0.1062E-01	0.2610E 01
0.3857E 02	0.6186E-02	0.2968E 01
0.4445E 02	0.2629E-02	0.3465E 01
0.4946E 02	0.1936E-02	0.3865E 01

RESULTS OF 775. CPS. DATA ANALYSIS

POSITION	AMPLITUDE	PHASE
0.	0.1000E 01	0.
0.5010E 01	0.5242E 00	0.3680E-00
0.9890E 01	0.2860E-00	0.7399E 00
0.1489E 02	0.1418E-00	0.1138E 01
0.1978E 02	0.7797E-01	0.1501E 01
0.2478E 02	0.3940E-01	0.1928E 01
0.2968E 02	0.2066E-01	0.2307E 01
0.3467E 02	0.1064E-01	0.2698E 01
0.3857E 02	0.6130E-02	0.3049E 01
0.4445E 02	0.2807E-02	0.3493E 01
0.4946E 02	0.1901E-02	0.3949E 01

RESULTS OF 800. CPS. DATA ANALYSIS

POSITION	AMPLITUDE	POSITION	PHASE
0.	0.1000E 01	0.	0.
0.1000E 01	0.8794E 00	0.1000E 01	0.5856E-01
0.1890E 01	0.7622E 00	0.2000E 01	0.1408E-00
0.2890E 01	0.6626E 00	0.8890E 01	0.6665E 00
0.3890E 01	0.5958E 00	0.2890E 01	0.1989E-00
0.4900E 01	0.5060E 00	0.3890E 01	0.2709E-00
0.6900E 01	0.3843E-00	0.4890E 01	0.3579E-00
0.7890E 01	0.3384E-00	0.5900E 01	0.4445E-00
0.1890E 01	0.5266E 00	0.2890E 01	0.2253E-00
0.6900E 01	0.3969E-00	0.7900E 01	0.6029E 00
0.1178E 02	0.1576E-00	0.7900E 01	0.6029E 00
0.1678E 02	0.7231E-01	0.1278E 02	0.9849E 00
0.2167E 02	0.3945E-01	0.1778E 02	0.1396E 01
0.2667E 02	0.1964E-01	0.2267E 02	0.1767E 01
0.3157E 02	0.1017E-01	0.2767E 02	0.2215E 01
0.3656E 02	0.5360E-02	0.3257E 02	0.2618E 01
0.4046E 02	0.3090E-02	0.3756E 02	0.3044E 01
0.4634E 02	0.1550E-02	0.4146E 02	0.3416E 01
0.5135E 02	0.9854E-03	0.4734E 02	0.3872E 01
		0.5235E 02	0.4314E 01

RESULTS OF 825. CPS. DATA ANALYSIS

POSITION	AMPLITUDE	POSITION	PHASE
0.	0.1000E 01	0.	0.
0.5010E 01	0.5174E 00	0.5010E 01	0.3845E-00
0.9890E 01	0.2757E-00	0.9890E 01	0.7712E 00
0.1489E 02	0.1331E-00	0.1489E 02	0.1187E 01
0.1978E 02	0.7185E-01	0.1978E 02	0.1563E 01
0.2478E 02	0.3488E-01	0.2478E 02	0.2017E 01

0.2968E 02	0.1748E-01	0.2968E 02	0.2440E 01
0.3467E 02	0.9211E-02	0.3467E 02	0.2919E 01
0.3857E 02	0.5257E-02	0.3857E 02	0.3300E 01
0.4445E 02	0.2810E-02	0.4445E 02	0.3848E 01
0.4946E 02	0.1755E-02	0.4946E 02	0.4264E 01
0.5434E 02	0.9205E-03		
0.5934E 02	0.4665E-03		

RESULTS OF 850. CPS. DATA ANALYSIS

POSITION	AMPLITUDE	POSITION	PHASE
0.	0.1000E 01	0.	0.
0.5010E 01	0.5156E 00	0.5010E 01	0.3914E-00
0.9890E 01	0.2728E-00	0.9890E 01	0.7816E 00
0.1489E 02	0.1308E-00	0.1489E 02	0.1199E 01
0.1978E 02	0.7012E-01	0.1978E 02	0.1576E 01
0.2478E 02	0.3348E-01	0.2478E 02	0.2018E 01
0.2968E 02	0.1618E-01	0.2968E 02	0.2436E 01
0.3467E 02	0.8259E-02	0.3467E 02	0.2959E 01
0.3857E 02	0.4530E-02	0.3857E 02	0.3344E 01
0.4445E 02	0.2451E-02	0.4445E 02	0.4012E 01
		0.4946E 02	0.4432E 01

RESULTS OF 875. CPS. DATA ANALYSIS

POSITION	AMPLITUDE	POSITION	PHASE
0.	0.1000E 01	0.	0.
0.5010E 01	0.5144E 00	0.5010E 01	0.4013E-00
0.9890E 01	0.2709E-00	0.9890E 01	0.7985E 00
0.1489E 02	0.1297E-00	0.1489E 02	0.1222E 01
0.1978E 02	0.6938E-01	0.1978E 02	0.1602E 01
0.2478E 02	0.3331E-01	0.2478E 02	0.2032E 01
0.2968E 02	0.1581E-01	0.2968E 02	0.2434E 01
0.3467E 02	0.7791E-02	0.3467E 02	0.2961E 01
0.3857E 02	0.4165E-02	0.3857E 02	0.3338E 01
0.4445E 02	0.2098E-02	0.4445E 02	0.4074E 01
0.4946E 02	0.1330E-02		

RESULTS OF 900. CPS. DATA ANALYSIS

POSITION	AMPLITUDE	PHASE
0.	0.1000E 01	0.
0.1000E 01	0.8410E 00	0.7390E-01
0.2000E 01	0.7154E 00	0.1439E-00
0.2890E 01	0.6225E 00	0.2292E-00
0.3890E 01	0.5508E 00	0.2147E-00
0.4890E 01	0.4815E-00	0.2907E-00
0.5900E 01	0.4070E-00	0.3625E-00
0.7900E 01	0.3031E-00	0.4797E-00

0.2890E 01	0.5923E 00	0.6280E 00
0.7900E 01	0.3031E-00	0.6281E 00
0.1278E 02	0.1585E-00	0.1036E 01
0.1778E 02	0.7559E-01	0.1473E 01
0.2267E 02	0.4036E-01	0.1862E 01
0.2767E 02	0.1967E-01	0.2296E 01
0.3257E 02	0.9299E-02	0.2695E 01
0.3756E 02	0.4566E-02	0.3214E 01
0.4146E 02	0.2493E-02	0.3568E 01
0.4734E 02	0.1170E-02	0.4287E 01

RESULTS OF 925. CPS. DATA ANALYSIS

POSITION	AMPLITUDE	POSITION	PHASE
0.	0.1000E 01	0.	0.
0.5010E 01	0.5073E 00	0.5010E 01	0.4239E-00
0.9890E 01	0.2619E-00	0.9890E 01	0.8396E 00
0.1489E 02	0.1235E-00	0.1489E 02	0.1291E 01
0.1978E 02	0.6546E-01	0.1978E 02	0.1692E 01
0.2478E 02	0.3212E-01	0.2478E 02	0.2149E 01
0.2968E 02	0.1499E-01	0.2968E 02	0.2557E 01
0.3467E 02	0.7505E-02	0.3467E 02	0.3091E 01
0.3857E 02	0.4104E-02	0.3857E 02	0.3445E 01
0.4445E 02	0.2038E-02		

RESULTS OF 950. CPS. DATA ANALYSIS

POSITION	AMPLITUDE	POSITION	PHASE
0.	0.1000E 01	0.	0.
0.5010E 01	0.2589E-00	0.5010E 01	0.4301E-00
0.9890E 01	0.1319E-00	0.9890E 01	0.8480E 00
0.1489E 02	0.6120E-01	0.1489E 02	0.1306E 01
0.1978E 02	0.3204E-01	0.1978E 02	0.1715E 01
0.2478E 02	0.1553E-01	0.2478E 02	0.2196E 01
0.2968E 02	0.7018E-02	0.2968E 02	0.2608E 01
0.3467E 02	0.3547E-02	0.3467E 02	0.3186E 01
0.3857E 02	0.1930E-02	0.3857E 02	0.3589E 01
0.4445E 02	0.1043E-02		
0.4946E 02	0.3889E-03		

RESULTS OF 975. CPS. DATA ANALYSIS

POSITION	AMPLITUDE	POSITION	PHASE
0.	0.1000E 01	0.	0.
0.5010E 01	0.5004E 00	0.5010E 01	0.4349E-00
0.9890E 01	0.2533E-00	0.9890E 01	0.8523E 00
0.1489E 02	0.1163E-00	0.1489E 02	0.1310E 01
0.1978E 02	0.6019E-01	0.1978E 02	0.1720E 01
0.2478E 02	0.2853E-01	0.2478E 02	0.2208E 01

0.2968E 02	0.1248E-01	0.2968E 02	0.2595E 01
0.3467E 02	0.6123E-02	0.3467E 02	0.3221E 01
0.3857E 02	0.3215E-02	0.3857E 02	0.3643E 01
0.4445E 02	0.1795E-02		

RESULTS OF 1000. CPS. DATA ANALYSIS

POSITION	AMPLITUDE	PHASE
0.	0.1000E 01	0.
0.5010E 01	0.4991E-00	0.4425E-00
0.9890E 01	0.2520E-00	0.8630E 00
0.1489E 02	0.1156E-00	0.1322E 01
0.1978E 02	0.5960E-01	0.1734E 01
0.2478E 02	0.2790E-01	0.2215E 01
0.2968E 02	0.1224E-01	0.2563E 01
0.3467E 02	0.5726E-02	0.3194E 01
0.3857E 02	0.2786E-02	0.3563E 01
0.4445E 02	0.1396E-02	0.4698E 01

RESULTS OF 1025. CPS. DATA ANALYSIS

POSITION	AMPLITUDE	POSITION	PHASE
0.	0.1000E 01	0.	0.
0.5010E 01	0.4971E-00	0.5010E 01	0.4530E-00
0.9890E 01	0.2498E-00	0.9890E 01	0.8820E 00
0.1489E 02	0.1146E-00	0.1489E 02	0.1352E 01
0.1978E 02	0.5901E-01	0.1978E 02	0.1773E 01
0.2478E 02	0.2768E-01	0.2478E 02	0.2253E 01
0.2968E 02	0.1253E-01	0.2968E 02	0.2589E 01
0.3467E 02	0.5817E-02	0.3467E 02	0.3194E 01
0.3857E 02	0.2785E-02	0.3857E 02	0.3491E 01
0.4445E 02	0.1048E-02		
0.4946E 02	0.5930E-03		

RESULTS OF 1050. CPS. DATA ANALYSIS

POSITION	AMPLITUDE	PHASE
0.	0.1000E 01	0.
0.5010E 01	0.4933E-00	0.4632E-00
0.9890E 01	0.2454E-00	0.9003E 00
0.1489E 02	0.1117E-00	0.1388E 01
0.1978E 02	0.5698E-01	0.1822E 01
0.2478E 02	0.2675E-01	0.2316E 01
0.2968E 02	0.1241E-01	0.2677E 01
0.3467E 02	0.5925E-02	0.3281E 01
0.3857E 02	0.3031E-02	0.3510E 01

RESULTS OF 1075. CPS. DATA ANALYSIS

POSITION	AMPLITUDE	PHASE
0.	0.1000E 01	0.
0.5010E 01	0.4891E-00	0.4693E-00
0.9890E 01	0.2404E-00	0.9083E 00
0.1489E 02	0.1073E-00	0.1409E 01
0.1978E 02	0.5378E-01	0.1852E 01
0.2478E 02	0.2485E-01	0.2363E 01
0.2968E 02	0.1146E-01	0.2764E 01
0.3467E 02	0.5590E-02	0.3409E 01
0.3857E 02	0.3116E-02	0.3624E 01

RESULTS OF 1100. CPS. DATA ANALYSIS

POSITION	AMPLITUDE	PHASE
0.	0.1000E 01	0.
0.5010E 01	0.4868E-00	0.4732E-00
0.9890E 01	0.2378E-00	0.9097E 00
0.1489E 02	0.1042E-00	0.1410E 01
0.1978E 02	0.5125E-01	0.1849E 01
0.2478E 02	0.2299E-01	0.2360E 01
0.2968E 02	0.1023E-01	0.2784E 01
0.3467E 02	0.4846E-02	0.3489E 01
0.3857E 02	0.2943E-02	0.3729E 01

RESULTS OF 1125. CPS. DATA ANALYSIS

POSITION	AMPLITUDE	POSITION	PHASE
0.	0.1000E 01	0.	0.
0.5010E 01	0.4863E-00	0.5010E 01	0.4798E-00
0.9890E 01	0.2378E-00	0.9890E 01	0.9174E 00
0.1489E 02	0.1033E-00	0.1489E 02	0.1413E 01
0.1978E 02	0.5054E-01	0.1978E 02	0.1841E 01
0.2478E 02	0.2228E-01	0.2478E 02	0.2329E 01
0.2968E 02	0.9652E-02	0.2968E 02	0.2743E 01
0.3467E 02	0.4192E-02	0.3467E 02	0.3448E 01
0.3857E 02	0.2744E-02	0.3857E 02	0.3753E 01
0.4445E 02	0.1242E-02		

RESULTS OF 1150. CPS. DATA ANALYSIS

POSITION	AMPLITUDE	POSITION	PHASE
0.	0.1000E 01	0.	0.
0.5010E 01	0.4856E-00	0.5010E 01	0.4915E-00
0.9890E 01	0.2375E-00	0.9890E 01	0.9378E 00
0.1489E 02	0.1030E-00	0.1489E 02	0.1436E 01
0.1978E 02	0.5070E-01	0.1978E 02	0.1862E 01
0.2478E 02	0.2254E-01	0.2478E 02	0.2329E 01
0.2968E 02	0.9861E-02	0.2968E 02	0.2739E 01

0.3467E 02	0.4118E-02	0.3467E 02	0.3349E 01
0.3857E 02	0.2801E-02	0.3857E 02	0.3745E 01
0.4445E 02	0.1119E-02		
0.4946E 02	0.5139E-03		

RESULTS OF 1175. CPS. DATA ANALYSIS

POSITION	AMPLITUDE	POSITION	PHASE
0.	0.1000E 01	0.	0.
0.5010E 01	0.4824E-00	0.5010E 01	0.5050E 00
0.9890E 01	0.2345E-00	0.9890E 01	0.9638E 00
0.1489E 02	0.1012E-00	0.1489E 02	0.1471E 01
0.1978E 02	0.4997E-01	0.1978E 02	0.1909E 01
0.2478E 02	0.2253E-01	0.2478E 02	0.2376E 01
0.2968E 02	0.1002E-01	0.2968E 02	0.2822E 01
0.3467E 02	0.4433E-02	0.3467E 02	0.3347E 01
0.3857E 02	0.3054E-02	0.3857E 02	0.3828E 01
0.4445E 02	0.1135E-02		

RESULTS OF 1200. CPS. DATA ANALYSIS

POSITION	AMPLITUDE	POSITION	PHASE
0.	0.1000E 01	0.	0.
0.5010E 01	0.4775E-00	0.5010E 01	0.5149E 00
0.9890E 01	0.2293E-00	0.9890E 01	0.9817E 00
0.1489E 02	0.9752E-01	0.1489E 02	0.1496E 01
0.1978E 02	0.4776E-01	0.1978E 02	0.1949E 01
0.2478E 02	0.2151E-01	0.2478E 02	0.2426E 01
0.2968E 02	0.9386E-02	0.2968E 02	0.2944E 01
0.3467E 02	0.4550E-02	0.3467E 02	0.3440E 01
0.3857E 02	0.3160E-02	0.3857E 02	0.4017E 01
0.4445E 02	0.1291E-02		

RESULTS OF 1229. CPS. DATA ANALYSIS

POSITION	AMPLITUDE	PHASE
0.	0.1000E 01	0.
0.1000E 01	0.8465E 00	0.8747E-01
0.2000E 01	0.7240E 00	0.1639E-00
0.2890E 01	0.6154E 00	0.2841E-00
0.3890E 01	0.5116E 00	0.2840E-00
0.2890E 01	0.6154E 00	0.3930E-00
0.7900E 01	0.2911E-00	0.8048E 00
0.1278E 02	0.1382E-00	0.1273E 01
0.1778E 02	0.5789E-01	0.1782E 01
0.2267E 02	0.2781E-01	0.2238E 01
0.2767E 02	0.1227E-01	0.2711E 01
0.3257E 02	0.4850E-02	0.3299E 01
0.3756E 02	0.2576E-02	0.3814E 01

0.4146E 02	0.1744E-02	0.4548E 01

RESULTS OF 1250. CPS. DATA ANALYSIS

POSITION	AMPLITUDE	PHASE
0.	0.1000E 01	0.
0.5010E 01	0.4717E-00	0.5253E 00
0.9890E 01	0.2234E-00	0.9955E 00
0.1489E 02	0.9349E-01	0.1497E 01
0.1978E 02	0.4464E-01	0.1947E 01
0.2478E 02	0.1962E-01	0.2395E 01
0.2968E 02	0.7029E-02	0.2974E 01
0.3467E 02	0.3893E-02	0.3508E 01

RESULTS OF 1275. CPS. DATA ANALYSIS

POSITION	AMPLITUDE	POSITION	PHASE
0.	0.1000E 01	0.	0.
0.5010E 01	0.4707E-00	0.5010E 01	0.5349E 00
0.9890E 01	0.2224E-00	0.9890E 01	0.1015E 01
0.1489E 02	0.9383E-01	0.1489E 02	0.1516E 01
0.1978E 02	0.4508E-01	0.1978E 02	0.1964E 01
0.2478E 02	0.2031E-01	0.2478E 02	0.2384E 01
0.2968E 02	0.6850E-02	0.2968E 02	0.2904E 01
0.3467E 02	0.3988E-02	0.3467E 02	0.3434E 01
0.3857E 02	0.1922E-02		
0.4445E 02	0.1133E-02		

RESULTS OF 1300. CPS. DATA ANALYSIS

POSITION	AMPLITUDE	POSITION	PHASE
0.	0.1000E 01	0.	0.
0.5010E 01	0.4683E-00	0.5010E 01	0.5479E 00
0.9890E 01	0.2188E-00	0.9890E 01	0.1042E 01
0.1489E 02	0.9282E-01	0.1489E 02	0.1557E 01
0.1978E 02	0.4496E-01	0.1978E 02	0.2018E 01
0.2478E 02	0.2109E-01	0.2478E 02	0.2439E 01
0.2968E 02	0.7044E-02	0.2968E 02	0.2937E 01
0.3467E 02	0.4503E-02	0.3467E 02	0.3458E 01
0.3857E 02	0.2048E-02		
0.4445E 02	0.9658E-03		
0.4946E 02	0.3748E-03		

RESULTS OF 1325. CPS. DATA ANALYSIS

POSITION	AMPLITUDE	POSITION	PHASE
0.	0.1000E 01	0.	0.
0.5010E 01	0.4642E-00	0.5010E 01	0.5597E 00

0.9890E 01	0.2122E-00	0.9890E 01	0.1061E 01
0.1489E 02	0.8931E-01	0.1489E 02	0.1595E 01
0.1978E 02	0.4303E-01	0.1978E 02	0.2080E 01
0.2478E 02	0.2080E-01	0.2478E 02	0.2526E 01
0.2968E 02	0.6672E-02	0.2968E 02	0.3055E 01
0.3467E 02	0.4865E-02	0.3467E 02	0.3604E 01
0.3857E 02	0.2300E-02		
0.4445E 02	0.1010E-02		
0.4946E 02	0.4343E-03		

RESULTS OF 1350. CPS. DATA ANALYSIS

POSITION	AMPLITUDE	POSITION	PHASE
0.	0.1000E 01	0.	0.
0.5010E 01	0.4601E-00	0.5010E 01	0.5687E 00
0.9890E 01	0.2058E-00	0.9890E 01	0.1062E 01
0.1489E 02	0.8509E-01	0.1489E 02	0.1605E 01
0.1978E 02	0.4005E-01	0.1978E 02	0.2107E 01
0.2478E 02	0.1945E-01	0.2478E 02	0.2588E 01
		0.2968E 02	0.3135E 01
		0.3467E 02	0.3783E 01

RESULTS OF 1375. CPS. DATA ANALYSIS

POSITION	AMPLITUDE	POSITION	PHASE
0.	0.1000E 01	0.	0.
0.5010E 01	0.4573E-00	0.5010E 01	0.5783E 00
0.9890E 01	0.2030E-00	0.9890E 01	0.1056E 01
0.1489E 02	0.8287E-01	0.1489E 02	0.1595E 01
0.1978E 02	0.3805E-01	0.1978E 02	0.2092E 01
0.2478E 02	0.1819E-01	0.2478E 02	0.2594E 01
		0.2968E 02	0.3016E 01

RESULTS OF 1400. CPS. DATA ANALYSIS

POSITION	AMPLITUDE	PHASE
0.	0.1000E 01	0.
0.5010E 01	0.4541E-00	0.5923E 00
0.9890E 01	0.2026E-00	0.1061E 01
0.1489E 02	0.8265E-01	0.1599E 01
0.1978E 02	0.3775E-01	0.2082E 01
0.2478E 02	0.1791E-01	0.2583E 01

RESULTS OF 1425. CPS. DATA ANALYSIS

POSITION	AMPLITUDE	PHASE
0.	0.1000E 01	0.
0.5010E 01	0.4480E-00	0.6083E 00

0.9890E 01	0.2009E-00	0.1079E 01
0.1489E 02	0.8197E-01	0.1628E 01
0.1978E 02	0.3780E-01	0.2111E 01
0.2478E 02	0.1813E-01	0.2616E 01

RESULTS OF 1450. CPS. DATA ANALYSIS

POSITION	AMPLITUDE	PHASE
0.	0.1000E 01	0.
0.5010E 01	0.4390E-00	0.6190E 00
0.9890E 01	0.1963E-00	0.1097E 01
0.1489E 02	0.7904E-01	0.1659E 01
0.1978E 02	0.3662E-01	0.2162E 01
0.2478E 02	0.1773E-01	0.2691E 01

PART 2 THE COMPLEX INVERSE RELAXATION LENGTH

FREQUENCY	OMEGA	RHO-REAL	ERROR-RE	RHO-IMAG	ERROR-IM
.1000E02	.6283E 02	.7995E-01	.1000E-02	.1805E-02	.1000E-04
.1500E02	.9425E 02	.7999E-01	.1000E-02	.2680E-02	.1000E-04
.2500E02	.1571E 03	.8010E-01	.1000E-02	.4510E-02	.5000E-04
.5000E02	.3142E 03	.8060E-01	.1000E-02	.9075E-02	.1000E-03
.6500E02	.4084E 03	.8105E-01	.1000E-02	.1175E-01	.3000E-03
.7500E02	.4712E 03	.8180E-01	.1000E-02	.1364E-01	.3000E-03
.1000E03	.6283E 03	.8255E-01	.1000E-02	.1730E-01	.3000E-03
.1100E03	.6911E 03	.8350E-01	.9000E-03	.1932E-01	.4000E-03
.1250E03	.7854E 03	.8420E-01	.9000E-03	.2178E-01	.5000E-03
.1500E03	.9425E 03	.8590E-01	.8000E-03	.2575E-01	.3000E-03
.1750E03	.1100E 04	.8795E-01	.8000E-03	.2902E-01	.2000E-03
.2000E03	.1257E 04	.9000E-01	.6000E-03	.3195E-01	.4000E-03
.2250E03	.1414E 04	.9180E-01	.6000E-03	.3562E-01	.3000E-03
.2500E03	.1571E 04	.9350E-01	.6000E-03	.3915E-01	.2000E-03
.2750E03	.1728E 04	.9590E-01	.5000E-03	.4201E-01	.3000E-03
.2900E03	.1822E 04	.9740E-01	.5000E-03	.4372E-01	.4000E-03
.3000E03	.1885E 04	.9810E-01	.6000E-03	.4492E-01	.3000E-03
.3250E03	.2042E 04	.1001E-00	.1000E-02	.4704E-01	.3000E-03
.3500E03	.2199E 04	.1025E-00	.1000E-02	.4871E-01	.4000E-03
.3750E03	.2356E 04	.1044E-00	.8000E-03	.5190E-01	.4000E-03
.4000E03	.2513E 04	.1071E-00	.1000E-02	.5235E-01	.4000E-03
.4250E03	.2670E 04	.1099E-00	.1000E-02	.5578E-01	.8000E-03
.4500E03	.2827E 04	.1111E-00	.1000E-02	.5823E-01	.7000E-03
.4510E03	.2834E 04	.1118E-00	.1000E-02	.5836E-01	.9000E-03
.4750E03	.2985E 04	.1139E-00	.1500E-02	.6043E-01	.1000E-02
.5000E03	.3142E 04	.1147E-00	.1000E-02	.6141E-01	.1000E-02
.5100E03	.3204E 04	.1152E-00	.2000E-02	.6191E-01	.1200E-02
.5250E03	.3299E 04	.1158E-00	.8000E-03	.6388E-01	.6000E-03
.5500E03	.3456E 04	.1179E-00	.8000E-03	.6603E-01	.1500E-02
.5750E03	.3613E 04	.1209E-00	.7000E-03	.6789E-01	.1500E-02
.6000E03	.3770E 04	.1228E-00	.1000E-02	.6955E-01	.1500E-02
.6250E03	.3927E 04	.1242E-00	.1000E-02	.7132E-01	.1000E-02
.6500E03	.4084E 04	.1240E-00	.1000E-02	.7255E-01	.1200E-02
.6750E03	.4241E 04	.1247E-00	.7000E-03	.7382E-01	.1500E-02
.7000E03	.4398E 04	.1277E-00	.1000E-02	.7546E-01	.1500E-02
.7250E03	.4555E 04	.1301E-00	.1000E-02	.7721E-01	.2000E-02
.7500E03	.4712E 04	.1314E-00	.2000E-02	.7851E-01	.2000E-02
.7750E03	.4869E 04	.1314E-00	.2000E-02	.7929E-01	.2000E-02
.8000E03	.5027E 04	.1358E-00	.1000E-02	.8237E-01	.1000E-02
.8250E03	.5184E 04	.1343E-00	.3000E-02	.8280E-01	.2000E-02
.8500E03	.5341E 04	.1387E-00	.2000E-02	.8444E-01	.3000E-02
.8750E03	.5498E 04	.1398E-00	.2000E-02	.8620E-01	.3000E-02
.9000E03	.5655E 04	.1415E-00	.1000E-02	.8750E-01	.2000E-02

.9250E03	.5812E 04	.1426E-00	.1000E-02	.8786E-01	.1000E-02
.9500E03	.5969E 04	.1453E-00	.1000E-02	.9030E-01	.1500E-02
.9750E03	.6126E 04	.1467E-00	.2000E-02	.9105E-01	.1500E-02
.1000E04	.6283E 04	.1483E-00	.2000E-02	.9200E-01	.1800E-02
.1025E04	.6440E 04	.1501E-00	.2200E-02	.9028E-01	.1800E-02
.1050E04	.6597E 04	.1500E-00	.2300E-02	.9220E-01	.2000E-02
.1075E04	.6754E 04	.1494E-00	.2300E-02	.9501E-01	.2300E-02
.1100E04	.6911E 04	.1523E-00	.2400E-02	.9650E-01	.2300E-02
.1125E04	.7069E 04	.1533E-00	.2600E-02	.9600E-01	.2700E-02
.1150E04	.7226E 04	.1536E-00	.2600E-02	.9542E-01	.2800E-02
.1175E04	.7383E 04	.1529E-00	.2800E-02	.9715E-01	.2800E-02
.1200E04	.7540E 04	.1525E-00	.3000E-02	.1006E-00	.3000E-02
.1229E04	.7722E 04	.1580E-00	.3200E-02	.1030E-00	.3200E-02
.1250E04	.7854E 04	.1609E-00	.3200E-02	.9977E-01	.3300E-02
.1275E04	.8011E 04	.1586E-00	.3400E-02	.9895E-01	.3300E-02
.1300E04	.8168E 04	.1588E-00	.3500E-02	.1001E-00	.3400E-02
.1325E04	.8325E 04	.1574E-00	.3500E-02	.1038E-00	.3400E-02
.1350E04	.8482E 04	.1611E-00	.3800E-02	.1070E-00	.3700E-02
.1375E04	.8639E 04	.1635E-00	.3800E-02	.1041E-00	.3700E-02
.1400E04	.8796E 04	.1640E-00	.3900E-02	.1055E-00	.3800E-02
.1425E04	.8954E 04	.1639E-00	.4000E-02	.1071E-00	.4000E-02
.1450E04	.9111E 04	.1655E-00	.4000E-02	.1097E-00	.4000E-02

PART 3 THE SQUARED COMPLEX INVERSE RELAXATION LENGTH

OMEGA	OMEGA**2	RHO**2-IM	ERROR-IM	RHO**2-RE	ERROR-RE
.6283E02	.3948E 04	.2886E-03	.5209E-05	.6389E-02	.1599E-03
.9425E02	.8883E 04	.4287E-03	.6960E-05	.6391E-02	.1600E-03
.1571E03	.2467E 05	.7225E-03	.1703E-04	.6396E-02	.1607E-03
.3142E03	.9870E 05	.1463E-02	.3427E-04	.6414E-02	.1630E-03
.4084E03	.1668E 06	.1905E-02	.7213E-04	.6431E-02	.1691E-03
.4712E03	.2221E 06	.2232E-02	.7636E-04	.6505E-02	.1718E-03
.6283E03	.3948E 06	.2856E-02	.8412E-04	.6515E-02	.1755E-03
.6911E03	.4777E 06	.3226E-02	.1016E-03	.6599E-02	.1658E-03
.7854E03	.6168E 06	.3668E-02	.1234E-03	.6615E-02	.1733E-03
.9425E03	.8883E 06	.4424E-02	.9274E-04	.6716E-02	.1529E-03
.1100E04	.1209E 07	.5105E-02	.8161E-04	.6893E-02	.1523E-03
.1257E04	.1579E 07	.5751E-02	.1103E-03	.7079E-02	.1336E-03
.1414E04	.1999E 07	.6540E-02	.9782E-04	.7158E-02	.1315E-03
.1571E04	.2467E 07	.7321E-02	.8438E-04	.7210E-02	.1279E-03
.1728E04	.2986E 07	.8057E-02	.9955E-04	.7432E-02	.1211E-03
.1822E04	.3320E 07	.8517E-02	.1216E-03	.7575E-02	.1324E-03
.1885E04	.3553E 07	.8813E-02	.1128E-03	.7606E-02	.1447E-03
.2042E04	.4170E 07	.9417E-02	.1541E-03	.7807E-02	.2284E-03
.2199E04	.4836E 07	.9986E-02	.1794E-03	.8134E-02	.2440E-03
.2356E04	.5552E 07	.1084E-01	.1666E-03	.8206E-02	.2086E-03
.2513E04	.6317E 07	.1121E-01	.1904E-03	.8730E-02	.2561E-03
.2670E04	.7131E 07	.1226E-01	.2874E-03	.8973E-02	.3091E-03
.2827E04	.7994E 07	.1294E-01	.2720E-03	.8957E-02	.3038E-03
.2834E04	.8030E 07	.1305E-01	.3180E-03	.9102E-02	.3287E-03
.2985E04	.8907E 07	.1376E-01	.4090E-03	.9317E-02	.4625E-03
.3142E04	.9870E 07	.1409E-01	.3522E-03	.9382E-02	.3522E-03
.3204E04	.1027E 08	.1426E-01	.5241E-03	.9433E-02	.6093E-03
.3299E04	.1088E 08	.1479E-01	.2412E-03	.9329E-02	.2619E-03
.3456E04	.1194E 08	.1558E-01	.4595E-03	.9549E-02	.3868E-03
.3613E04	.1305E 08	.1641E-01	.4577E-03	.1001E-01	.3729E-03
.3770E04	.1421E 08	.1708E-01	.5075E-03	.1024E-01	.4543E-03
.3927E04	.1542E 08	.1772E-01	.3911E-03	.1034E-01	.3911E-03
.4084E04	.1668E 08	.1800E-01	.4428E-03	.1012E-01	.4222E-03
.4241E04	.1799E 08	.1841E-01	.4775E-03	.1011E-01	.3961E-03
.4398E04	.1934E 08	.1927E-01	.5340E-03	.1062E-01	.4818E-03
.4555E04	.2075E 08	.2009E-01	.6749E-03	.1097E-01	.5691E-03
.4712E04	.2221E 08	.2063E-01	.8395E-03	.1109E-01	.8395E-03
.4869E04	.2371E 08	.2084E-01	.8427E-03	.1098E-01	.8427E-03
.5027E04	.2527E 08	.2237E-01	.4363E-03	.1165E-01	.4363E-03
.5184E04	.2687E 08	.2224E-01	.4036E-04	.1118E-01	.4745E-03
.5341E04	.2852E 08	.2342E-01	.1170E-02	.1209E-01	.1061E-02
.5498E04	.3023E 08	.2410E-01	.1184E-02	.1211E-01	.1076E-02
.5655E04	.3198E 08	.2476E-01	.7409E-03	.1236E-01	.6330E-03

.5812E04	.3378E 08	.2506E-01	.4610E-03	.1262E-01	.4610E-03
.5969E04	.3563E 08	.2625E-01	.6166E-03	.1297E-01	.5616E-03
.6126E04	.3753E 08	.2671E-01	.8043E-03	.1323E-01	.8599E-03
.6283E04	.3948E 08	.2728E-01	.9018E-03	.1352E-01	.9243E-03
.6440E04	.4148E 08	.2710E-01	.9375E-03	.1437E-01	.9854E-03
.6597E04	.4352E 08	.2766E-01	.1024E-02	.1400E-01	.1059E-02
.6754E04	.4562E 08	.2840E-01	.1125E-02	.1331E-01	.1125E-02
.6911E04	.4777E 08	.2939E-01	.1164E-02	.1388E-01	.1175E-02
.7069E04	.4996E 08	.2944E-01	.1327E-02	.1429E-01	.1316E-02
.7226E04	.5221E 08	.2932E-01	.1357E-02	.1450E-01	.1333E-02
.7383E04	.5450E 08	.2972E-01	.1400E-02	.1395E-01	.1400E-02
.7540E04	.5685E 08	.3066E-01	.1518E-02	.1313E-01	.1518E-02
.7722E04	.5963E 08	.3254E-01	.1670E-02	.1436E-01	.1670E-02
.7854E04	.6168E 08	.3210E-01	.1700E-02	.1593E-01	.1688E-02
.8011E04	.6418E 08	.3139E-01	.1720E-02	.1537E-01	.1732E-02
.8168E04	.6672E 08	.3179E-01	.1780E-02	.1518E-01	.1792E-02
.8325E04	.6931E 08	.3269E-01	.1797E-02	.1399E-01	.1808E-02
.8482E04	.7195E 08	.3447E-01	.2005E-02	.1451E-01	.2016E-02
.8639E04	.7464E 08	.3405E-01	.2001E-02	.1589E-01	.2013E-02
.8796E04	.7738E 08	.3461E-01	.2069E-02	.1575E-01	.2081E-02
.8954E04	.8017E 08	.3510E-01	.2168E-02	.1541E-01	.2168E-02
.9111E04	.8300E 08	.3630E-01	.2201E-02	.1534E-01	.2201E-02

BIOGRAPHICAL SKETCH

Ray Sturgis Booth was born in Miami, Florida, on October 5, 1938. He was graduated in June, 1956, from South Dade High School in Homestead, Florida. In January, 1961, he received the degree of Bachelor of Electrical Engineering from the University of Florida and was admitted to the University's Graduate School. He was awarded the degree of Master of Science in Nuclear Engineering in August, 1962. While pursuing his graduate studies, he was a research assistant in the Department of Nuclear Engineering.

Ray Sturgis Booth is married to the former Judith Anne Bridges. He is a student member of the American Nuclear Society and of the American Institute of Electrical Engineers.

This dissertation was prepared under the direction of the chairman of the candidate's supervisory committee and has been approved by all members of that committee. It was submitted to the Dean of the College of Engineering and to the Graduate Council, and was approved as partial fulfillment of the requirements for the degree of Doctor of Philosophy.

April 24, 1965

Thomas F. Martin Jr.
Dean, College of Engineering

Dean, Graduate School

Supervisory Committee:

Chairman

G. R. Dalton

A P Sage

Robert E Uhrig

R G Selfridge

273
1 5591